THE INTERACTIONS OF ANTIMONY AND BISMUTH WITH GALLIUM ARSENIDE {111} SURFACES

A thesis submitted to

DUBLIN CITY UNIVERSITY

for the degree of

Doctor in Philosophy

Colm McGinley, B.A.

School of Physical Sciences

Dublin City University

Research Supervisor

Dr. A.A. Cafolla

March 1998

Declaration

I hereby certify that this material, which I now submit for assessment on the programme of study leading to the award of Ph.D. is entirely my own work and has not been taken from the work of others save and to the extent that such work has been cited and acknowledged within the text of my work

Signed: Colm Mc Ginley ID No.: 93701110

Date: 11 March 1998

Contents

Abstract

Four GroupV-GaAs{111}-(2×2) surfaces were studied by Low Energy Electron Diffraction (LEED) and Photoelectron Spectroscopy (PES). The growth modes of these systems were established as Volmer-Weber growth for both Bi and Sb on GaAs(111)B and Stranski-Krastanov for Sb and Bi on GaAs(111)A. Deposition of Bi on GaAs(111)B had the effect of removing some of the As trimers of the clean surface but this effect was not found for Sb deposition. For Bi deposition on GaAs(111)A, a new chemical environment was found for the surface Ga. This is evidence for a Ga-Bi chemical bond, in contrast to Sb on GaAs(111)A, where the Sb bonds to the As. These results are inferred from core level photoelectron spectroscopy. A series of anneals was performed for each system over the temperature range for which the adsorbed layer remained on the surface. Bi fully desorbed from the GaAs(111)A surface at 425°C and from the GaAs(111)B surface at 475°C. In the case of Sb, desorption was complete at 600°C for both GaAs(111)A and (111)B. After desorption of both Sb and Bi overlayers from GaAs(111)A, the (2×2) symmetry of the clean surface was regained. The GaAs(111)B surface was faceted after Sb desorption and for Bi desorption the symmetry increased to (1×1). Temperature induced changes in the crystal symmetry of the adsorbate systems were followed using LEED. New surface reconstructions observed were Sb\GaAs(111)A-$(2\sqrt{3}\times 2\sqrt{3})R30°$ [500°C-550°C], Sb\GaAs(111)B-$\begin{pmatrix} 3 & -1 \\ -1 & 3 \end{pmatrix}$ [475°C-550°C] and Bi\GaAs(111)B-c(4×2) [110°C-375°C]. Structural models for these reconstructed systems, which take photoemission evidence for the chemical bonding into account, were derived in agreement with the electron counting rule. LEED pattern simulations were demonstrated for two of these structural models. For Bi-GaAs(111)A, the (2×2) symmetry of the original clean surface remained for the whole experiment. Changes in the surface band bending for each system were also measured.

Acknowledgements

'Night time is the Right time'
- Duke Ellington

First I have to thank my supervisor, Tony Cafolla, for giving me the opportunity to do this work and for securing the funding to allow me complete it. I am grateful for his direction in experimental work, various discussions and encouragement.

The direction this work took came from a curious study with bizarre LEED patterns seen at the Daresbury synchrotron on a very late night. More late nights followed and night time was the right time for most of the work described in this thesis. I am seriously grateful to those who collaborated on the 8am shuffle, Philip Moriarty, Charles Markham, Brigid Murphy and Dave Teehan. I thank (in order of appearance) Chris Dunscombe, Rob Petrie, Brian Lawless and Eilish McLoughlin for helping with the day work at beamline 6.2 and David Woolf for the impeccably made samples. The commitment and generosity of everyone contributed enormously to the success of the Daresbury trips.

For conversation, discussion and help on surface physics I must thank, Brigid, Philip and Dave (all again) and Greg Hughes and Enda McGlynn of D.C.U. Another thank you to Alan Hughes for all his help with bureaucracy and Al Devine for assistance with photographic work.

Thanks to all the postgrads who helped make my time in building N a good time and to Paul Quinn and Eilish McLoughlin for proof reading this thesis.

Finally I thank my family for their support and understanding during the last few years and most of all, Joan, for encouragement, companionship and everything.

Funding from Forbairt, Basic Science Award SC/95/456, is acknowledged

Table of Acronyms

ARPES	Angle Resolved Photoelectron Spectroscopy
CBM	Conduction Band Minimum
CHA	Concentric Hemispherical Analyser
DOS	Density of States
ECLS	Epitaxial continued layer structure
EDC	Energy Distribution Curve
ESCA	Electron Spectroscopy for Chemical Analysis
FWHM	full width at half maximum
IPE	Inverse Photoemission
LEED	Low Energy Electron Diffraction
ML	Monolayer
PES	Photoelectron Diffraction
QCM	Quartz Crystal Monitor
RHEED	Reflection High Energy Electron Diffraction
SCLS	Surface Core Level Shift
SIMS	Secondary Ion Mass Spectrometry
SRS	Synchrotron Radiation Source
STM	Scanning Tunneling Microscopy
SXPS	Soft X-ray photoelectron Spectroscopy
TEM	Transmission Electron Microscopy
TGM	Toroidal Grating Monochromator
UHV	Ultra High Vacuum
VBM	Valence Band Maximum
XPS	X-ray Photoelectron Spectroscopy

Chapter I

Introduction

The importance of the surface properties of semiconductors in device technology has been recognised ever since the first germanium transistors were built in the 1940's. Semiconductor surfaces have electronic and structural properties that are different from those of the bulk and the need to account for these surface modifications has led to major advances in experimental and theoretical research over the last 50 years. In III-V semiconductors, such as GaAs, the relationship between crystal structure and electronic properties is an interesting area of study. Since the early 1980's the research interest in the growth of Sb and Bi on III-V surfaces has steadily increased. Much of this work concentrated on Schottky barrier formation and investigating the possibility of epitaxial growth. Motivation for the former derived from interest in the rectification properties of electronic diodes and while studies in epitaxy complemented this work, the possibility of new device applications was an impetus for crystal growers. Initially, the interaction of Sb and Bi with the (110) cleavage plane of the III-V semiconductors served as a model system for the study of these interfaces in general. Within ten years this type work progressed as far as developing alternative non-linear optical devices. This class of interfaces was also used to test newly emerging experimental techniques such as IV-LEED, X-ray standing wave (XSW), scanning tunnelling microscopy (STM) and angle resolved ultraviolet photoelectron spectroscopy (ARUPS) most of which had already been successful for the analysis of low coverage adsorbates on metals and some elemental semiconductors. Theoretical calculations performed during the 1980's were mainly directed towards low index clean GaAs surfaces but there were some important successes with regard to the group V adsorbates on the cleavage plane.

This study began with an investigation of the interaction of Sb with the GaAs (111)A and (111)B surfaces. This was done by annealing in stages after an initial Sb deposit of approximately 1 monolayer. Structural transitions were observed for both surfaces at a temperature of 500°C. With the crystal symmetry of the surfaces given by electron diffraction and knowledge of surface chemical bonding given by core level photoemission, structural models of these surfaces could be proposed. A simple theoretical principle

which has been successfully used to describe various III-V surfaces was invoked to justify the structural models. The principal conclusions from this work concern the structure of these surfaces.

For comparison, the interaction of Bi with the GaAs{111} surfaces was then examined. The Bi-GaAs(111)B surface exhibited a reconstruction and has similarities with the Sb terminated (111)B surface. Only for Bi on the GaAs(111)A surface, was the clean surface symmetry unaltered by the annealing process. There was evidence however that Bi chemically bonds directly to this surface. Structural models were proposed to explain experimental results in both cases.

With the nature of the surface reconstructions determined, a detailed study of overlayer growth was carried out. Sb and Bi were found to have the Stranski-Krastanov growth mode on the (111)A surface. A different growth mode (Volmer-Weber) was established for both overlayers on the (111)B surface. With regard to the electronic properties of these systems, the process of deposition and annealing affected the surface band bending in a manner depending on which surface was used, not which overlayer. Simulations of diffraction patterns recorded for two of the surfaces studied are also carried out.

A general background to both semiconductor surfaces and the experimental techniques used are given in chapters II and III. A brief review of recent research on low index GaAs surfaces and their termination with Group V elements is given in chapter IV. The emphasis here is on structural studies. Chapters V and VI give results and discussion for the interaction of Sb and Bi with the GaAs(111)A surface. Chapters VII and VIII describe Sb and Bi on the GaAs(111)B surface. General comparisons between the four systems and concluding remarks are made in chapter IX.

Chapter II

Theoretical details

This chapter begins with a description of the nature of semiconductor surfaces. Surface crystallography and the surface reciprocal lattice are then described. Electronic properties are discussed from the point of view of band bending at surfaces. Photoemission spectroscopy and its application to probing atomic core levels in the solid state is then introduced. Finally, a description of the growth modes of adsorbates on surfaces is given.

2.1 The structure of Semiconductor Surfaces [1]

The creation of a surface modifies the crystal structure of a material and creates local electronic states which differ from those in the bulk. In the case of a semiconductor, electronic states arising due to an unmodified surface will have an energy in the bulk band gap. Nonpolar semiconductors, such as Silicon or Germanium, have the (111) plane as that of lowest surface energy, as the creation of a surface with this orientation involves breaking the minimum number of bonds per unit area. In the polar semiconductors, like GaAs and other III-V compounds, the (110) surface has the lowest surface energy. The (110) plane is therefore the natural cleavage plane. For a III-V semiconductor, the (111) orientation has one face entirely metallic (Group III terminated) and the opposite face purely non-metallic (Group-V terminated). This results in a surface energy higher than that of the (110) surface. This explains why the lowest energy surfaces are different for polar and nonpolar semiconductors. To achieve bulk termination with an orientation different to the natural cleavage plane the sample must be prepared using a technique such as molecular beam epitaxy (MBE).

At a semiconductor surface, broken bonds protrude out into the vacuum. In tetrahedral semiconductors these are sp^3 hybridised bond orbitals, the same as those in the bulk, but they are on average only half filled. This electron deficiency is the origin of the electronic and crystal structure differences between the surface and the bulk.

2.1.1 Surface Reconstruction [1]

A semiconductor surface which has exactly the same atomic positions and bond lengths as an equivalent bulk plane would have too high an energy to be stable so it undergoes either relaxation or reconstruction or both.

An unmodified surface would have partially filled dangling bond states with an energy in the band gap which is energetically unfavourable. A modification of the crystal structure is necessary to remove the surface electronic states from the band gap.

Relaxation is simply a modification of the bulk bond lengths and bond angles. Reconstruction of the surface involves the rebonding of surface atoms in a manner not found in the bulk. Reconstruction also includes the possibility of bond rehybridisation at the surface. A lowering of symmetry takes place when a surface reconstructs. This is due to the degeneracy of the unreconstructed surface. The degeneracy is explained by the fact that for any distribution of electrons among the dangling bonds, all situations have the same energy. A surface reconstruction is therefore a Jahn-Teller distortion. The lowering of symmetry may be seen in surface crystallography or else in the bond rehybridisation.

2.1.1.1 Surface crystallography and Woods notation [2]

Surface crystallography relates the symmetry of the surface to the symmetry of the underlying bulk planes. If primitive translation vectors for a bulk plane are $\mathbf{b_1}$ and $\mathbf{b_2}$ and the reconstructed surface has primitive translation vectors of $\mathbf{s_1} = m\mathbf{b_1}$ and $\mathbf{s_2} = n\mathbf{b_2}$, where m and n are integers, then the surface reconstruction is called (m×n). This is called Woods notation. If m and n are non integers then the (m×n) surface unit cell is rotated with respect to the bulk (1×1) unit cell. For this notation the angle between $\mathbf{b_1}$ and $\mathbf{b_2}$ is equal to the angle between $\mathbf{s_1}$ and $\mathbf{s_2}$.

The GaAs {111} surfaces are used as an example. GaAs has two distinct (111) surfaces, as mentioned above, the (111)A, ideally terminated by a monolayer of Ga atoms, and the (111)B, ideally terminated by plane of As atoms. The (111)A surface has a (2×2) reconstruction [3] while the (111)B exhibits a temperature dependent progression of reconstructions, i.e. (2×2) → (1×1) → ($\sqrt{19}\times\sqrt{19}$) → (1×1) [4]. Shown in figure 2.1 are schematic models for the (2×2) reconstructions of GaAs (111)A and (111)B.

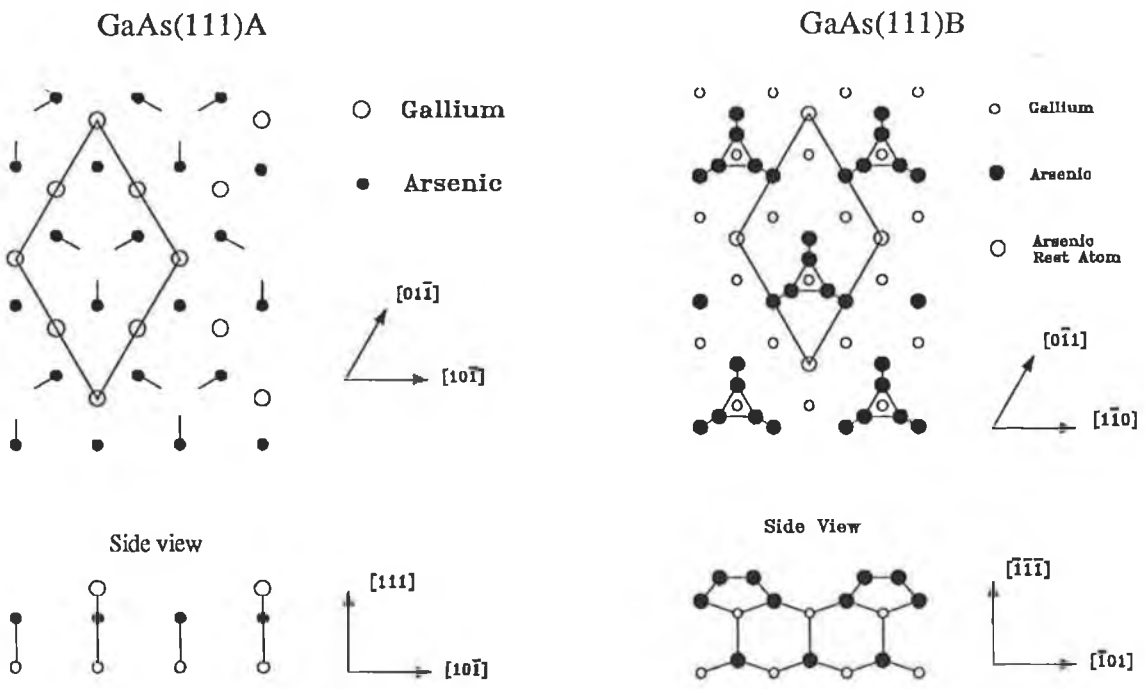

Figure 2.1. The GaAs (111)A and (111)B (2×2) surfaces. The (2×2) cells are marked with dashed lines.

GaAs (111)A is terminated by ¾ monolayers of Ga and the resulting Ga vacancies expose As dangling bonds in the layer beneath. These Ga vacancies have a unit cell or mesh which has four times the area of the bulk (1×1) mesh. This reconstruction is stable for an MBE grown sample up to the melting temperature (~650°C).

The As terminated GaAs(111)B surface shown in figure 2.1 is covered with As trimers in a (2×2) arrangement. The As rest atom in the GaAs(111)B surface contains a dangling bond with two electrons protruding directly out of the surface. Variations on both of these terminations are possible after temperature annealing and will be discussed in detail later.

2.1.1.2 Surface crystallography and matrix notation

Surface reconstructions for which the angles of the bulk and surface unit cells are not equal require a matrix notation.

$$\mathbf{s}_1 = m_{11}\mathbf{b}_1 + m_{12}\mathbf{b}_2$$
$$\mathbf{s}_2 = m_{21}\mathbf{b}_1 + m_{22}\mathbf{b}_2$$

or

$$\begin{pmatrix}\mathbf{s}_1\\ \mathbf{s}_2\end{pmatrix} = \begin{pmatrix}m_{11} & m_{12}\\ m_{21} & m_{22}\end{pmatrix}\begin{pmatrix}\mathbf{b}_1\\ \mathbf{b}_2\end{pmatrix} = M\begin{pmatrix}\mathbf{b}_1\\ \mathbf{b}_2\end{pmatrix} \qquad (2.1)$$

The surface reconstruction is then denoted by the matrix $\begin{pmatrix}m_{11} & m_{12}\\ m_{21} & m_{22}\end{pmatrix}$. In the case of an adsorbate system, the symmetry of the surface is often lower then that of the equivalent bulk plane. The symmetry of the adsorbate layer and the bulk are related in the same manner as for a reconstructed surface (equation 2.1). If the m_{ij} are rational the surface reconstruction is called commensurate. For non rational m_{ij}, the reconstruction is non-commensurate. This type of reconstruction occurs when there is no chemical bond between the substrate and overlayer.

2.1.2 The Reciprocal Lattice and Diffraction [5]

The III-V semiconductors have a zincblende crystal structure where a two dimensional reciprocal lattice can be defined for a given surface plane in a similar way to the three dimensional case. For surface primitive translation vectors $\mathbf{s}_1$ and $\mathbf{s}_2$, the reciprocal lattice vectors are given by

$$\mathbf{s}_1^* = 2\pi\frac{\mathbf{s}_2 \times \hat{\mathbf{n}}}{\mathbf{s}_1 \cdot (\mathbf{s}_2 \times \hat{\mathbf{n}})}, \quad \mathbf{s}_2^* = 2\pi\frac{\mathbf{s}_1 \times \hat{\mathbf{n}}}{\mathbf{s}_1 \cdot (\mathbf{s}_2 \times \hat{\mathbf{n}})} \qquad (2.2)$$

where $\hat{\mathbf{n}}$ is the unit vector normal to the surface. The surface reciprocal lattice can be determined by Low Energy Electron Diffraction (LEED). From the diffraction pattern the surface real space lattice can be determined.

For a reconstructed surface or an adsorbed surface layer, surface and bulk reciprocal lattice vectors are related by

$$\mathbf{s_1}^* = m_{11}^* \mathbf{b_1}^* + m_{12}^* \mathbf{b_2}^*$$
$$\mathbf{s_2}^* = m_{21}^* \mathbf{b_1}^* + m_{22}^* \mathbf{b_2}^*$$

or

$$\begin{pmatrix} \mathbf{s_1}^* \\ \mathbf{s_2}^* \end{pmatrix} = \begin{pmatrix} m_{11}^* & m_{12}^* \\ m_{21}^* & m_{22}^* \end{pmatrix} \begin{pmatrix} \mathbf{b_1}^* \\ \mathbf{b_2}^* \end{pmatrix} = M^* \begin{pmatrix} \mathbf{b_1}^* \\ \mathbf{b_2}^* \end{pmatrix} \tag{2.3}$$

The vectors $\mathbf{s_1}^*$ and $\mathbf{s_2}^*$ can be found from a LEED pattern. The matrix M* is related to M of equation 2.1 by

$$M^* = (M^{-1})^T$$

or

$$m_{11} = \frac{m_{22}^*}{\det M^*} \qquad m_{12} = \frac{-m_{21}^*}{\det M^*}$$
$$m_{21} = \frac{-m_{21}^*}{\det M^*} \qquad m_{22} = \frac{m_{22}^*}{\det M^*} \tag{2.4}$$

Equations 2.4 are useful for complicated surface reconstructions as the reciprocal space coefficients m_{ij}^* can be found directly from LEED patterns. The matrix M which describes the real space symmetry of the adsorbate system can then be derived.

2.2 Electronic Properties

The other important surface modification of a crystal involves that of surface electronic states. Surface states can be described by exponentially decaying solutions to the Bloch condition. The wave function describing a surface state decays into the bulk and has maximum amplitude at the surface [6, 7]. These states may arise from the charge in the dangling hybrid bonds protruding into the vacuum or from surface bonds to another element in the case of an adsorbate. These states can have an energy which lies in the bulk band gap.

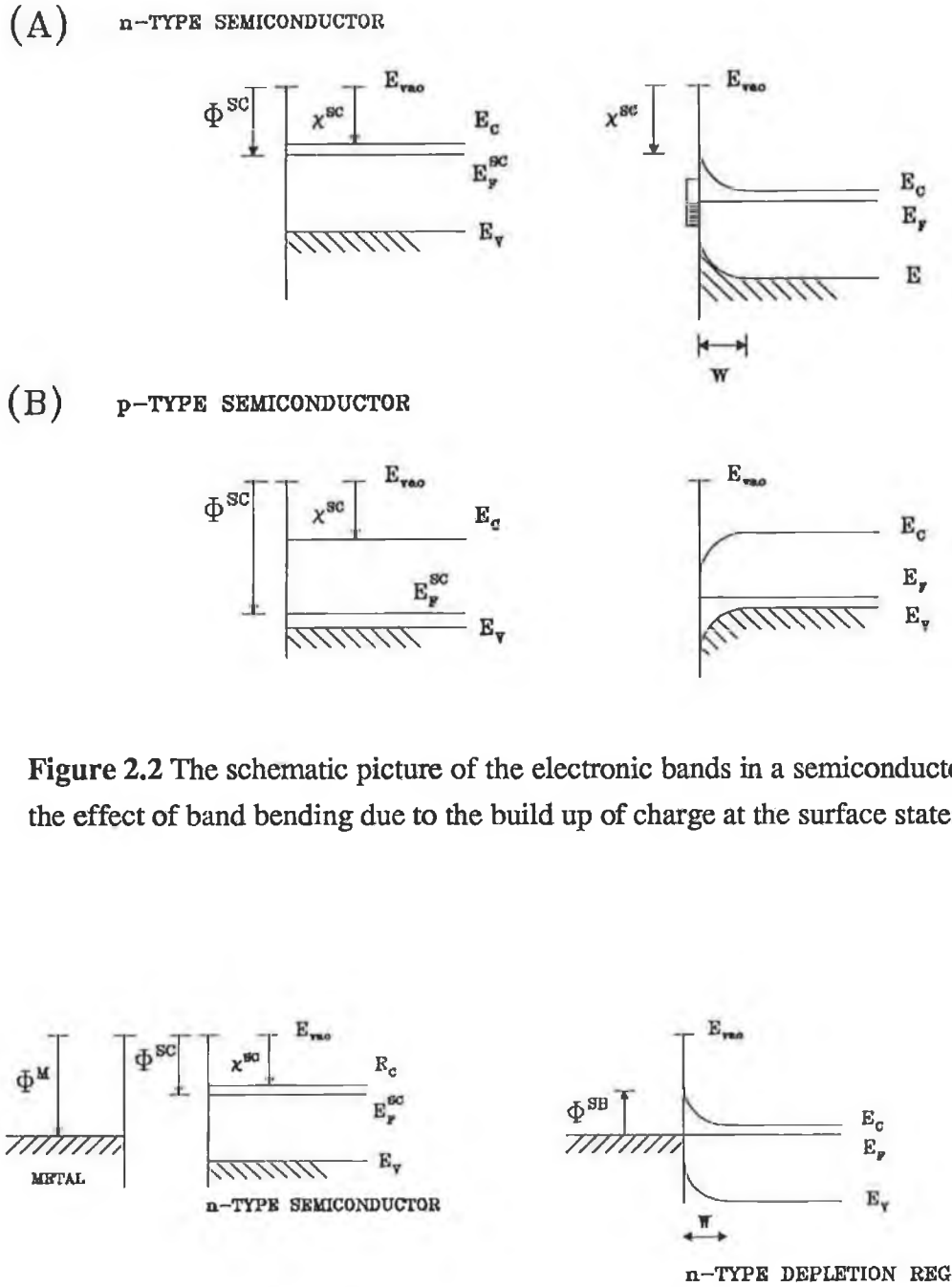

Figure 2.2 The schematic picture of the electronic bands in a semiconductor with the effect of band bending due to the build up of charge at the surface states.

Figure 2.3 The situation before and after a metal is brought into contact with a semiconductor in the Schottky description of the Schottky barrier. Φ^{SB} is the height of the schottky barrier.

2.2.1 Band Bending at Surfaces [8]

The existence of electronic states within the bandgap can lead to band bending. In the case of a n-type material band bending occurs when conduction electrons lower their energy by filling the surface states. This flow of charge to the surface results in the region close to surface having uncompensated donor ions and so the electrostatic potential at the surface is raised. This change in the surface potential is called band bending. The band bending increases until all the surface states are filled or else until the occupied level of surface states reaches the Fermi level (see figure 2.2). For p-type material, the majority carriers are holes and an equivalent process to that in n-type material leads to band bending in the opposite direction.

In figure 2.2 the diagrams on the right show the band bending. E_C, E_V and E_F are the conduction band minimum, valence band maxima and Fermi level respectively. Φ and χ are the work function and electron affinity of the semiconductor. In both the n-type and p-type cases shown in figure 2.2, the Fermi level is said to be 'pinned mid-gap'.

2.2.2 Band bending at a metal/semiconductor interface

Band bending in the case of a metal/semiconductor interface is illustrated in figure 2.3. If the work function of the metal is greater than that of the semiconductor ($\Phi^M > \Phi^{SC}$), then a potential barrier will be formed at the interface, known as the Schottky barrier. The size of the Schottky barrier depends on the characteristics of the two materials involved. There are two early models which attempt to describe the electronic state of the interface, one due to Schottky and a second by Bardeen. Both of these models represent extreme situations and any real interface lies between these two extremes but the models do give a basic explanation for the two main causes of band bending.

2.2.2.1 The Schottky Model

The Schottky model explains band bending in terms of the bulk properties of the two materials involved. Figure 2.3 shows a metal and n-type semiconductor before and after contact. When the two materials are brought together, electrons flow from the semiconductor conduction band into the metal leaving behind a region which is positively

charged. This 'depletion' region has a width w and the situation causes band bending due to the increase in potential at the surface. The resulting potential barrier at the interface is called the Schottky barrier Φ^{SB} and, as shown in the diagram, is given by

$$\Phi^{SB} = \phi^{M} - \chi^{S} \tag{2.5}$$

where ϕ^{M} and χ^{S} are the work function of the metal and the electron affinity of the semiconductor respectively. This model was developed in the 1930's by Schottky, Mott and Davydov independently but was soon found to be inadequate. The Schottky barrier does not have a linear dependence on the metal work function but is usually independent of it.

2.2.2.2 The Bardeen Model

The Bardeen model is an improvement on the Schottky model and relies on the role of surface states to explain band bending. Figure 2.4 shows a metal/(n-type)semiconductor interface where electrons flow into the metal but they originate from the surface states in the semiconductor, not from the bulk. These surface states are the origin of band bending (section 2.2.1). If there is a sufficiently high density of states at the surface then all of the charge transfer comes from the surface. The band bending therefore remains unchanged and the Schottky barrier is independent of the work function and is given by,

$$\Phi^{SB} = V^{B} + \xi. \tag{2.6}$$

Here V^{B} is the band bending before contact and $\xi = E_C - E_F$. As stated before the two models are two extremes and any real case usually involves charge from both the bulk and the surface states of the semiconductor. More sophisticated models such as the Unified Defect Model of Spicer [9] or the Metal Induced Gap States Model of Heine [10] have been introduced to explain more recent experimental results but their validity can depend on how particular surfaces are prepared [8].

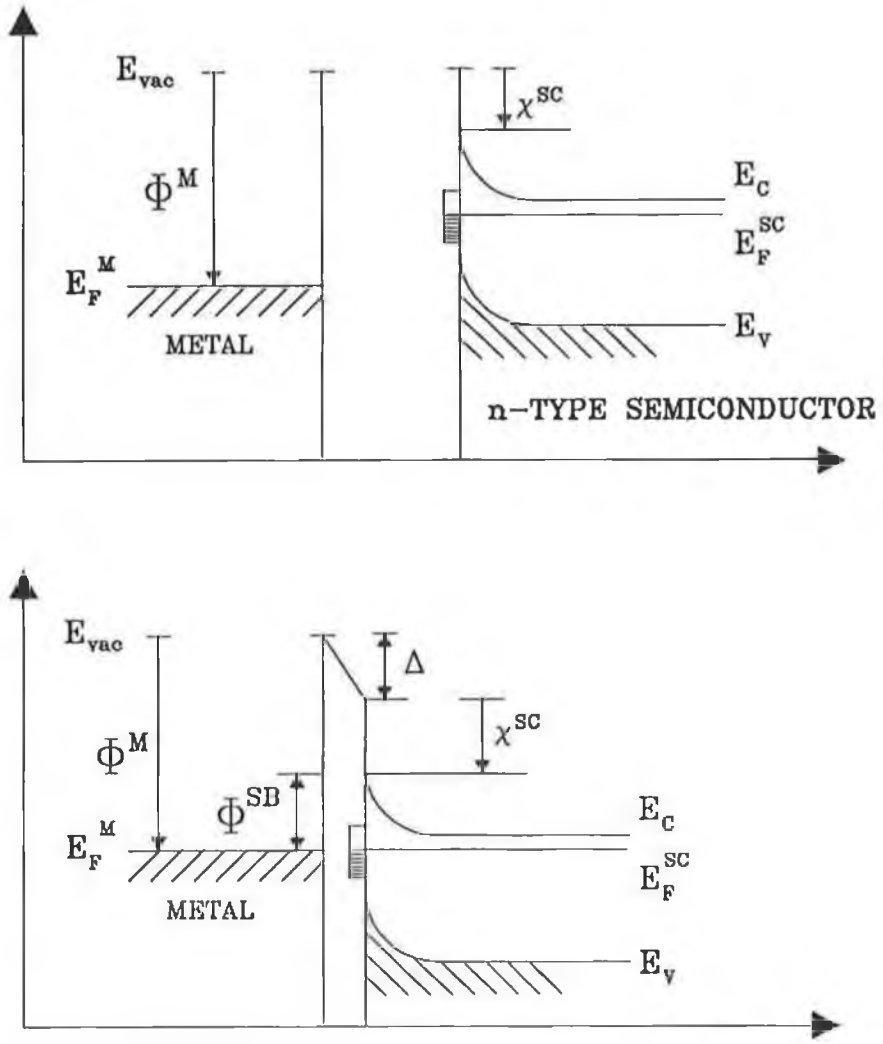

Figure 2.4 The Bardeen model shows how the height of the Schottky barrier may be considered to be independent of the work function of the metal.

2.3 Photoemission [12]

Photoemission spectroscopy is a widely used technique in surface science and variations of the technique have contributed to many different areas of the subject. The applications of photoemission are numerous but significant uses of the technique in surface physics include measuring the electronic structure of materials, investigating chemical bonding by core level photoemission and determining crystal structure by photoelectron diffraction [12].

For surface science photoemission experiments, radiation in the ultra-violet to soft X-ray range (10-300eV) is extremely useful. Photons in this energy range can be used to produce spectra both of the valence bands and a number of atomic core levels. Photoelectron spectroscopy has been greatly improved by the use of synchrotron radiation sources (section 3.1) as the photon energy used can be chosen to ensure that the photoelectron energy corresponds to that for which the electron has its minimum escape depth from the material. In most materials an electron has its minimum escape depth at an energy of approximately 40eV (figure 2.5) [11]. The surface sensitivity of the experiment can therefore be optimised by selecting a suitable photon energy so that the photoelectrons have a kinetic energy of approximately 40eV. Seah and Dench [11] have given an empirical expression for the photoelectron escape depth in an inorganic solid as

$$\lambda_m = 2170E^{-2} + 0.72(aE)^{1/2} \qquad (2.7)$$

where E is the electron energy above the Fermi level (eV) and a is a monolayer thickness (nm).

In this work, core level photoemission spectroscopy is used which combined with LEED allows the surface structure of new adsorbate systems to be determined. These systems are the Sb and Bi terminated GaAs(111)A and (111)B surfaces.

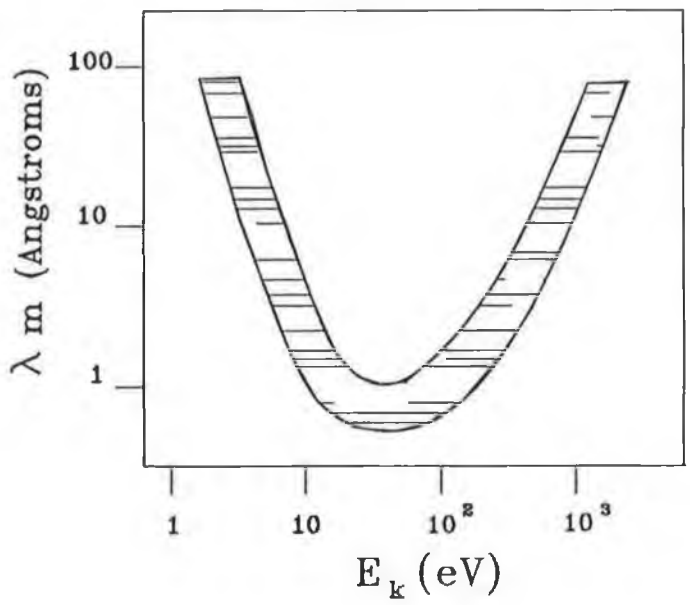

Figure 2.5 The dependence of the escape depth of photoelectrons, λ_m, on their kinetic energy E_k. The specific plots for most materials fall within the shaded region. The minimum escape depth corresponds to the maximum in surface sensitivity.

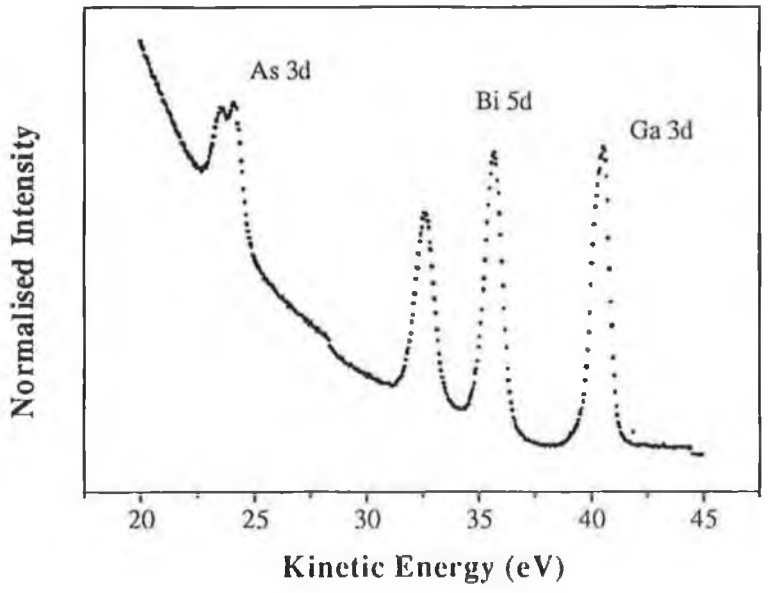

Figure 2.6 A photoemission spectrum showing Ga 3d, As 3d and Bi 5d core levels and the secondary electron tail.

2.3.1 The Photoemission process

The production of photoelectrons in a material is conveniently described as a 3-step process :

1. Ionisation of an atom in the bulk material
2. Transport of the photoelectron to the surface
3. Emission of the photoelectron into the vacuum

Each stage has its own interaction cross section which contributes to the intensity distribution of the primary photoelectrons - these are electrons which reach the surface without scattering. Secondary electrons are those which are inelastically scattered en route to the surface in step (2). These electrons contribute a rapidly decreasing tail to the spectrum produced. The spectra in figure 2.6 illustrates this. If the secondary electrons are ignored the spectrum is related to the density of electron states in the solid. The energy range of the states probed depends on the energy of the photons used.

A full description of the photoemission spectrum described above is complex [12] but in a simple one electron approximation the kinetic energy of a primary electron (E_k) is given by

$$E_k = h\nu - E_b - \phi \qquad (2.8)$$

where $h\nu$ is the photon energy, ϕ is the work function and E_b the binding energy of the electron in the solid. This equation does not take into account the relaxation of the electrons in the vicinity of the hole left by the emitted electron.

2.3.2 Core Level Spectroscopy

A core level spectrum corresponds to the density of states of an atomic level referred to by the principle and orbital angular momentum numbers n and l. In this work the As 3d, Ga 3d, Sb 4d and Bi 5d levels are studied for Sb and Bi adsorbed on GaAs{111} surfaces. In principle the more tightly bound s or p core levels could be studied, but this would require a photon energy outside the range of the beamline monochromator (section 3.2) and the interaction cross sections for these levels are ~100 times lower than those for the d levels.

All of the d states have l=2 and splitting is observed due to the coupling of the orbital and spin angular momenta of the electrons. Parallel or antiparallel coupling of spin and orbital moments result in different energies for the electrons whose total angular momentum is given by $j = l \pm s$. In the case of parallel coupling, j = l + s, and electrons in this state are shifted to lower binding energy while for electrons with antiparallel coupling, j = l - s, and the state is shifted to higher binding energy. The energy difference between the two states is called the 'spin-orbit splitting'. The two states have different degeneracy given by $m_j = 2j + 1$ so that the ratio of the intensities of the two components in the spectrum is given by

$$R = \frac{2(l+s)+1}{2(l-s)+1}. \qquad (2.9)$$

The Spin orbit splitting and the branching ratio of a Bi 5d spectrum are shown graphically in figure 2.7. For a d level the branching ratio is ideally 1.5 but this may change due to diffraction effects.

2.3.3 Core level broadening

Core level photoemission spectra have a finite width (see figure 2.7). In the atomic case, the core level width ΔE is given by,

$$\Delta E = \sqrt{\Gamma^2 + \Delta E_{ph}^2 + \Delta E_{an}^2} \qquad (2.10)$$

ΔE_{ph} and ΔE_{an} are the full width at half maximum (FWHM) of Gaussian functions which represent the resolution of the photon source and the electron analyser respectively. These are discussed in more detail in chapter 3. Γ is the FWHM of a Lorentzian function and represents the uncertainty in energy due to the lifetime of the core hole after photoemission has taken place. For an excited state lifetime of ~ 10^{-15} s, Γ is approximately 0.2eV.

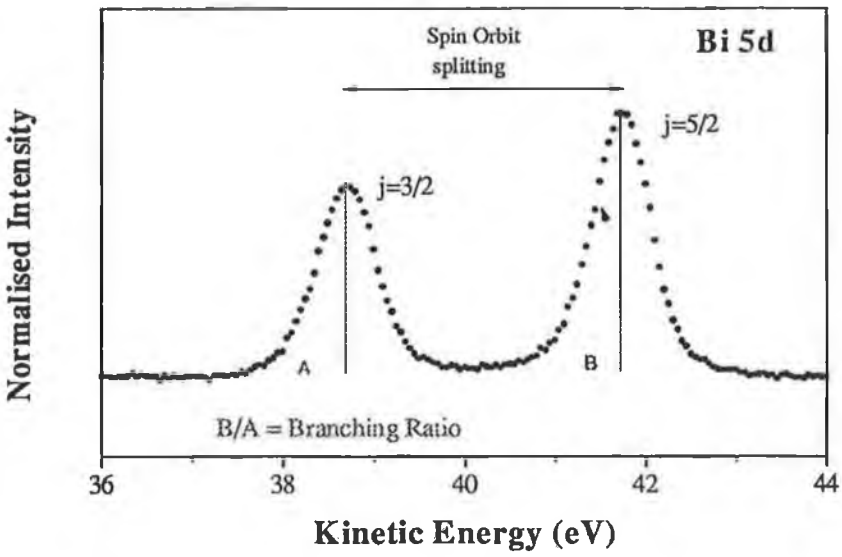

Figure 2.7 Bi 5d photoemission core level spectrum showing the spin orbit splitting and branching ratio.

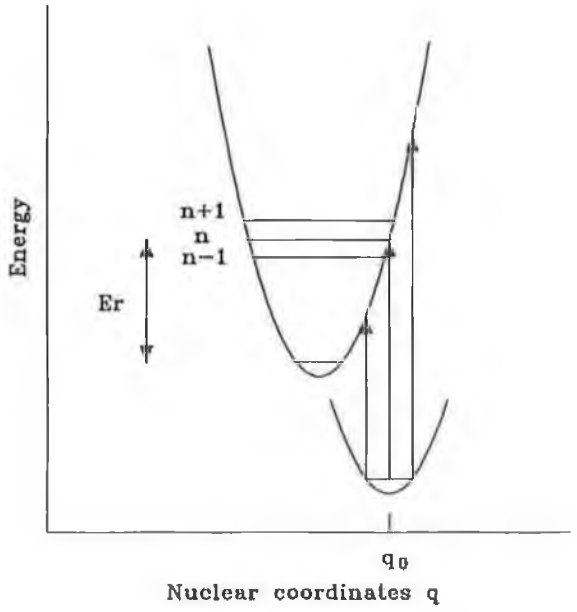

Figure 2.8 The Franck-Condon diagram representing the ground state and the hole state in the photoemission process. This shows the origin of phonon broadening in the core level spectra.

In the solid state further core level broadening may be observed [12]. Phonon broadening in polar compounds increases the width of the core level by an amount which depends on the deviation from the equilibrium position of the atom in the crystal due to lattice vibrations. If an As 3d photoelectron is produced, the charge of the As atom is reduced by one and the surrounding Ga atoms are no longer in their equilibrium positions with respect to the As ion. A lattice transition must therefore take place after the photoemission process and the number of phonons produced effects the width of the photoemission feature. The transition is visualised in figure 2.8. The Franck-Condon principle states that electronic transitions are represented by a line of constant nuclear position so that the energy of the excited state depends on the position of the atom when photoemission takes place. It can therefore be seen that small variations in the atomic positions lead to large fluctuations in the energy of the excited state. Lattice relaxation is achieved by phonon emission. The broadening of the spectral feature depends on E_R, the vibrational relaxation energy.

In semiconductors where band bending occurs, the Fermi level may be pinned in the middle of the band gap (section 2.2.1 above). As the amount of band bending is influenced by the density of surface states, defects in the surface crystal structure will cause the amount of band bending to vary over the surface. This means that the Fermi level, which is the energy reference point, is inhomogeneously pinned and this contributes a further Gaussian broadening to the core level spectra.

2.3.4 Chemical Shifts in Core levels [12]

In core level spectroscopy, the binding energy of a particular atomic state depends on chemical environment. For example, the binding energy of the As 3d core level differs by ~1eV between amorphous As and GaAs. This is shown in figure 2.9. The binding energy difference between the two situations is called a chemical shift.

This energy shift ΔE_i between the two bonding configurations is given by

$$\Delta E_i = K_C(q_i^1 - q_i^2) + (V_i^1 - V_i^2) + (E_R^1 - E_R^2) \qquad (2.11)$$

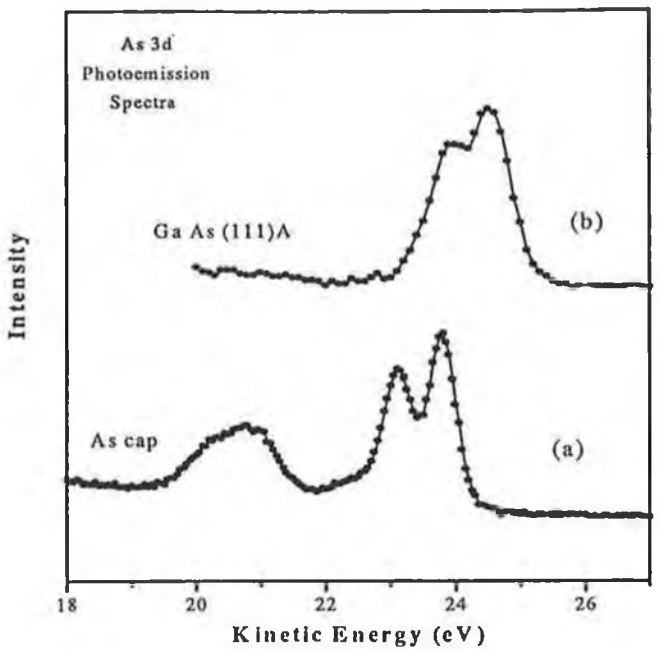

Figure 2.9 As 3d core level spectra for bulk As (a) and GaAs (b). The kinetic energy of the photoelectrons are related to their binding energy by equation 2.7

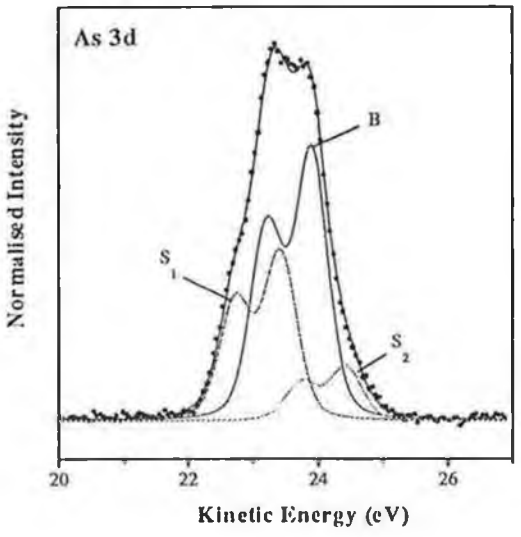

Figure 2.10 As 3d core level spectrum fitted with three components showing the surface shifted components.

where q_i is the charge on atom i. E_R is the relaxation energy which is due to the movement of negative charge toward the hole left by the photoemission proces. K_c is a coupling constant between the core and valence electrons so that $K_c q_i$ is equivalent to a classical screening potential

$$K_c q_i = \frac{q_i}{4\pi\varepsilon_0 r_{av}} \tag{2.12}$$

where r_{av} is the average radius of the valence shell of the i^{th} atom.

The term V_i in (2.11) has the form of a madelung potential and is due to the 'point charges' of the surrounding j atoms in the crystal,

$$V_i = \sum_{j \neq i} \frac{1}{4\pi\varepsilon\varepsilon_0} \frac{q_j}{r_{ij}} \tag{2.13}$$

This description is taken from Cardona and Ley [11]. An alternative method is to describe the chemical shift purely in terms of the charge transfer of the chemical bond [6]. This latter method relies on accurate knowledge of the length of the chemical bond so it works well for chemical shifts in bulk photoemission.

In general, the binding energy of a core level increases or decreases depending on whether charge is transferred from or to the atom in a chemical bond. In the GaAs chemical bond, charge is transferred to the As atom so the binding energy of the 3d core level is less than that for bulk As (see figure 2.9).

2.3.5 Final State Effects [14]

Relaxation effects can have a signifigant impact on the measured binding energy E_B of a photoelectron. Electron rearrangements that occur during photoemission result in the lowering of the value of E_B. Contributions to the relaxation energy arise from both the atom containing the core hole (intra-atomic relaxation) and its surrounding atoms (extra-atomic relaxation). Most of the atomic relaxation component (E_A) is due to the rearrangement of outer shell electrons, which have a smaller E_B then the photoelectron.

The inner shell electrons whose E_B is larger than the emitted photoelectron, have a smaller contribution to the atomic relaxation energy and are neglected. The form of extra-atomic relaxation (E_R) depends on the material being examined. In metals and highly doped semiconductors for instance, valence band electrons can move from one atom to the next to screen the core hole.

2.3.6 Surface Core Level Shifts

Surface atoms generally have a lower coordination than equivalent atoms in the bulk. This results in a surface core level shift where the surface atoms contribute a component to the spectrum which is shifted in binding energy relative to the bulk component. Shown in figure 2.10 is an As 3d core level spectrum with surface shifted components. Each component is due to a different chemical environment for the As atoms, one for the As in bulk GaAs and the other two are surface core level shifts. This core level has been fitted by a method described in chapter III.

It is convenient to visualise the surface shift as being due to a charge transfer to or from the surface atom. Such a charge transfer will shift the core level to higher binding energy relative to the bulk position if the charge transfer is from the surface atom. This is the basis for identifying chemical bonds specific to the surface of the material.

There is a problem with calculating the charge transfer involved in a surface chemical bond. Even though the surface chemical shift is easily found from the core level spectra, the calculation of the amount of charge transfer relies on accurate knowledge of the length of the relevant surface chemical bond. Surface bond lengths may be found from methods such as I-V LEED or the X-ray standing wave technique [13]. Without accurate knowledge of these bond lengths, the charge transfer involved cannot be calculated.

2.4 Modes of thin film growth

Photoemission spectroscopy may be used to characterise different modes of film growth. Types of growth include [15, 16]:

1. Layer-by-layer (Frank-van der Merwe growth), where the adsorbate grows on the substrate one full monolayer at a time.

2. Layer plus islanding (Stranski-Krastanov growth). Here one full monolayer is adsorbed on the surface after which islanding takes place.

3. Complete islanding (Volmer-Weber growth), in which the deposited material immediately forms islands on the surface.

Photoemission spectroscopy may be used to determine the growth mode of an adsorbate. As photoelectrons are emitted from substrate or adsorbate atoms they have to penetrate a certain amount of material before they leave the crystal. Core level spectra of the adsorbate or substrate adatoms can then be recorded as the material is deposited. The change in line intensity as a function of deposited thickness is indicative of different growth modes. In the simplest case of layer-by-layer growth, the change in the photoemission line intensity is linear for the first monolayer deposited after which there is a change in slope followed by another linear change in intensity and so on for each monolayer deposited (figure 2.11). In the case of island growth the change in line intensity is linear. For layer plus islanding there is one change in slope of the line intensity at a coverage of 1 monolayer.

If the photoemission lineshape (or core level) is fitted as described in section 3.9 then the intensities of the different components within the core level can also be measured as a function of the amount of adsorbate deposited. This process is used in later chapters to study the growth of Sb and Bi overlayers on GaAs{111} surfaces.

The reason why the different growth modes described above occur can be understood in terms of the relative surface energies of the deposit and substrate materials. Surface energy is defined as the excess internal energy of the solid-vacuum system over that of an imaginary system with two homogeneous phases separated by an ideally discontinuous change at a mathematical surface between them [17]. Surface energy differs from bulk energy because of the rebonding and relaxation at the surface. Islanding occurs when the surface energy of the deposit material is high compared to that of the substrate. For monolayers to form on the substrate surface, the deposit must have a lower surface energy than the substrate. After the formation of a monolayer, further growth is either in the form of more layers or islands. It is assumed that the initial monlayer is strained because of the

difference in the substrate and deposit lattice spacings and the type of growth which ensues depends on the relative sizes of the deposit strain energy and the deposit surface energy. If the strain energy is low compared to its surface energy then continued layer growth is expected. If, however, the deposit strain energy is high, growth of a second layer may be impossible due to strain related defects and so further growth is in the form of islands.

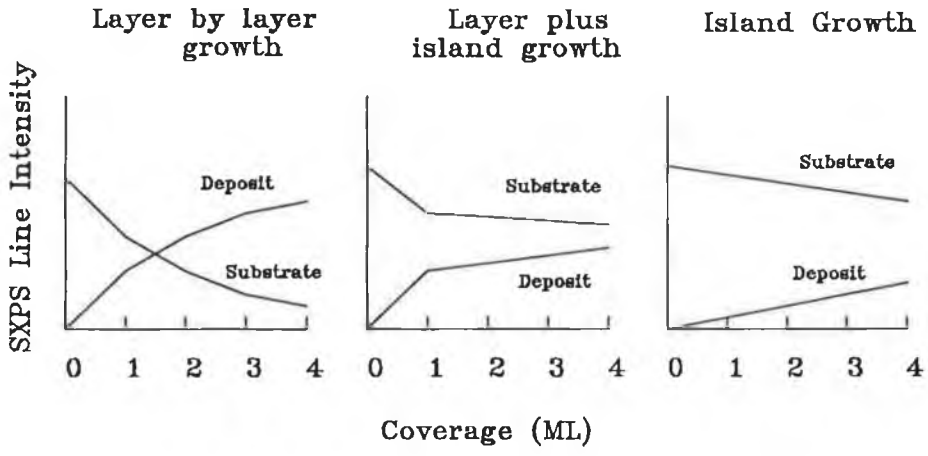

Figure 2.11 The change in the intensities of the photoemission lineshapes of the deposit and the substrate as a function of the amount deposited.

References for chapter II

1. W. A. Harrison, *Electronic Structure, The physics of the chemical bond*

2. M.A. Van Hove, W.H. Weinberg and C. M. Chan, *Low Energy Electron Diffraction* (Springer Verlag 1985)

3. S.Y. Tong, G. Xu and W.N. Mei, Phys. Rev Lett. **52**, 1693 (1984)

4. D.K.Biegelsen, R.D. Bringans, J.E. Northrup and L.E. Swartz, Phys. Rev Lett. **65**, 452 (1990)

5. D. G. Castner and G.A. Somorjai, Chemical Reviews, **79** 235 (1979)

6. W. Monch, *Semiconductor Surfaces and Interfaces,* (Springer 1995)

7. S. G. Davison and Maria Steslicka, *The Basic Theory of Surface States* (Clarendon Press, 1992)

8. E. H. Rhoderick and R. H. Williams, *Metal-Semiconductor Contacts* (O.U.P., 1986)

9. W.E. Spicer et al, J. Vac. Sci. Technol., **17** 1019 (1980)

10. V. Heine Phys. Rev. A, **138** 168 (1965)

11. M. P. Seah and W.A. Dench, Surf. Interface and Anal., **1** 2 (1979)

12. L.Ley and M.Cardona, *Photoemission in Solids Vol.I* , (Springer-Verlag, Berlin, 1979)

13. D. P. Woodruff and T. A. Delchar, *Modern Techniques of Surface Science* (Cambridge University Press, 1994)

14. J.C. Vickerman, *Surface Analysis - The Principal Techniques*, Wiley, 1997

15. H. Luth Surfaces and Interfaces of Solids (Springer-Verlag, 1993)

16. L. C. Feldman and J. W. Mayer *Fundamentals of Surface and Thin Film Analysis* (North-Holland, 1986)

17. M. Prutton, *Surface Physics*, Oxford University Press, 1983

Chapter III

Experimental Procedures

3.1 Synchrotron Radiation [1]

A synchrotron is a most useful radiation source for performing a wide range of spectroscopy experiments. The distinguishing characteristics of synchrotron radiation are a continuous spectrum from the infra red to the hard X-ray (figure 3.1), linear polarization and high intensity relative to conventional discharge tube radiation.

In a synchrotron electrons are accelerated along a circuital path by the application of transverse magnetic fields in 'bending magnets'. When relativistic velocities are achieved, the centripetal acceleration of the charged particle causes the emission of dipole radiation which forms a highly collimated beam tangential to the electron path. This radiation contains harmonics of the electron orbital frequency which cannot be resolved and is polarised in the plane of the electron orbit. The synchrotron 'ring' comprises bending magnets and straight sections which contain focussing magnets and an RF cavity which replaces the energy lost radiatively by the electrons.

Synchrotron Radiation gets its name from the fact that the beam energy and magnetic field are increased synchronously so as to keep the electrons in a constant orbit. A more useful adaptation of the synchrotron is the storage ring where the electron beam is kept stable for several hours so that experiments can be performed without interruption. The beam gradually decays due to collisions between electrons or between the electrons and the walls of the ring. The beam is replaced with a new beam at regular intervals. To establish the beam initially, electrons are linearly accelerated into a small synchrotron, accelerated further, and from there they are injected in bunches into the main ring. For experimental work there a number of beamlines around the storage ring which, by a combination of mirrors and monochromators direct the radiation into ultra high vacuum (UHV) chambers containing the experimental instrumentation.

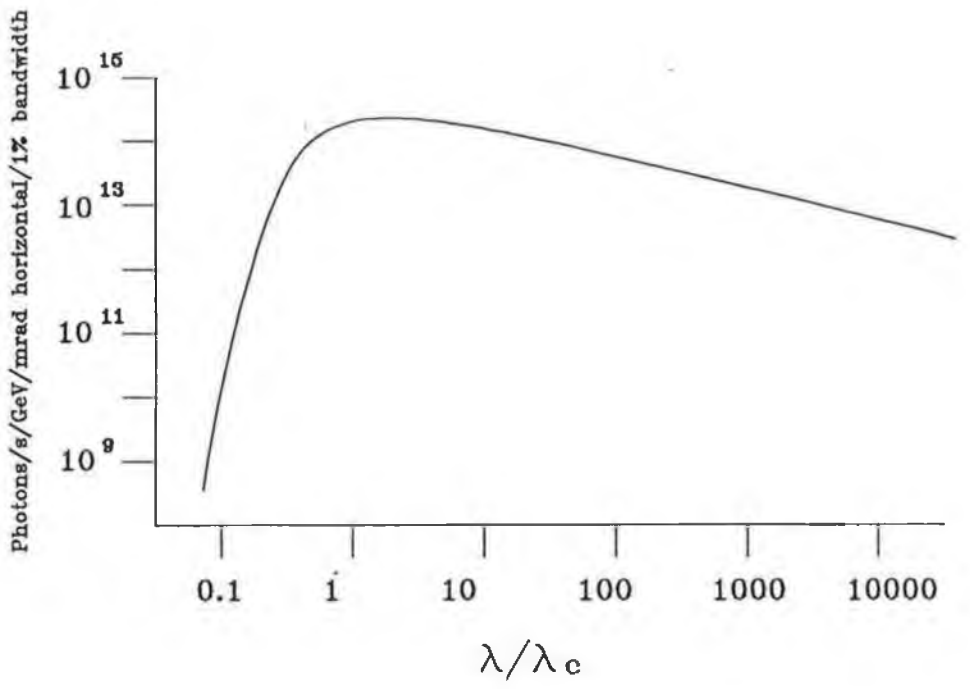

Figure 3.1 Spectral distribution of the radiation emitted by a storage ring. λ_c is a critical wavelength characteristic of a particular storage ring where $\lambda_c = 19/B(T)E(GeV)^2$. E and B being the particle energy and magnetic field of the dipole magnet respectively.[1] For the Daresbury SRS, E = 2GeV and B = 1.2 T. $\lambda_c = 4.0$Å.

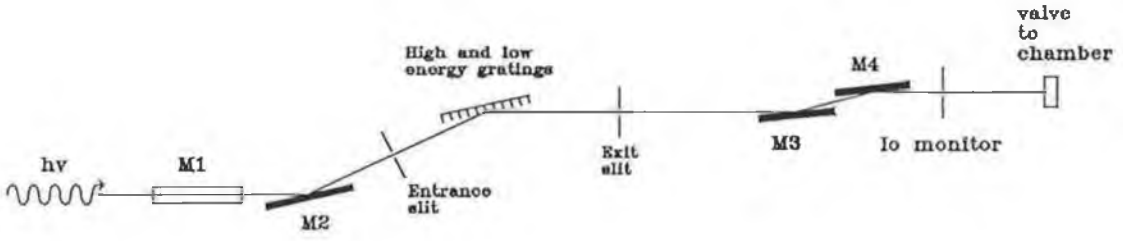

Figure 3.2 Schematic drawing of beamline 6.2.

3.2 The toroidal grating monochromator and beamline 6.2

A toroidal grating monochromator with two gratings were available on beamline 6.2 at the Daresbury Synchrotron Radiation Source: the first, a low energy grating, with 700 lines/mm and a second, the high energy grating, with 1800 lines/mm. The transmission characteristics of the gratings were such that the low energy grating (15-50 eV) is most useful for work on the low lying electronic levels in the valence band while the high energy grating (40-100eV) provides photons with an energy suitable for recording core level spectra. Table 3.1 below shows the minimum photon energy required to probe the core levels relevant in this work. In practice a photoelectron spectra of core levels contains a secondary electron tail above which we would like to observe the core level features. In this case a photon energy of at least 70eV is preferable for the atomic levels listed in table 3.1.

Table 3.1

Core level	Binding Energy (eV)	Electron kinetic energy ($h\nu$ = 70eV)
Ga $3d_{3/2}$	18.7	46.0
As $3d_{3/2}$	41.7	23.9
Sb $4d_{3/2}$	33.44	32.0
Bi $5d_{3/2}$	26.9	38.7

Table 3.1 The binding energies of the core levels studied in this work, taken from Cardona and Ley [2]. The kinetic energy of the photoelectrons produced are from experimental data for Sb and Bi on the GaAs(111)A surface.

A schematic of beamline 6.2 is shown in figure 3.2. As well as the monochromator and the four mirrors used to direct the beam of radiation to the chamber, the other significant feature is an incident light intensity (I_0) monitor. This monitor continually records the intensity of the light so that photoemission spectra can be normalised as the data is being recorded.

3.3 The experimental chamber

The experimental chamber on beamline 6.2 is designed for surface sensitive photoemission experiments. The system enables ultra high vacuum (UHV) to be achieved in about 24 to 36 hours and maintained for a two week experimental run. A base pressure of 10^{-10} mbar could be achieved with one turbo pump, 2 titanium sublimation pumps and liquid nitrogen traps. Standard equipment on the chamber included a sample manipulator with electron beam heating facility, LEED optics and a VG ADES 400 electron spectrometer. A sample transfer system and Sb and Bi evaporation sources were added for this work. A plan view of the chamber is shown in Figure 3.3.

3.3.1 The sample transfer mechanism

The sample transfer system (figure 3.4) allows As capped GaAs samples to be placed into the UHV chamber from the lab without losing main chamber vacuum. A valve, as shown in figure 3.4, which can withstand the pressure differential between UHV and atmospheric pressure was attached to the chamber. To this valve a four way cross piece with a hinged window port and a magnetically driven linear transfer mechanism (LTM) were fitted. This transfer system could be pumped down to ~5×10^{-7} mbar independently of the chamber with a separate turbo pump.

To transfer a sample into the chamber the valve was closed and the LTM let up to atmospheric pressure with nitrogen flowing through the system. A sample was inserted into a holder on the linear drive and then the whole mechanism pumped down to high vacuum. The sample was then transferred to the manipulator, by sliding the magnet along the LTM, without any irreversible effect on the base pressure of the chamber.

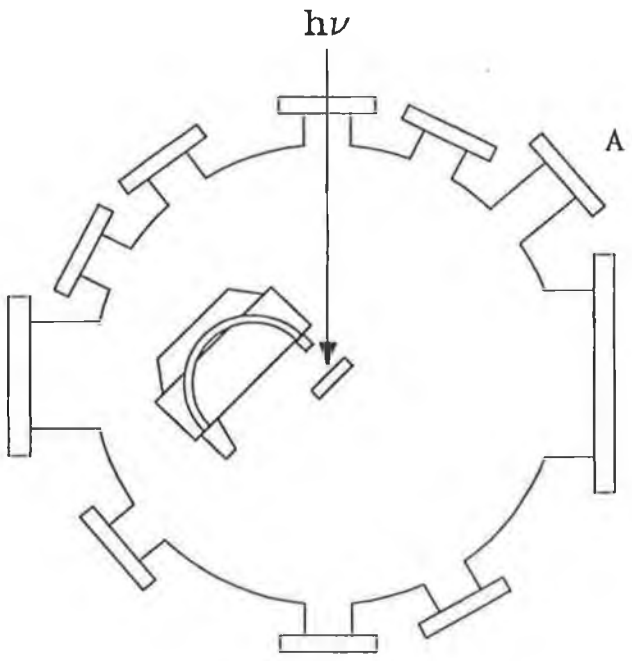

Figure 3.3. Plan view of the UHV chamber on beamline 6.2. The system was assembled to allow XPS, LEED and overlayer depositions to be performed without moving the sample from the holder.

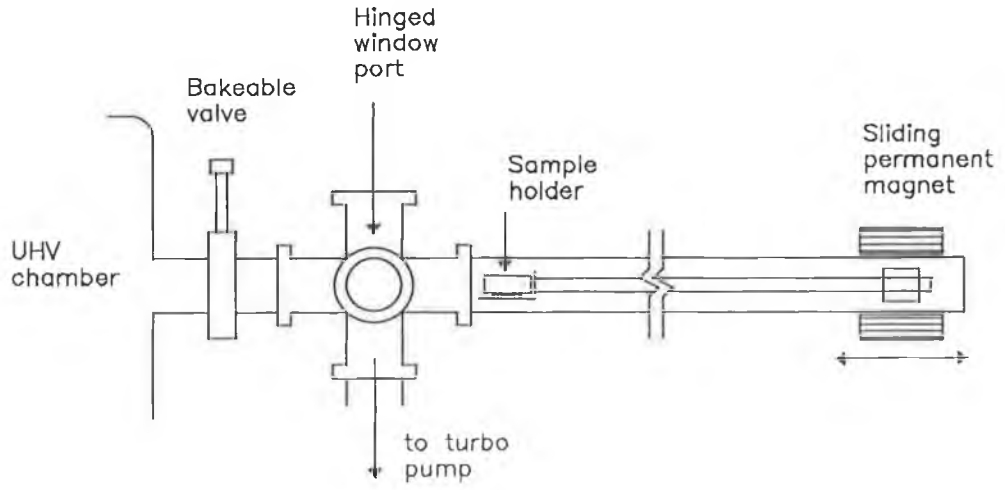

Figure 3.4 The Linear transfer mechanism. This allows quick transfer of samples into the chamber which would other wise be destroyed during the 'bake out' of the system.

3.3.2 Sample heating system and evaporation sources

Samples could be heated by two methods, radiative and electron beam. Radiative heating was by two tungsten filaments attached to the manipulator behind the sample holder. The filaments were connected to a regulated power supply which delivered a current of up to 5 Amps. This method achieved a maximum sample temperature of ~ 400°C. For further heating a potential of up to 400 Volts was applied to a plate attached to the back of the sample holder which caused electrons emitted from the tungsten filaments to be accelerated toward the sample holder. The impact of the electrons heated the sample further, up to a maximum temperature of approximately 800°C. Temperature was measured by a chromel alumel thermocouple.

The Sb and Bi evaporation sources were constructed as follows: pellets of Sb (or Bi) were placed in tantalum foil cylinders which were sealed at each end. Tungsten wire was wound around the foil packets to act as a heating element. These were inserted into four way cross piece attachments on the chamber. With a current of ~9 amps flowing in the tungsten element, the material in the foil evaporated through the two sets of punched holes, one set directed toward the sample in the centre of the chamber and the other set toward a quartz crystal oscillator (QCO). This oscillator was connected to a calibrated frequency monitor which calculated the thickness deposited. The difference in distance between the source and the QCO and the source and the sample resulted in a QCO to sample deposition ratio of 50:1 for Bi and 70:1 for Sb. These ratio differences are most likely due to differences in the construction of the sources and were determined by calibration on a separate but identical chamber which had a QCO placed at the sample position in the centre of the chamber.

3.3.3 The ADES 400 electron spectrometer

A concentric hemispherical analyser (the ADES 400) was used to record the photoelectron spectra. An electric field between the two concentric hemispherical surfaces disperses the electrons entering the spectrometer and only those electrons within a given energy range will complete the circular path and be detected by a channeltron (figure 3.5).

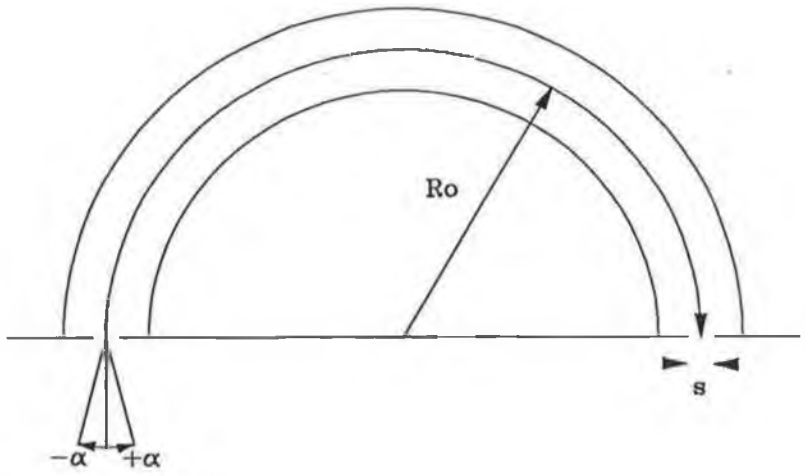

Figure 3.5 The Concentric Hemispherical Spectrometer (CHA), after reference [3]. Parameters are as described above.

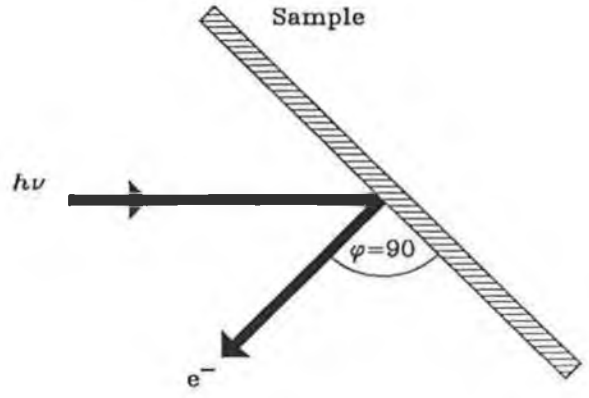

Figure 3.6 Experimental geometry showing the directions of the incident light and the outgoing photoelectrons.

The resolving power of the analyser is given by,

$$\frac{\Delta E}{E} = \frac{s}{2R_o} + \alpha^2 \qquad (3.1)$$

where s is the width of the entrance and exit slits (1mm), R_O is the mean radius of the cylinder (50mm) and α is the acceptance angle (4°). In these experiments E, the electron pass energy was chosen to give a resolution approximately equal to the photon resolution. For a pass energy of 10eV, the resolution ΔE of the spectrometer is 0.15eV.

The analyser was operated in a constant pass energy mode. In this mode the electrons were decelerated by grids at the entrance slits so that the electrons detected have a constant energy and the resolution is constant throughout the spectrum.

The spectrometer could be rotated by 300° in the plane of the synchrotron and by 90° in the plane perpendicular to this. Given that photoelectrons are emitted from a sample in all directions, this spectrometer can be used to record electron spectra at different polar and azimuthal angles to the surface. By positioning the analyser at a grazing incidence angle to the surface the detected electrons are more likely to originate from surface atoms and so the surface sensitivity is increases. The highest count rate is achieved for 'normal emission' geometry which is illustrated in figure 3.6.

3.3.4. Low Energy Electron Diffraction [3]

Low energy electron diffraction (LEED) is used to find the two-dimensional symmetry of the surface. The technique relies on the fact that at low energies (20-300 eV) electrons have a penetration depth of about 10Å in crystals. This short penetration depth is due to the fact that electrons in this energy range have a high scattering cross section with the core electrons of the solid. The scattered electrons constructively interfere to form a diffraction pattern.

If diffraction from the top layer of atoms in a surface is considered, then the surface atomic periodicity does not extend in the direction normal to the surface. This is equivalent to a three dimensional lattice with infinite separation between lattice points in the direction of the surface normal. Transforming this situation into reciprocal space gives

an infinitely dense column of reciprocal lattice points or rods normal to the atomic plane. These rods are labelled by the Miller indices h and k, and a general reciprocal lattice vector G_{hk} lies in the plane of the surface and is given by,

$$G_{hk} = hs_1^* + ks_2^* \tag{3.2}$$

Figure 3.7 shows the Ewald sphere construction which is the standard method for considering diffraction. The tip of the incident wavevector k_o is placed at the origin of the reciprocal lattice and a sphere of radius k_o is drawn. Diffraction occurs everywhere the Ewald sphere cuts a reciprocal lattice rod and the diffracted beams k′ can be labelled with the Miller indices of the rod causing it. In three dimensions, the condition for diffraction from a periodic lattice is

$$\mathbf{k}' = \mathbf{k}_o + \mathbf{G}_{hkl} \qquad \text{and} \qquad |\mathbf{k}'| = |\mathbf{k}_o| \tag{3.3}$$

These conditions are relaxed by the loss of periodicity in one dimension to

$$\mathbf{k}'_{//} = \mathbf{k}_{o//} + \mathbf{G}_{hk} \qquad \text{and} \qquad |\mathbf{k}'| = |\mathbf{k}_o| \tag{3.4}$$

where the subscript // refers to the component of the vector parallel to the surface.

The apparatus used was a Vacuum Generators rear view LEED system, a schematic of which is shown in figure 3.8. The LEED optics consists of an electron gun which delivers a beam of low energy electrons to the sample. Electrons scattered from the sample travel in straight lines to the spherical grids as the first of these is held at the same (ground) potential as the sample. The next two grids eliminate inelastically scattered electrons by being held at a potential close to that of the primary source. Elastically scattered, diffracted, electrons are then accelerated toward a fluorescent screen where they produce a fluorescent image of the diffraction pattern which was viewed from behind the electron gun.

3.3.4.1 Kinematic and Dynamical LEED theories

A useful technique in surface analysis is to generate LEED patterns by computational modelling of the diffraction process. Theories which describe the interaction of the

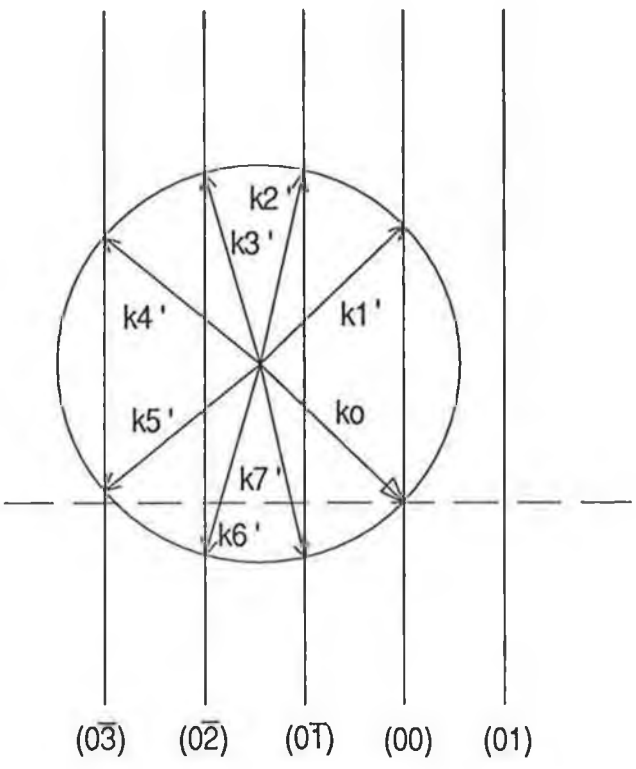

Figure 3.7 Ewald sphere construction applied to a square net of atoms of side a. The spacing between the reciprocal lattice rods is $2\pi/a$. The diagram shows the beams scattered in the (0k) plane only but more beams will be scattered in directions out of the plane of the page.

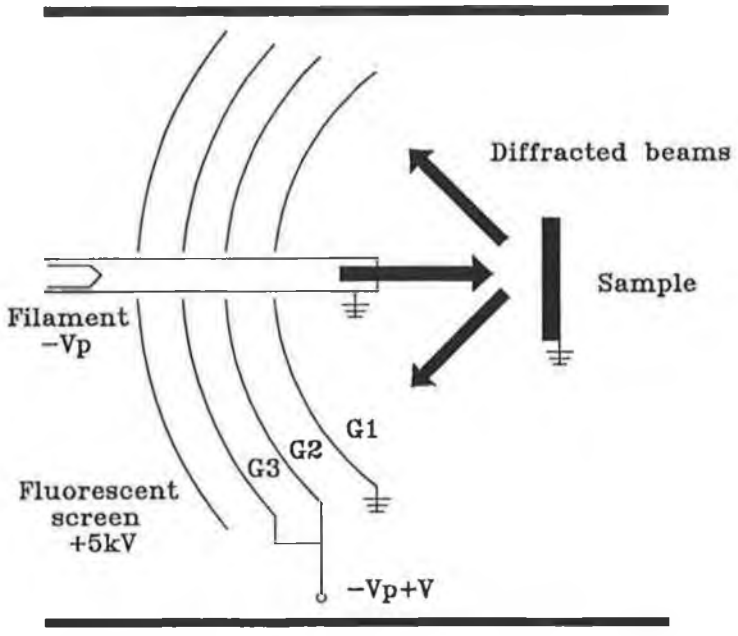

Figure 3.8 LEED optics for viewing diffraction patterns. The pattern was viewed on the screen from behind the electron gun. This gives a better view of the pattern than that from behind the sample as the sample holder is quite bulky.

incident electrons with the surface are grouped into two types: the kinematic and dynamical theories of LEED. The kinematic theory which is simpler and more limited was developed first. Kinematical theory can account for the positions of the various spots in the diffraction pattern but not their relative intensities. This theory assumes that the electrons interact only weakly with the surface atoms, all collisions are elastic and multiple scattering is ignored. For surface analysis, the theory can be used to verify approximate structural models. Dynamical LEED theory accounts for multiple scattering between surface atoms and includes a large number of phase shifts in the scattering process to simulate the interaction between the incident electron and the many different electrons of different momentum within the atom cores. This theory allows accurate calculation of beam intensities and so experimental beam intensity versus incident electron energy curves can be fitted to establish the surface structure in fine detail.

If scattering of an electron at an isolated atom is considered and then extended across an array of atoms then the total scattered wave which results from the superposition of the waves originating from the single atoms can be written as

$$\phi \propto \sum_j f_j(k_0,k')\left(e^{i(k'-k_0)R_j}\right) \tag{3.5}$$

k_0 incident electron wave vector
k' scattered electron wave vector
f_j atomic scattering factor
R_j position of the j^{th} atom

By replacing the atomic scattering factor with the structure factor F for the crystallographic unit cell, equation (3.5) becomes

$$\phi \propto F \sum_{n_1=1}^{M_1} e^{in_1a_1.(k'-k_0)} \sum_{n_2=1}^{M_2} e^{in_2a_2.(k'-k_0)} \tag{3.6}$$

M_1, M_2 Number of lattice points
a_1, a_2 Unit cell vectors where $R_i = n_1a_1 + n_2a_2$

Equation (3.6) can be simply written as

$$\phi \propto F.G \tag{3.7}$$

where G is called the lattice factor.

The measurable quantity is not the amplitude but the intensity I of a diffracted beam which is defined as the ratio of electron current in the diffracted beam i to that in the primary beam i_O. The intensity is given by the square of the amplitude

$$I \propto |F|^2.|G|^2 \tag{3.8}$$

The difference between the kinematic and dynamical theory is contained in the structure factor F. For single scattering, F is composed from a superposition of the atomic scattering factors multiplied by the corresponding phase shifts due to the individual atoms within the unit cell. In the dynamical theory however, the effects of multiple scattering and inelastic interactions are included in the calculation of the scattered wave. F depends on both k' and k_0 separately, whereas in the kinematic theory, the structure factor is only a function of the difference $(k'-k_0)$.

3.3.4.2 Modelling the LEED patterns

A previously developed LEED simulation program was used to qualitatively verify the structures proposed for the GaAs {111} surfaces with Sb or Bi overlayers. The simulation code was developed by Panagiotides et. al. [4]. This program simulated LEED patterns from a scattered electron wavefield composed of both single and double scattering contributions. There are two sets of input parameters in the program : structural parameters, which concern the surface crystallography and non-structural parameters which relate to the electron beam, scattering phase shifts and scattering amplitudes. For periodic structures such as those investigated here, the basis of the surface in cartesian coordinates and the primary translation vectors only are required to generate the surface structure within a user defined area (typically 100 Å each side). The program performs all the calculations for individual scatter pair contributions to the outgoing electron wavefield, using a muffin tin potential for the atomic core and using s-wave phase shifts only. This

latter simplification takes no account of the directionality of the covalent bonding in semiconductors. It is therefore appropriate for LEED simulation of metal surfaces. The program was however expected to produce good qualitative results for the structural models proposed.

3.4 MBE grown As capped GaAs substrates

For surface studies, apart from those on the natural cleavage plane of the crystal, samples prepared by molecular beam epitaxy (MBE) are ideal. All the samples used for this work were prepared at the University of Wales, College Cardiff and the technical considerations of the growth process have been comprehensively described [5].

In MBE growth, a substrate of the (111) orientation is cut and cleaned in ultra high vacuum by sequences of ion bomberding and annealing. A (2×2) RHEED pattern indicates high quality growth and there is a range of temperature and As flux values under which this is achieved. Samples are typically grown at a temperature of 500-550°C for the (111)B surface and 550-650°C for the (111)A [5]. These samples were doped with Zn (p-type : p = $10^{19}cm^{-3}$) and Si (n-type : n=$10^{18}cm^{-3}$) for the (111)A and (111)B respectively.

To allow samples to be stored and transferred to another experimental chamber they are covered with a protective layer (several microns thick) of amorphous As. This is achieved by switching off the Ga flux after growth of the GaAs epilayer and cooling the sample to about -50°C. Arsenic then condenses on the surface and this 'cap' protects the surface from oxidation or other contamination while the sample is moved to another experimental site.

3.4.1 Sample preparation - removal of the As cap

De-capping the MBE grown samples was the first procedure in the experiments described here. By heating the sample to ~350°C As was seen to desorb. Desorption was monitored on the mass spectrometer by the intensity of a peak due to As_2. When the intensity of this peak began to drop, the sample was allowed to cool to room temperature and then re-annealed to 380°C.

Successful removal of the As cap was judged by core level photoemission. This is illustrated in figure 3.9. The As 3d core level spectrum for the As cap contains two features, a broad peak due to surface As_2O_3 and a component with clearly resolved spin orbit splitting due to the amorphous As. After cap removal, characteristic As 3d core level spectra for the (111)A and (111)B surfaces were observed. A clear (2×2) LEED pattern was observed for both surfaces and the final test for a suitable clean surface was to compare the valence band spectra at normal emission with previous work [6].

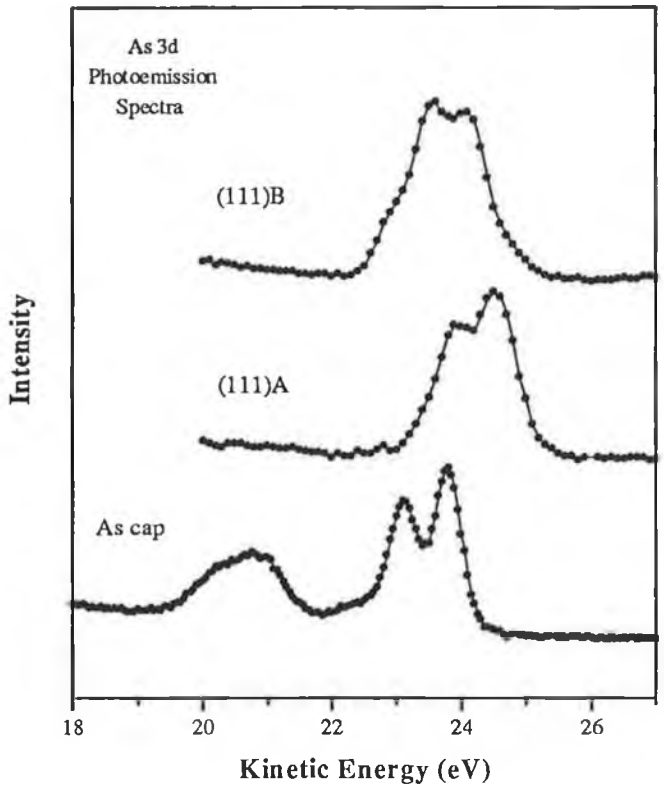

Figure 3.9 Photoemission spectra of the As 3d region. The spectrum of the As cap has a well resolved doublet due to the amorphous arsenic and a much broader peak at lower kinetic energy which is due to the arsenic oxides on the surface of the cap. After de-capping, the differences in the chemical bonding of the Arsenic on the (111)A and (111)B surfaces is already apparent in the different shape of the two spectra.

3.5 Fermi level determination

A good electrical contact between the GaAs sample and the Mo spade is ensured by the use of In solder. In this situation the Fermi level (E_f) of the sample and the metal spade are at the same energy so that E_f for the semiconductor can be found using photoemission from the molybdenum. This can be compared with the energy of the valence band maximum (VBM) to determine the amount of band bending at the semiconductor surface.

A Fermi level scan is shown in figure 3.10. This was fitted in a simple way to the equation for a Fermi function:

$$I = I_{max}\left(\frac{1}{1+e^{(E-E_f)/akT}}\right) + I_{back} \qquad (3.9)$$

This expression could be convoluted with a Gaussian function to represent the experimental resolution but a good answer for E_f is achieved by introducing the variable a into the fitting equation. This has the effect of thermal broadening to a non-physical temperature but the value obtained for E_f from fitting the spectrum is reliable. The other variables in equation 3.9 are shown graphically in figure 3.10.

Determination of the Fermi level has two purposes. First is to ensure that the photon energy is exact and has not drifted due to heating of the spectrometer grating. Secondly, E_f is needed to measure the band bending at the surface. Recording a valence band spectra and finding the valence band maximum by extrapolation (figure 3.11) is useful as E_f–VBM gives the size of the surface band bending.

3.6 Core level fitting - Deconvolution of parameters

A core level spectrum usually contains one component for each chemically inequivalent state. Each component is a convolution of the experimental broadening with the intrinsic lineshape of the core level, known as a Voigt function. As the binding energy difference of the different components is about the same size as the width of the various Voigt functions, the components usually appear as a single broad peak. To determine the contribution of each component to the spectrum a numerical fitting routine must be used

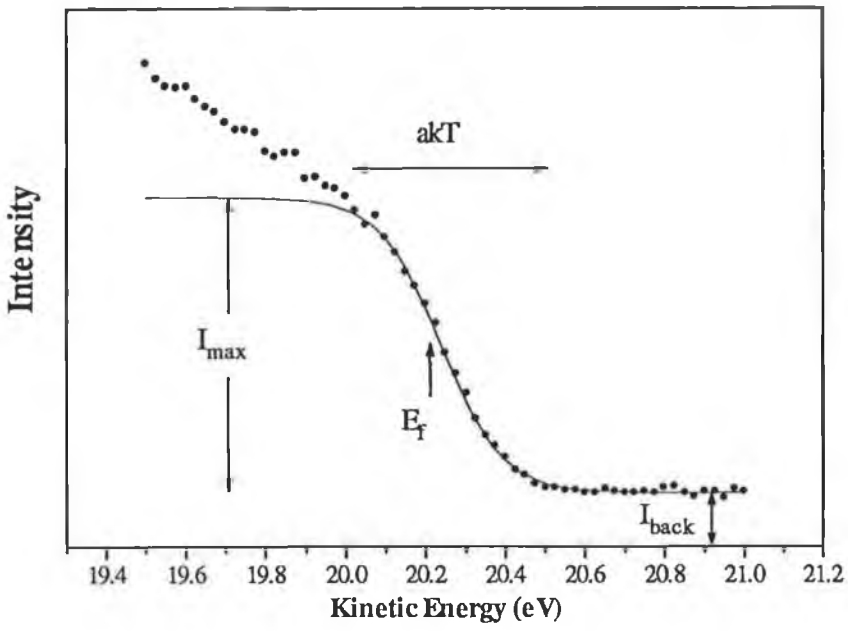

Figure 3.10 Photoemission spectrum of a Fermi edge fitted to a Fermi function as described below.

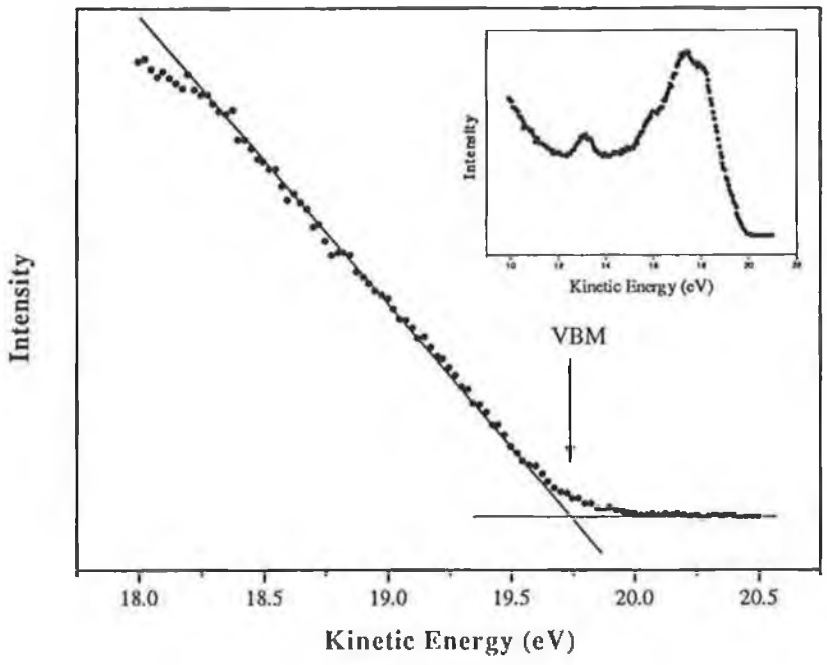

Figure 3.11 A photoemission spectra of the valence maximum with the full scan of the valence band shown in the inset. The valence band maximum (VBM) is taken to be the intersection point of the linear extrapolation of the band edge and the background signal

to separate the components and evaluate such parameters as the Lorentzian and the Gaussian widths. The program used for numerical fitting was 'TCFIT' which allowed for up to four spin-orbit split peaks. Other variables were peak intensity, peak position, Lorentzian and Gaussian widths and a polynomial background. The program then minimised the difference between the experimental and modelled spectra using a Simplex routine [7].

References for Chapter III

1. G. Margaritondo, *Introduction to Synchrotron Radiation,* (O.U.P, Oxford, 1988)

2. L.Ley and M.Cardona, *Photoemission in solids Vol. II*, (Springer-Verlag, Berlin, 1979)

3. D.P. Woodruff and T.A. Delchar, *Modern techniques of surface science,* (Cambridge University Press, 1986)

4. N. Panagiotides, D. Batchelor and D. A. King, Chem. Phys. lett., **177** (1991) 419

5. D. A. Woolf, D. I. Westwood and R. H. Williams, Appl. Phys. Lett. **62** (12), 1370 (1993) and Semicond. Sci. Technol. **8**, 1075 (1993).

6. A. D. Katnani and D. J. Chadi, Phys. Rev. **B 31**, 2554 (1985).

7. W. H. Press et al, *Numerical Recipes, the Art of Scientific Computing,* (Cambridge University Press, 1986).

Chapter IV

Low index GaAs surfaces and Group V overlayers

4.1 The electron counting model

Surface reconstruction involves the rebonding of atoms in the top few layers of the crystal so as to lower the energy and symmetry of the surface. A successful description of the rearrangement of valence electrons resulting from the reconstruction of III-V semiconductors is given by a technique called the electron counting model developed by Pashley [1]. An earlier version of the electron counting model was produced by Farrell et. al. where the emphasis was on explaining the MBE growth of GaAs(100) [2]. These authors described the growth of one GaAs bilayer as a series of stages where one As or Ga dimer is added to an As rich (2×4) surface unit cell at each stage until a new layer is complete. Each step in the process represented a new surface reconstruction each of which was accepted if all the dangling bonds on Ga atoms were empty while those on the As atoms were full. These states are electronically stable and so the associated atoms have a long residence time on the surface at growth temperatures. Species with excited electronic states are expected during growth but were considered to be unstable against diffusion. Therefore the surface reconstructions considered were those that resemble structures seen under static UHV conditions.

In general a reconstruction involves the movement of charge from the electropositive element (Group III) to the electronegative element (Group V). So for a GaAs surface, the Ga atom has three electrons distributed among four tetrahedral bonds or 3/4 electrons per sp^3 orbital. With the As atom containing 5/4 electrons per bond, a transfer of the charge from one Ga atom to one As atom fulfils the above criteria and the viability of a surface reconstruction model can be checked using this simple condition. With no filled electronic states above the valence band, the surface is semiconducting which is a useful way to summarise the purpose of the model : those reconstructions are possible which produce a semiconducting surface. Another way to consider the surface structure of polar semiconductors is in terms of surface charge, as described by Harrison [3]. In this

description of III-V surface reconstruction, all As dangling bonds are full and Ga dangling bonds are empty. Structural models give rise to a charge redistribution at the surface and are rejected if a potential gradient or surface dipole is created in the crystal, as this raises the total energy of the system. Only those reconstructions which reduce the surface charge to zero are considered acceptable. The requirement of zero net surface charge is exactly equivalent to the electron counting rule so that reconstructed surfaces which obey the electron counting principle are both semiconducting and possess no net surface charge.

A convenient use of the electron counting model is to propose surface structural models using STM data where the general form of the reconstruction is quickly established and the same can also be done when the periodicity of the surface has been given by LEED. In the latter case, it is useful to use the known structure of similar surfaces or other reconstructions on the same surface to suggest the bonding configuration within the surface unit cell. Also useful for bonding determination is photoemission spectroscopy as surface core level shifted components in a spectra are associated with some specific chemical environment for the atom type which can be deduced from studies of other surfaces [4, 5, 6]. With information on the surface bonding established and knowledge of the surface periodicity from diffraction, structural models can be proposed.

4.2 The GaAs {111} clean surfaces

After the decapping process is performed on both GaAs (111)A and (111)B surfaces, a (2×2) LEED pattern is observed. This LEED result had been established as early as 1961 by Haneman for the (111)A surface [7] and by MacRae in 1966 for the (111)B orientation [8]. Correct structural models for these systems were eventually described in the 1980's with the advent of techniques such as IV-LEED and STM and these models serve as good examples of the use of the electron counting principle.

4.2.1 The GaAs (111)A surface

Haneman's original model for the (2×2) (111)A surface consisted of a Ga terminated surface where ¼ of the Ga atoms were raised upwards from their ideal positions and the remaining Ga atoms receded into the bulk. For this buckled surface the raised Ga atoms

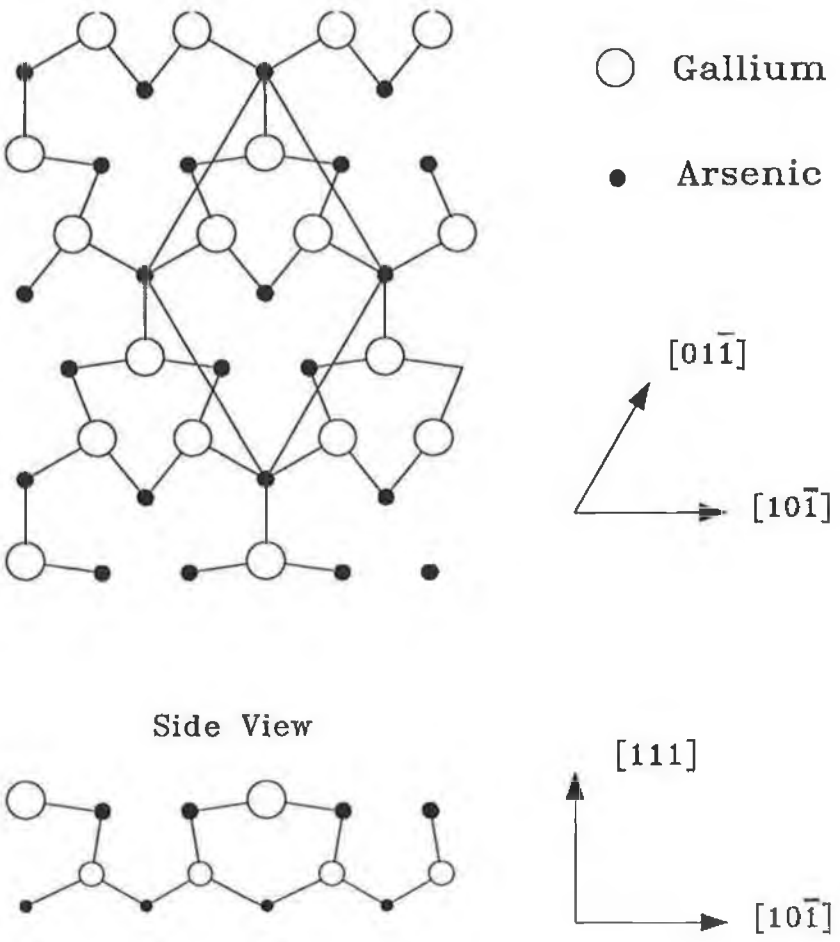

Figure 4.1 The vacancy buckling model for the GaAs(111)A - (2×2) surface, after Tong et. al. [9]. This reconstruction converts the surface from polar to non-polar [13] and the dimensions for this model as found by IV - LEED and total energy calculations are given in references 9 and 13 respectively.

then created the necessary (2×2) array. This situation was considered improbable as it requires the surface atoms to have two different hybridisation states [9] but the concept of buckling is relevant to models for the non polar (110) surface described below. In 1984 the structure of the (111)A surface was determined by Tong et. al. using IV-LEED [9]. Their model is called the vacancy buckling model where in each (2×2) surface unit cell there is one Ga atom missing and the three As atoms in the layer underneath have one dangling bond each (Figure 4.1). This cation vacancy description was guessed intuitively and was a major success for the complex technique of dynamical LEED calculations. With regard to the electron counting model, there are three Ga atoms and three As atoms per unit cell which undergo bond rehybridisation. Each Ga atom loses ¾ electron to an As atom, leaving the Ga and As with sp^2 and s^2p^3 hybridisation respectively. This is typical of III-V reconstructions and it is noted that the As dangling bond is s-like in character.

Tong's calculations showed that the (2×2) periodicity was not confined to the top bilayer but extended into the bulk until the fifth monolayer. These subsurface distortions are to accommodate the buckling in the top bilayer where the Ga sp^2 bonds have planar geometry and the As s^2p^3 bonds are pyramidal - the As dangling bond is directed towards the Ga vacancy and the three remaining bonds to Ga atoms are mutually perpendicular. Other experimental techniques such as grazing-incidence X-ray diffraction [10, 11] and STM [12] have verified this structure for GaAs (111)A as well as for In Sb (111)A [11]. Extensive theoretical studies supporting the model include the tight binding total energy method [13], *ab initio* pseudopotential methods [14] and the Hartree Fock molecular orbital technique [15].

Another (2×2) reconstruction is also stable on this surface, but its structure was not established experimentally until 1994 [16] despite the interest this surface had generated over the preceding ten years. An early mention of the possibility of a second (2×2) reconstruction was made by Cho and Arthur [17] when they observed a change of intensity in the half-order RHEED spots during MBE growth when the As_2 flux was increased. Thornton et. al. [16] established that for a decapped (111)A surface, the Ga vacancy model is created at 350°C, but if the cap is slowly removed at 315°C the surface contains no Ga vacancies and is stabilised by one As trimer per unit cell. This model had been suggested in the theoretical study of Kaxiras et. al. [14] some years earlier and was estimated to have the lowest energy of a variety of models including the vacancy model. Compared to the ideal unreconstructed (1×1) surface, energy reductions of 5.0eV and 3.3eV per unit cell were calculated for the trimer and vacancy models respectively while

the other models considered resulted in significantly less energy reduction. The least favoured models were not consistent with the electron counting model and so their total energy is expected to be too high to adequately stabilise the surface. Although these calculations favoured the As trimer structure over the then more widely accepted vacancy model, the effect of varying the chemical potential of the constituent atoms through a 2.0eV range simulated the effect of changing the environment of the surface from Ga rich to As rich. With this consideration the Ga vacancy model had the lowest energy over the greatest range of ambient conditions, with the As trimer structure prevailing for the As rich environment. These results of Kaxiras [14], Thornton [16] and Cho [17] are therefore all in agreement and the As trimer (111)A structure is also compatible with the electron counting principle.

From the electron counting point of view the As trimer structure is seen to stabilise the surface by a transfer of charge from the group III cation to the group V anion. There are a number of ways to count up the total number of valence electrons at the surface but their distribution among the bonding orbitals is unique. A (2×2) cell has one As trimer containing 9 bonds altogether, 3 each of As dangling bonds, As-As bonds within the trimer and As-Ga backbonds to the surface. Eighteen electrons fill the requirement, 15 of which are from the 3 As atoms and 3 more electrons from the 4 Ga atoms in the (2×2) unit cell each having ¾ electrons which lower their energy by filling the As trimer bonds. The rehybridisation that this produces should then cause the Ga atoms to recede into the bulk (planar sp^2 geometry) and the As trimer atoms should display a distorted pyramidal s^2p^3 geometry. Each unit cell also contains a Ga rest atom with an empty dangling bond at the surface.

4.2.2 The GaAs (111)B surface

A variety of surface reconstructions have been reported for the GaAs(111)B surface. Depending on surface preparation structures as diverse as (2×2) [8, 18, 19, 20], (3×3) [20] ($\sqrt{3}\times\sqrt{3}$) [21] and ($\sqrt{19}\times\sqrt{19}$) [18, 21, 22] have been observed although a thorough study of reconstructions found during MBE growth by Woolf et. al. [23, 24] and Yang et. al. [25] limit the possibilities to the progression (2×2) → (1×1) → ($\sqrt{19}\times\sqrt{19}$) → (1×1) as temperature and As_4 flux are varied. The (3×3) and ($\sqrt{3}\times\sqrt{3}$) structures have received little attention. They were observed on samples prepared by ion bombarding and annealing the surface and are not found on MBE prepared samples. Surface contaminants could possibly have a role to play in these experimental results. All GaAs(111)B surfaces prepared in this

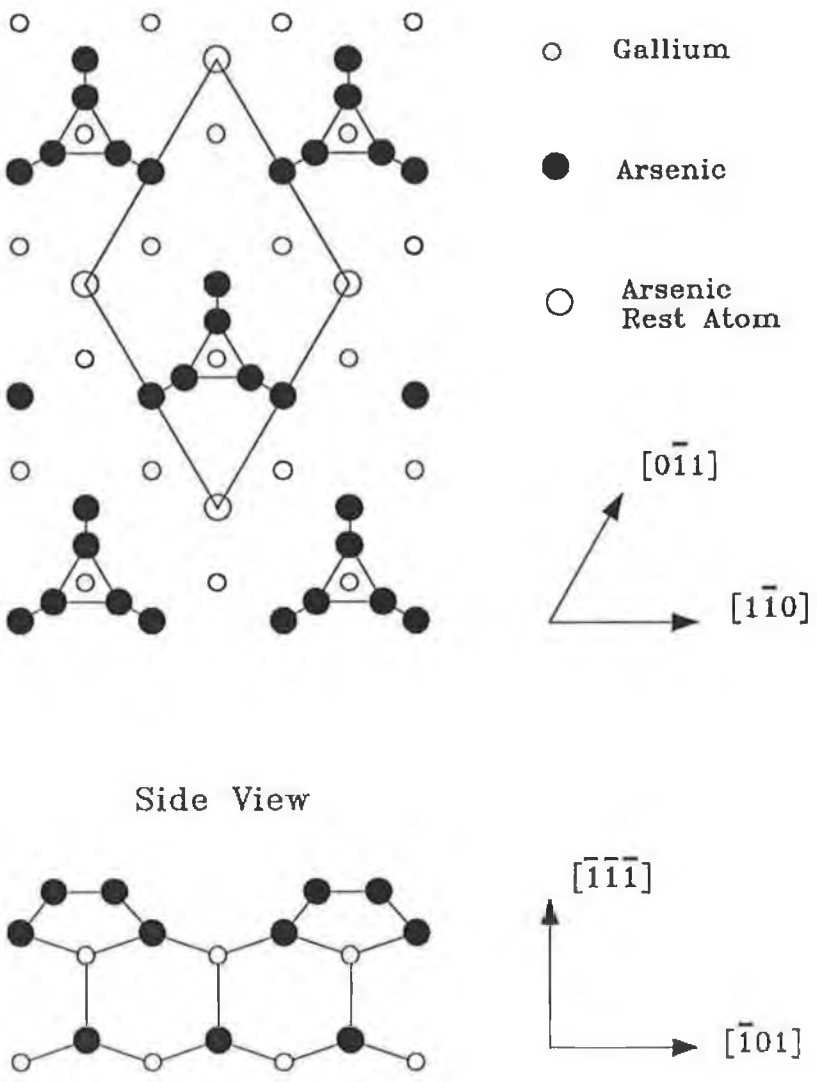

Figure 4.2 This trimer model for the GaAs(111)B - (2×2) surface was first suggested by Kaxiras et. al. as a result of a comprehensive total energy analysis of many different reconstructions [27]. STM results later confirmed that this is the correct model for the R.T. to 500°C temperature range [28].

work showed a (2×2) LEED pattern, the structure of which has been extensively investigated by a variety of experimental and theoretical techniques.

An early theoretical study of the GaAs(111)B-(2×2) surface by Chadi [26] dismissed the possibility that the surface was stabilised by As vacancies as their formation was found to be endothermic. Surface stabilisation by a (2×2) array of As trimers was first postulated by Kaxiras et. al. following their total energy calculations [27] - the As trimer reduced the energy of the surface by 4.5 eV per unit cell with respect to the unreconstructed clean surface. Despite this favourable result the authors dismissed the model as being unstable against steric restrictions but the model is now known to be correct. This was finally established STM studies in 1990 [28] and the model is shown in Figure 4.2.

As with other III-V surfaces which usually display the same reconstruction regardless of the species of the anion and cation, the (111)B face of InSb has a (2×2) trimer structure. This was first established by the transmission electron diffraction technique [29]. This method gave the Sb-Sb bond length of the trimer atoms (8% larger than the bond length in bulk antimony.) It had been known since 1984 that the (2×2) surface was semiconducting after the surface band structure was mapped using angle resolved photoemission [30] and so the electron counting rule should be satisfied. The rule is satisfied but as their is no Ga surface environment the extra charge needed to fill the dangling bond of the As rest atom (see figure 4.2) originates from the excess charge of the As trimer. In contrast with the trimer structure on the GaAs(111)A surface where the trimer is charge deficient and receives ¾ electrons from the Ga rest atom, charge transfer takes place in the opposite sense on the (111)B face. The trimer is backbonded to surface As atoms giving these As-As bonds excess charge which then fills the charge deficient As dangling bond of the rest atom (see figure 4.2).

Annealing this surface to 500 °C produces the ($\sqrt{19}\times\sqrt{19}$) R23.4° structure. This structure is complex and not fully understood. The model given by Biegelsen et. al. does not obey the electron counting rule and thermal desorption studies suggest that ~0.5 ML of As leaves the surface to produce the structure whereas Biegelsen's model requires the removal of 1.07 ML of As from the initial (2×2) trimer structure. The transition to ($\sqrt{19}\times\sqrt{19}$) was also found to be abrupt. More recently it has been shown by STM that the transition to ($\sqrt{19}\times\sqrt{19}$) happens continuously over a 50°C temperature range when under a constant As_4 flux [31]. This transitional phase is called (1×1) in the work of Woolf et. al. [23]. More complexity was suggested by the fact that free Ga migrating across the surface

plays a role in the formation of the ($\sqrt{19}\times\sqrt{19}$) structure which further complicates the aim of establishing the structure as the amount of surface species involved in the reconstruction is unknown. Unfortunately, the only theoretical work on this reconstruction [32] arrives at a model which shows no resemblance to the corresponding STM images.

4.3.1 MBE grown GaAs (100) surfaces

A large number of different reconstructions can be observed on this surface by varying the substrate temperature and As_4 flux during the MBE growth procedure. As the flux of the As_4 beam is reduced the As/Ga ratio of the surface decreases and the series of reconstructions from As rich to Ga rich are : c(4×4) → (2×4)-c(2×8) → (1×6) → (4×6) → (4×2)-c(8×2) [33]. The As rich (2×4) surface (figure 4.3) has been extensively studied and it was established, initially from RHEED intensity studies, that it exhibits three different phases. These are called α, β and γ which have As coverages of ½, ¾, 1 ML respectively according to an STM study by Farrell and Palmstrom [34]. Other authors have disputed these coverages on the basis of STM and dynamical RHEED calculations [35]. Further complexity is added by the observation of extra LEED spots in c(2×8) positions coexisting with the (2×4) pattern but this has been explained by the presence of defects where alternate (2×4) surface unit cells are shifted by one substrate lattice vector to form a c(2×8) surface net [36]. It is this (2×4) termination which was used in a study of Sb adstructures on the (100) surface, reviewed below.

4.3.2 The GaAs(110) surface

In contrast to the complexity of the GaAs(100) surface, the (110) surface is quite straightforward. This might be expected as the cleavage plane has the lowest surface energy and it is non polar, i.e. it contains equal numbers of anions and cations. All III-V(110) surfaces have show a (1×1) LEED pattern [37] so the system does not reconstruct but the relaxation is significant as it involves a rehybridisation of the bonding orbitals which ensures that the surface remains semiconducting. This distortion is consistent with the electron counting model. To accommodate this rehybridisation, the cation (planar sp^2) moves towards the bulk and the anion (pyramidal s^2p^3) moves away from the surface with no significant change in the bond lengths. This (1×1) surface is characterised by a buckling angle ω (figure 4.4) which lies within the range 29°±3° for almost all III-V (110) surfaces. Further details are discussed in a recent review [37].

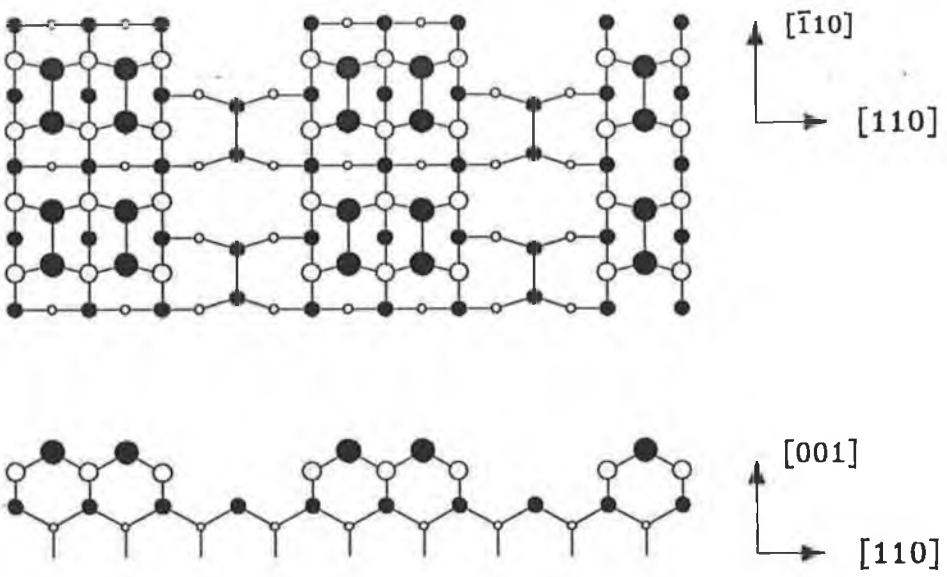

Figure 4.3 A model for the GaAs(100) - (2×4) surface. Known as the β_2 structure this is one of a number of various models proposed for this surface [35].

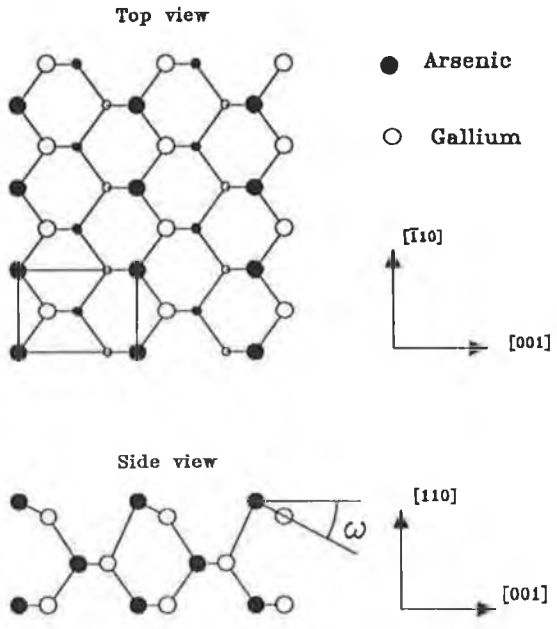

Figure 4.4 The accepted model for the GaAs(110)-(1×1) surface, the buckling is a structural relaxation which reduces the total energy of the surface.

4.4 The interaction of Sb and Bi with III-V surfaces

Since the early 1980's the research interest in the growth of Sb and Bi on III-V surfaces has steadily increased. Much of this work concentrated on Schottky barrier formation and investigating the possibility of epitaxial growth. Motivation for the former derived from interest in the rectification properties of electronic diodes and while studies in epitaxy complemented this work, the possibility of new device applications was an impetus for crystal growers. Initially, the interaction of Sb and Bi with the (110) cleavage plane of the III-V semiconductors served as a model system for the study of these interfaces in general. Within ten years this type work progressed as far as developing alternative non-linear optical devices. This class of interfaces was also used to test newly emerging experimental techniques such as IV-LEED, X-ray Standing Wave (XSW), Scanning Tunnelling Microscopy (STM) and angle resolved ultraviolet photoelectron spectroscopy (ARUPS) most of which had already been successful for the analysis of low coverage adsorbates on metals and some elemental semiconductors. Theoretical calculations performed during the 1980's were mainly directed towards low index clean GaAs surfaces but there were some important successes with regard to the group V adsorbates on the cleavage plane. A review of these is given below to highlight how the development of these analytical techniques progressed in tandem with further understanding of Sb and Bi adsorbates on the III-V semiconductors.

4.4.1 Antimony and Bismuth on GaAs (110)

The Group V elements form well ordered overlayers when deposited on III-V surfaces at room temperature [37]. Antimony in particular, always exhibits a (1×1) structure for monolayer coverages while Bi sometimes deviates from this and forms a structure with a lower periodicity in one direction.

A number of alternative models for the monolayer coverage of Sb on the (110) surface had been proposed [38] after Skeath et. al. [39, 40] had established the growth of one epitaxial monolayer of Sb on GaAs(110). These authors found that Sb bonds to two different sites in the surface unit cell. Dynamical LEED studies performed by Duke et. al. [41] then established that the *epitaxial continued layer structure* (ECLS) model was correct (figure 4.5). In this structural model Sb forms zig-zag chains across the surface

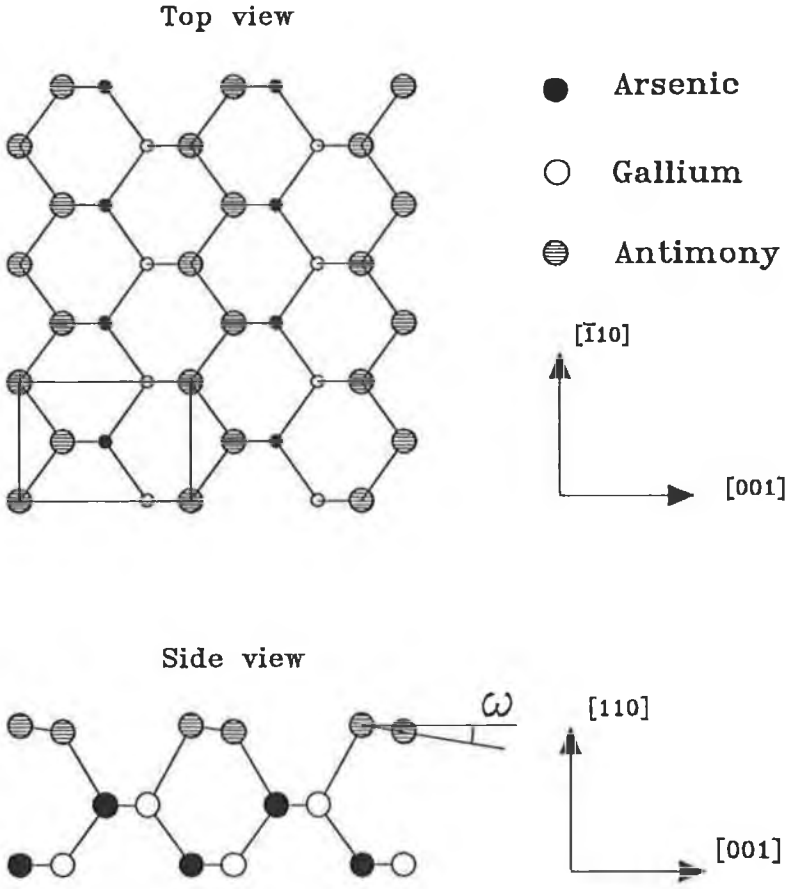

Figure 4.5 A number of models were initially proposed for the III-V(110)-Sb(1×1) surface. Shown here is the epitaxial continued layer structure which was first established by dynamical LEED calculations ([41]. Antimony forms this structure on all III-V surfaces while Bi has the same local structure but defects cause the formation of a (1×6) or (1×3) superlattice on some III-V substrates.

with the adatoms bonded alternately to As and Ga atoms along the $[\bar{1}10]$ direction. The buckling angling ω, which is analogous to the buckling angle of the clean surface, has been calculated both from LEED data and *ab initio* calculations for Sb and Bi on a wide range of III-V (110) surfaces and lies in the 3.5°±2° range. This buckling angle is considerably less then the 29°±3° of the clean surface but it has the effect of sweeping the surface states out of the bulk band gap [42, 43]. This latter fact was verified by scanning tunnelling spectroscopy and also holds on well ordered terraces with gap states present at the terrace edges. More recently theoretical [44, 45], LEED [46] and XSW [47] studies have shown that Sb grows in the ECLS mode with no significant relaxation of the underlying substrate. Beyond the first monolayer Sb continues to form three dimensional islands in a Stranski-Krastanov mode but further annealing to 600°C removes all excess Sb leaving a sharp (1×1) LEED pattern.

Bi also grows in the Stranski-Krastanov mode on the GaAs(110) and InP(110) surfaces but the effect of annealing is slightly different as it creates regular dislocations with missing adatoms every 6 unit cells in the $[\bar{1}10]$ direction [48, 49]. This trend is consistent enough to produce sixth order fractional spots in the LEED pattern and is possibly due to the larger size of the Bi atoms as compared to the Sb atoms.

4.4.2 Sb on the GaAs(100) surface

In comparison with the almost comprehensive literature that exists for the model systems of group V overlayers on III-V materials, other low index III-V surfaces have been somewhat overlooked. Maeda et.al. [50] were the first group to deposit Sb on the clean GaAs(001) surface and their RHEED and photoemission experiments revealed transitions through a series of reconstructions with increasing temperature arriving at a (2×4) reconstruction which they suggested had three Sb dimers per unit cell. Another study of this reconstruction was by XSW [51], where the authors gave values for the Sb-Sb dimer bond length (2.95 ± 0.06Å) and the separation between the Sb atoms and the Ga atoms in the surface plane below (1.81± 0.02Å). The three dimer model was replaced by a one dimer model consistent with STM images [52] which recent electronic structure calculations have shown is semiconducting [53].

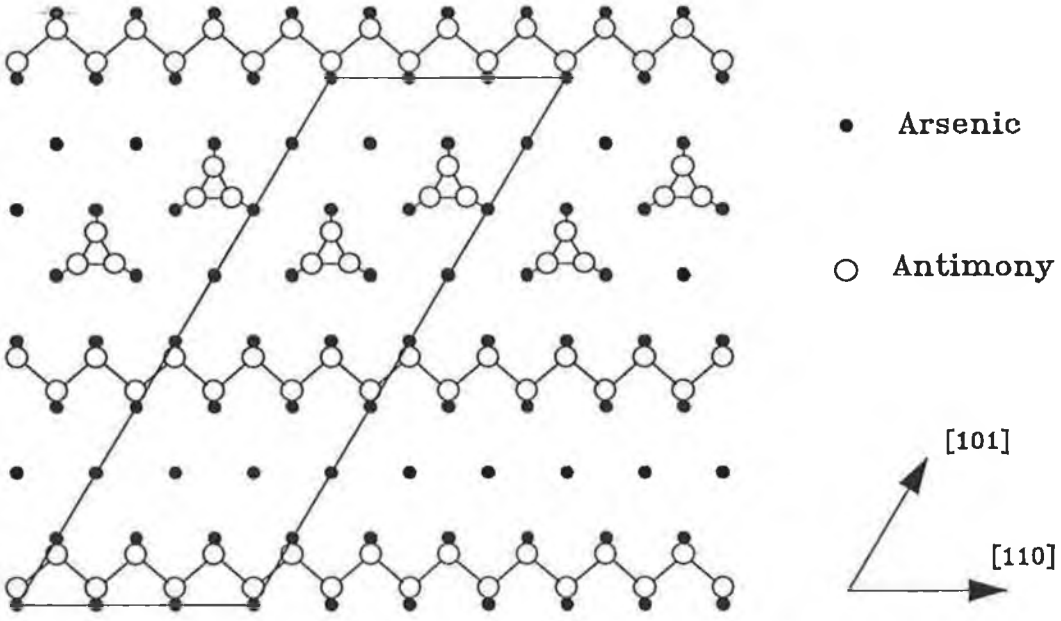

Figure 4.6 Antimony forms reconstructions on the GaAs(111)B surface which are based on pairs of chains of adatoms extending across the surface [54]. The (3×8) reconstruction shown here is in full agreement with the electron counting rule.

4.4.3 Sb on the GaAs(111)B surface

Only three studies were found in the literature involving the deposition of a group V overlayer on a GaAs(111) surface [54, 55, 56]. Moriarty et. al. [54, 55] found that a sub monolayer coverage of Sb on GaAs(111)B produces a complex group of reconstructions all of which contain double chains of Sb adatoms which are separated by different arrangements of Sb trimers. These reconstructions coexist on the surface after annealing to 370°C. All of the Sb chains are separated by three substrate unit cells and the spacing between these chain pairs varies from p = 2,3,4,5 rows of substrate atoms. The chains are parallel to the (110) direction and the periodicity m of the reconstruction in this direction depends on p. Even though the STM images showed domains of four different structures, the electron counting model fully accounts for all of them. If there are n trimers per unit cell and as there are (p+5)m substrate As atoms per unit cell then there are 3n+4m of these As atoms bonded to Sb. Electron counting the requires that

$$(3n+4m)/4=3\{m(p+5)-3n-4m\}/4.$$

This equation then gives the lowest integer values of m and n for some value of p observed in the STM images :

p = 2,	m = 12, n = 5
p = 3,	m = 3, n = 2
p = 4,	m = 12, n = 11
p = 5,	m = 6, n = 7.

Shown in Figure 4.6 is the (3×8) reconstruction where p = m = 3. The STM image of this reconstruction is given in figure 4.7. The justification of these reconstructions represents some success for the electron counting model and shows its validity even for large unit cells such as (12×7), ie, where p = 2.

A separate study of the Sb-GaAs(111)B was also performed by Moriarty et. al. [56]. On annealing to 525°C, the surface reconstructed to (1×3) symmetry. This reconstruction comprises of Sb chains oriented parallel to the {110} directions and separated by three bulk primitive lattice vectors. This model represents a breakdown of the electron counting rule as the surface unit cell is charge deficient. This means that a surface As atom not bonded to Sb has a dangling bond with an energy in the bulk band gap. The reason given

for this situation is that the surface energy is minimised by the reduction in surface strain due to the formation of Sb chains. This effect dominates over the need for charge neutrality and so the electron counting model breaks down.

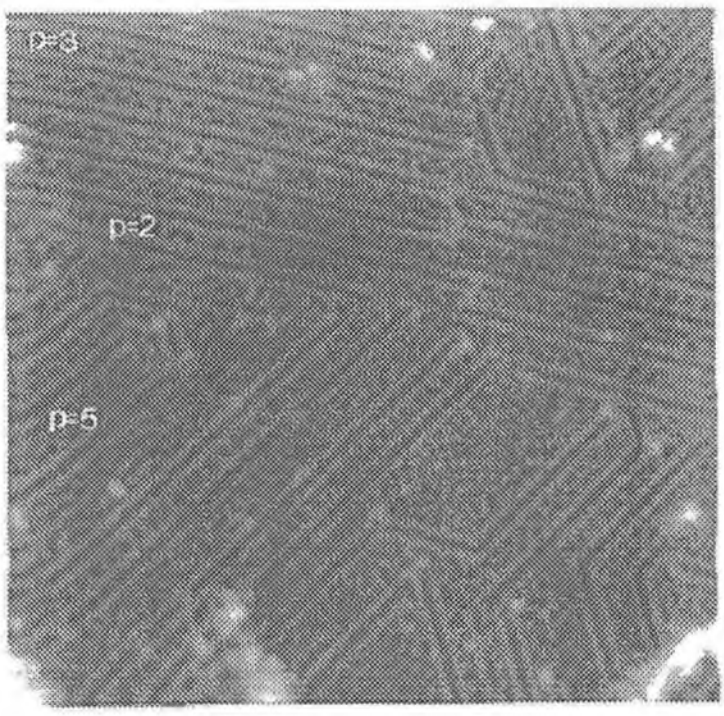

Figure 4.7 STM image of the Sb/GaAs surface at 375°C. The three regions labelled p=2,3,5 have different reconstructions as described in the text. This image is taken from ref.(54), used with permission.

4.5 Limitations of the Electron counting Model

This chapter emphasises the success of the electron counting rule in describing surface reconstructions in III-V semiconductors. The surface energy is a minimised if the anion dangling bonds contain two electrons and cation dangling bonds are empty. Other factors which contribute to the surface energy and are not accounted for by electron counting are electrostatic interactions and strain effects. Examples of the importance of these effects are given for III-V (100) surface reconstructions.

Northrup and Froyen [57] have shown that if two structural models are proposed, both of which agree with the electron counting rule, the most likely reconstruction is that with the lowest Coulomb interaction between the atomic charges at the surface. The reconstruction considered was GaAs(100)-(2×4). The energy arising from the Coulomb interactions is found by performing a Madelung summation over the As and Ga charges at the surface,

$$S = \frac{1}{2}\Sigma q_i q_j / |R_i - R_j|$$

where R_i is the position of the charge q_i. If S is found for two structural models, then the energy difference between the two is $\Delta S/\varepsilon$. Dividing by the dielectric constant ε takes screening into account. This method was used to find the lowest energy of two proposed models for the GaAs (100)-(2×4) surface and the results agree with first principle total energy calculations. The authors concluded that electrostatic interactions are the driving force for ordering on polar semiconductor surfaces. This interaction is not taken into account in the electron counting model.

Another contribution to the surface energy which the electron counting principle does not consider is surface strain. Monch [58] describes how the increase in elastic strain energy due to the formation of a dimer is approximately 2eV on all (100) semiconductors. Larsen et al. [59] calculated that the As dimer bond state on the GaAs(100) surface lies 3.5eV below the valence band maximum. The surface energy is therefore reduced by ~1.5eV per dimer. The As dimer on the GaAs(100) surface, like the As trimer on the (111)B surface ensures that all As dangling bonds at the surface contain a lone pair of electrons, a condition of the electron counting rule. This minimises the energy of the surface only because the increase in strain energy is relatively small. Some authors suggest that those surface reconstructions which violate the electron counting rule are driven by the minimisation of surface strain. The example of the Sb\GaAs(111)B-(3×1) [56] was discussed in section **4.4.3**. Other violations of electron counting caused by the reduction of surface stress are the GaSb c(2×10) and (2×10) reconstructions [60]. These systems are weakly metallic and the cause of this is attributed to a competition between the energy gain from the formation of Sb dimers and the energy loss from the increased surface stress.

References for Chapter IV

1. M. D. Pashley, Phys. Rev. B **40** 10481 (1989)
2. H. H. Farrell, J. P. Harbison and L. D. Peterson, J. Vac. Sci. Technol. B **5** 1482 (1987)
3. W. A. Harrison, J. Vac. Sci. Technol. **16** 1492 (1979)
4. D. E. Eastman, T. C. Chiang, P. Heimann and F. J. Himpsel, Phys. Rev. Lett. **45** 656 (1980). This and the following two references are only examples of the many surfaces which have been analysed using core level photoemission with the aim of establishing the nature of the surface bonding.
5. J. F. van der Veen, P. K. Larsen, J. H. Neave and B. A. Joyce, Solid State Comm. **49** 659 (1984)
6. C. J. Spindt, M. Yamada, P. L. Meissner, K. E. Miyano, T. Kendelewicz, A. Herrera-Gomez, W. E. Spicer and A. J. Arko, Phys. Rev. B **45** 11108 (1992)
7. D. Haneman, Phys. Rev. **121** 1093 (1961)
8. A. U. MacRae, Surf. Sci. **4** 247 (1966)
9. S. Y. Tong, G. Xu and W. N. Mei, Phys. Rev. Lett. **52** 1693 (1984)
10. C. Xu, W. Hu, M. W. Puga, S. Y. Tong et. al., Phys Rev B, **32** 8473 (1985)
11. J. Bohr, R. Feidenhans, M. Nielsen, M. Toney, R. L. Johnson and I.K. Robinson, hys. Rev. Lett. **54** 1275 (1985).
12. K. W. Haberen and M. D. Pashley, Phys. Rev. B **41** 3226 (1990)
13. D. J. Chadi, Phys. Rev. Lett. **52** 1911 (1984)
14. E. Kaxiras, et. al., Phys Rev. B **35** 9625 (1987)
15. J. G. Ping and H. E. Ruda, J. Appl. Phys. **75** 5332 (1994)
16. J. M. C. Thornton, P. Weightman, D. A. Woolf and C. J. Dunscombe, Phys. Rev B **51** 14459 (1994)
17. A. Y. Cho and J. R. Arthur, Prog. Solid State Chem. **10** 157 (1975)
18. A. Y. Cho and I. Hayashi, Solid-States Electron. **14**, 125 (1971)
19. J. R. Arthur, Suf. Sci. **43** 449 (1974)
20. M. Alonso, F. Soria and J. L. Sacedon, J. Vac. Sci. Technol. A **3** 1595 (1985)
21. K. Jacobi, C. Muschwitz and W. Ranke, Surf. Sci. **82**, 270 (1979)
22. K. Jacobi, G. Steinert and W. Ranke, Surf. Sci. **57** 571 (1976)
23. D. A. Woolf. D. I. Westwood and R. H. Williams, Appl. Phys. Lett. **62** 1370 (1993)
24. D. A. Woolf, D. I. Westwood and R. H. Williams, Semicond. Sci. Technol. **8** 1075 (1993)
25. K. Yang and L. J. Schowalter, Appl. Phys. Lett. **60** 1851 (1992)
26. D. J. Chadi, Phys. Rev. Lett. 52 1911 (1984)

27. E. Kaxiras, Y. Bar-Yam, J. D. Joannaopoulus and K. C. Pandey, Phys. Rev. B 35 9636 (1987)
28. D. K. Biegelsen, R. D. Bringans, J.E. Northrup and L.-E. Swartz, Phys. Rev. Lett., **65** 452 (1990)
29. T. Nakada and T. Osaka, Phys. Rev. Lett., **67** 2834 (1991)
30. R. D. Bringans and R. Z. Bachrach, Phys. Rev. Lett. **53** 1954 (1984)
31. A. R. Avery, E. S. Tok and T. S. Jones, Surf. Sci. **376** L397 (1997)
32. E. Kaxiras, Y. Bar-Yam, J. D. Joannaopoulus and K. C. Pandey, Phys. Rev. B **57** 106 (1986)
33. P. Drathen, W. Ranke and R. Jacobi, Surf. Sci. **77** L162
34. H. H. Farrell and C .J. Palmstrom, J. Vac. Sci. Technol. B **8** 903 (1990)
35. T. Hashizume, Q. K. Xue, J. Zhou, A. Ichimiya and T. Sakuri, Phys. Rev. Lett. **73** 2208 (1994)
36. M. D. Pashley, K. W. Haberen, W. Friday, J. M. Woodall and P. D. Kirchner, Phys. Rev. Lett. **60** 2176 (1988)
37. G. P. Srivistava, Rep. Prog. Phys. **60** 561 (1997)
38. W. G. Schmidt, F. Bechstedt and G.P. Srivistava, Surf. Sci. Rep., **25** 141 (1996)
39. P. Skeath, C. Y. Su, I. Lindau and W. E. Spicer, J. Vac. Sci. Technol., **17** 874 (1980)
40. P. Skeath, C. Y. Su, W. A. Harrison, I. Lindau and W. E. Spicer, Phys. Rev. B **27** 6246 (1983)
41. C. B. Duke, A Paton, W. K. Ford, A. Kahn and J. Carelli, Phys Rev B **26** 803 (1982)
42. R. M. Feenstra and P. Martensson, Phys. Rev. Lett. **61** 447 (1988)
43. P. Martensson and R. M. Feenstra, Phys. Rev. B **39** 7744 (1989)
44. G. P. Srivistava, Phys. Rev B **47** 16616 (1993)
45. W. G. Schmidt, B Wenzein, and F. Bechstedt, Phys. Rev B **49** 4731 (1994)
46. W. K. Ford, T. Guo, D. L. Lessor and C. Duke, Phys. Rev. B **42** 8952 (1990)
47. Kendelewicz et. al. J. Vac. Sci. Technol. A **11** 2351 (1993)
48. R. Ludeke, A Taleb-Ibrahami, R. M. Feenstra and A. B. McLean, J. Vac. Sci. Technol. **B 7** 936 (1989)
49. J. J. Joyce, J. Anderson, M. M. Nelson, C. Yu and G. J. Lapeyre, J. Vac. Sci. Technol. **A 7** 850 (1989)
50. F. Maeda, Y. Watanabe and M. Oshima, Phys. Rev. B **48** 14733(1993)
51. M. Sugiyama, S. Maeyama, F. Maeda and M. Oshima, Phys. Rev. B **52** 2678 (1995)
52.P. Moriarty, P. H. Beton, Y-R. Ma, M. Henini and D. A. Woolf, Phys. Rev. B **53** 16148 (1996)

53. G.P. Srivistava, Conference presentation, European Conference on Surface Science, Genoa, 1996.
54. P. Moriarty, P. H. Beton, and D. A. Woolf, Phys. Rev. B **51** 7950 (1995)
55. P. Moriarty, P. H. Beton, M. Henini and D. A. Woolf, J. Vac. Sci. Technol., B **14** 1024 (1996)
56. P. Moriarty, P. H. Beton, M. Henini and D. A. Woolf, Surf. Sci. **365** L663 (1996)
57. J. E. Northrup and S. Froyen, Phys. Rev. B, **50** 2015 (1994)
58. W. Monch, *Semiconductor Surfaces and Interfaces*, Springer, (1995)
59. P.K. Larsen, J. F. van der Veen, A. Mazur, J. Pollman, J. H. Neave and B. A. Joyce, Phys. Rev B **26** 3222 (1982)
60. L.J. Whitman, P.M. Thibado, S.C. Erwin, B.R. Bennett and B.V. Shanabrook, Phys. Rev. Lett. **79** 693 (1997)

Chapter V

Antimony on GaAs(111)A

5.1 Introduction

This chapter begins with a description of the growth of an Sb overlayer on the GaAs(111)A-(2×2) surface. Two chemical environments for the Sb overlayer are observed. One environment is associated with an interfacial Sb layer. Above this layer Sb growth is in a layer-plus-island mode. By annealing the system to 500°C a $(2\sqrt{3}\times2\sqrt{3})R30°$ reconstruction was formed for which a structural model is proposed. The effect of the Sb overlayer on the surface electronic band bending is also described.

5.2 The growth of Antimony on GaAs(111)A

The initial growth of Sb on GaAs(111)A is consistent with Stranski-Krastanov growth. Evidence for this is seen in the plot of the intensities of the components in the Sb 4d photoelectron spectrum as a function of the amount deposited (figure 5.1). In this figure it is the area of the core level components (see figure 5.2) divided by both the incident light intensity and a background intensity taken directly from the core level spectrum which are plotted. This normalisation procedure allows comparison between spectra taken with different incident light intensities as the flux from the synchrotron decays and also accounts for the fact that the sample has to be moved for each deposition of Sb which could give slight inaccuracies if the sample is not returned to exactly the same position every time.

There are two Sb core level components, one of which is identified with Sb-surface bonding which saturates at a low coverage. More significant is the Sb-Sb component, the intensity of which initially increases linearly and then the slope changes at a depth of 2.0± 0.1Å. This 'break point' in the Sb-Sb curve is indicative of a change in growth mode. A change in slope such as this is either associated with layer plus island growth or layer-by-

layer growth as described above. For layer-by-layer growth, the curve representing the Sb-Sb component should be contained within an exponential envelope [1]. Attempts to fit this with an exponential function were unsuccessful, so the growth of Sb is assumed to be in a layer plus island mode. This is therefore Stranski-Krastanov growth and this has been observed for Sb growth on the GaAs(110) surface [2] and further justification for this result is given below.

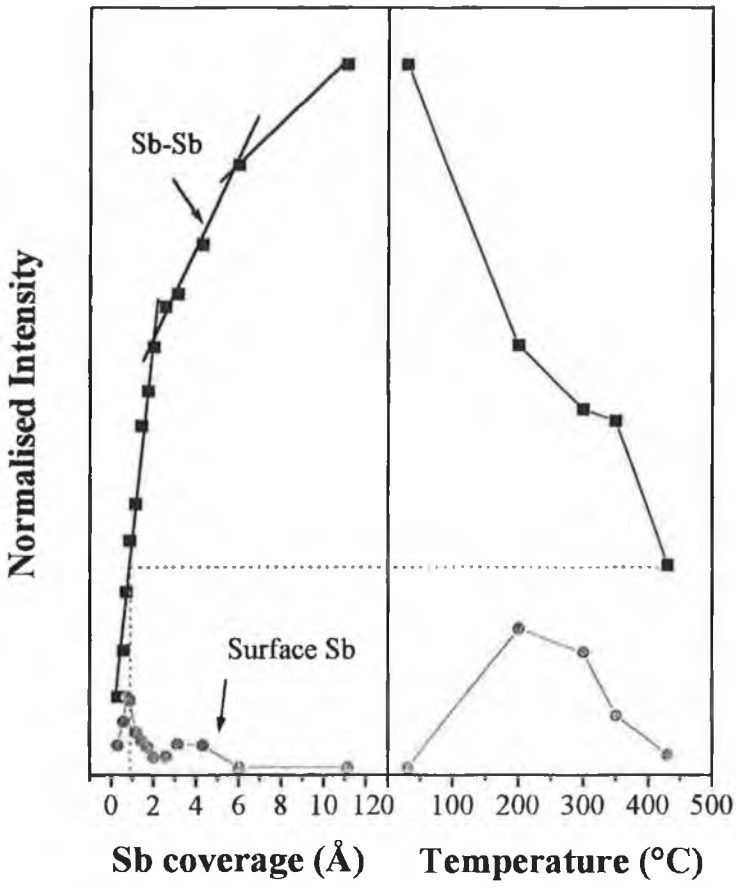

Figure 5.1 The normalised intensity of the two components in the Sb core level as a function of the nominal depth deposited. Also shown is the effect on these intensities as the sample is annealed. The lines are drawn to guide the eye.

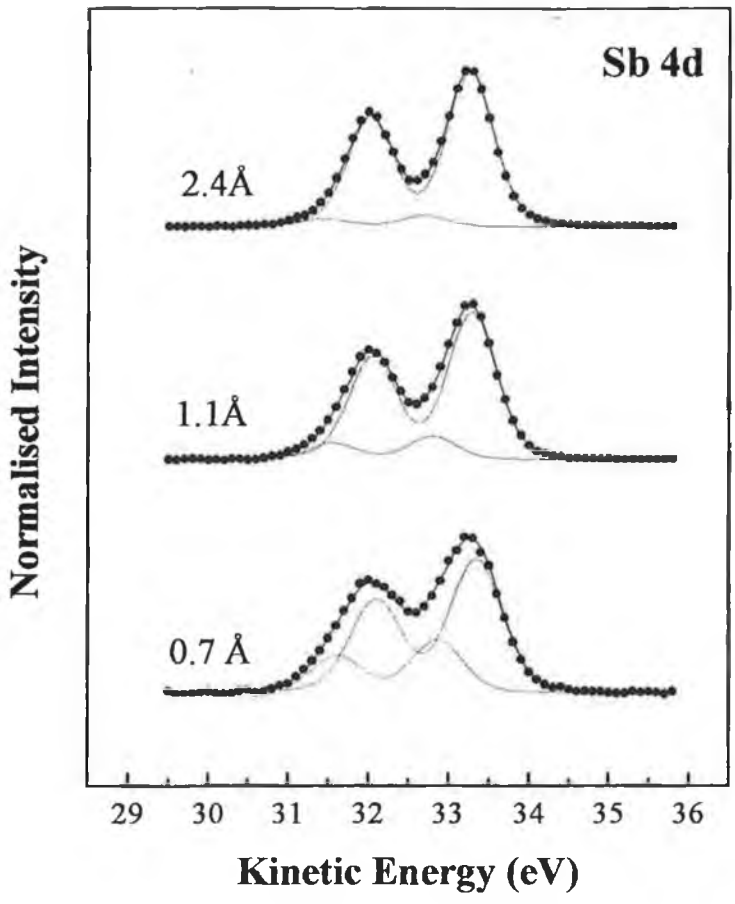

Figure 5.2 Fitted Sb core levels at different Sb coverages during the growth study.

It is useful to now compare these results with the growth of Sb on another III-V (111) surface. Epitaxial growth of Sb has been achieved on a Ga Sb (111)A substrate. Golding et. al. [3] synthesised heterojunctions and elementary multilayered structures of Sb\GaSb by molecular beam and migration enhanced epitaxies. By comparing the lattice parameters of GaAs and GaSb we can see why layer plus island growth of Sb is favoured on GaAs while epitaxy is achieved for GaSb. The interatomic nearest neighbour distances on the (111) plane are 4.00 Å for GaAs and 4.31 Å for GaSb. Bulk Sb is rhombohedral and the interatomic distance for the (111) plane is also 4.31 Å. The maximum planar mismatch between these orientations of Sb and GaAs has been given as 0.0006 at 273 K [3] so no significant strain is to be expected at the interface and epitaxial growth results. In this

study the planar mismatch between Sb and GaAs is 0.072 or 7% and this difference is enough to create a strain in the overlayer which prevents layer by layer growth.

Also shown in Figure 5.1 is the effect of annealing temperature on the intensities of the core level components. At 250°C the intensity of the bulk component is the same as that before annealing while the surface component has dramatically increased in intensity. This is unusual as the total Sb core level intensity seems to increase, but is probably due to a reorganisation of the bulk Sb which exposes more surface Sb and so increases the relative surface signal.

On annealing the sample to 500°C, the intensity of the Sb-Sb component in the Sb 4d core level spectrum has decreased to an intensity equivalent to 0.9±0.1 Å. This estimate of the final coverage will be used below in discussing the structural model for the surface reconstruction observed at this temperature.

5.3 LEED Results

A separate study of the Sb-GaAs(111)B system was performed to establish if new reconstructions would form. The sample was heated from room temperature to 600°C, where the Sb had completely desorbed, in intervals of 50°C. LEED patterns were observed and photoemission spectra taken to monitor any structural or chemical bonding changes at the surface.

After the deposition of Sb on the GaAs(111)A surface, a weak (2×2) LEED pattern with a high background was observed. The Sb coverage at this initial stage is of the order of 4 ML and the faint evidence of a (2×2) structure suggests that the original clean surface Ga vacancy structure is still preserved beneath the overlayer. A series of temperature anneals was performed through which further structure began to appear in the LEED pattern, where the faint (2×2) spots began to split along the direction of the bulk spots. This is indicative of a new reconstruction forming and the surface as a whole becoming more ordered. At 500°C a ($2\sqrt{3}\times2\sqrt{3}$) R30° LEED pattern was observed (figure 5.3), from which a structural model for the surface is suggested below. Annealing the sample to 600°C caused the complete desorbtion of the Sb.

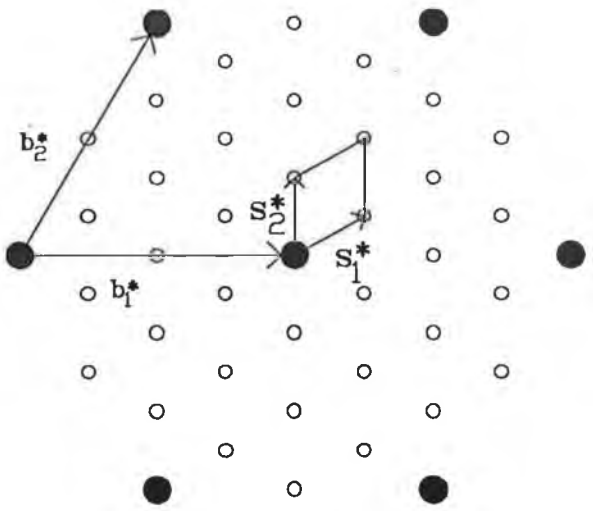

Figure 5.3 The (2√3×2√3)R30° LEED pattern observed for the Sb-GaAs(111)A surface at 500°C. The bulk reciprocal lattice unit cell is represented by the vectors $\mathbf{b_1}^*$ and $\mathbf{b_2}^*$. The vectors $\mathbf{s_1}^*$ and $\mathbf{s_2}^*$ define the adsorbate reciprocal lattice from which the real space surface reconstruction is derived. The photograph of this pattern is also shown on the following page.

At this stage it is worth considering this (2√3×2√3) LEED pattern from a structural point of view as it contains information with regard to the crystallographic unit cell of this surface which will be discussed in the next section. The pattern gives evidence for a unique (2√3×2√3) unit cell. The possibility of coexisting domains of (2×2) and (√3×√3) is ruled out as this situation would give rise to fewer spots in the LEED pattern. This multidomain surface might be argued as possible as the clean surface has (2×2) symmetry and the arrangement of adatoms in a (√3×√3) surface structure is common on the (111) facets of both metals and semiconductors [4]. If this were the case the final reconstruction at 500°C would contain regions of the restored clean surface, after the desorption of some Sb, coexisting with (√3×√3) domains. The reason why this can be disregarded is that the LEED pattern for this multidomain situation would contain fewer spots than are observed, i.e., LEED would only show a superposition of (2×2) and (√3×√3) patterns. This is illustrated in Figure 5.4.

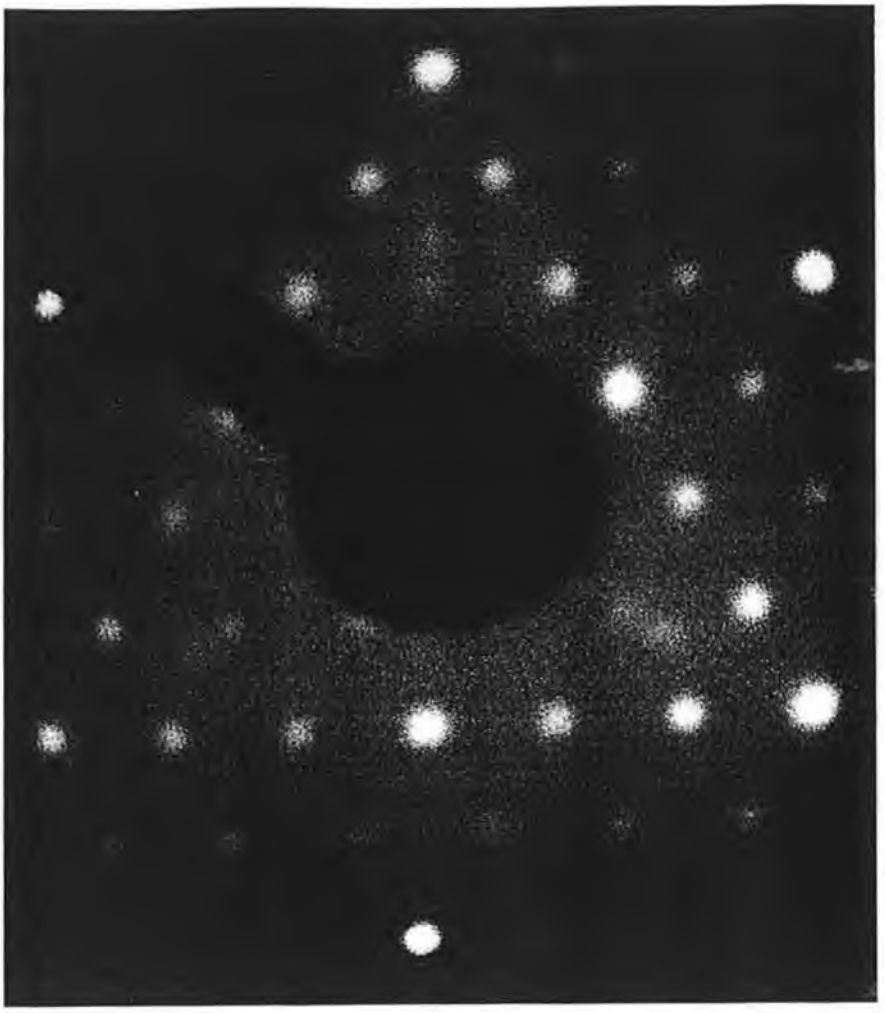

The $(2\sqrt{3}\times 2\sqrt{3})R30°$ LEED pattern

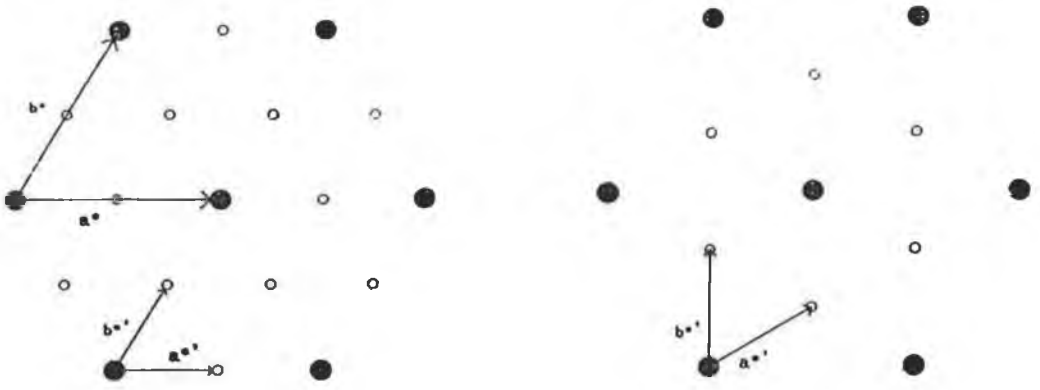

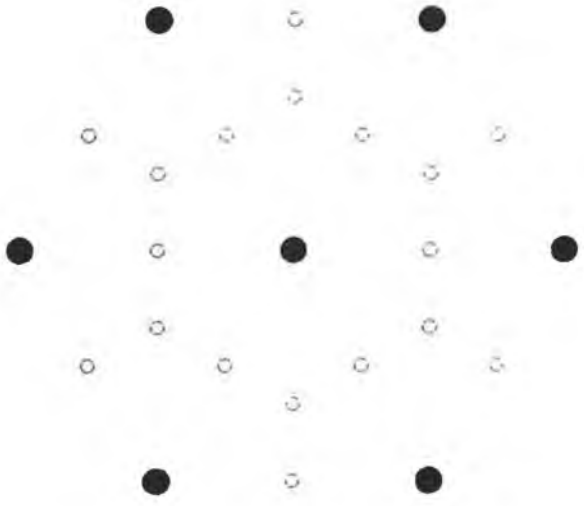

Figure 5.4 A compound LEED pattern (below) which would result if a surface contained separate domains of (2×2) and (√3×√3) reconstructions. The pattern is simply the superposition of the two LEED patterns at the top of the diagram.

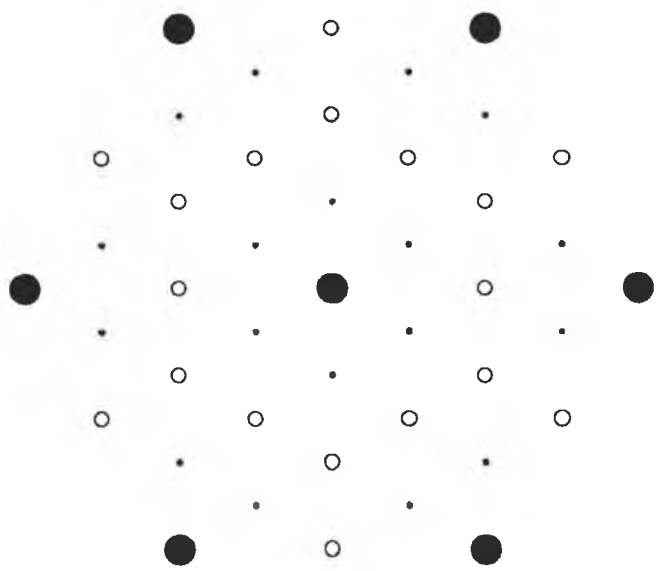

Figure 5.5 This diagram illustrates the LEED pattern expected if the Sb-GaAs(111)A surface at 500°C were composed of a substrate with a (2× 2) reconstruction with an overlayer exhibiting an independent ($\sqrt{3}\times\sqrt{3}$) structure. The pattern is the same as that of figure 5.4 with the extra spots being due to multiple scattering.

A variation on the preceding idea could also be suggested. If the (2×2) vacancy structure of the original clean surface were to remain intact underneath the adsorbed layer of Sb and the effect of temperature annealing was to create an independent ($\sqrt{3}\times\sqrt{3}$) Sb adstructure on top of the vacancy structure we would effectively have two independent structures contributing to the LEED pattern. Such a compound structure would produce the diffraction spots shown in figure 5.4 but there would also be extra spots due to *multiple scattering*. Each multiply scattered beam would be due to the interference of electrons scattered both from atoms involved in the substrate (2×2) array and from Sb adatoms above. A diffraction spot due entirely to multiple scattering is generally accepted to be a factor of ten weaker than the other fractional order spots which are due to singly scattered electrons [5]. This type of pattern is shown schematically in figure 5.5. This pattern has spots in all the same positions as in figure 5.3 (which represents what was actually seen in the experiment) but those spots due to multiple scattering (•) would be less intense than the singly scattered spots and this was not seen. All of the fractional order spots were seen

to have approximately the same maximum intensity as judged by eye and by examination of the photographs after the experiment. Even though these reconstruction induced spots have a maximum intensity at different primary beam energies (a familiar effect in an IV-LEED experiment) there was no suggestion that some of the spots were weak enough to be due to multiple scattering only. With this information from the LEED pattern the possibility of the surface being composed of a ($\sqrt{3}\times\sqrt{3}$) Sb overlayer bonded to the (2×2) structure of the original clean surface is dismissed.

5.4.1 Core Level Photoemission Spectroscopy

Figures 5.6 (a), (b) and (c) show the core level photoemission spectra recorded for the clean surface, after Sb deposition and for a series of anneals up to 600°C where the Sb had completely desorbed. The clean surface spectra are in agreement with those of the (2×2) Ga vacancy model [6], and section **4.2.1**. There is a surface core level shifted component in both the Ga 3d and As 3d spectra, associated with empty Ga and full As dangling bonds respectively (figure 4.1). This data agrees with the results of Thornton et al [7] .

After the deposition of the Sb overlayer, the Sb 4d core level initially has two components, one associated with the Sb-Sb bonding and the other with Sb-surface bonding as mentioned above. At this stage the As 3d core level has a surface shifted core level component on the low kinetic energy side of the spectrum. This component has a higher binding energy than the bulk As which is indicative of charge transfer from the As to Sb and so the surface Sb is at this stage bonded to the As atoms exposed at the surface by the Ga vacancy.

After annealing to 500°C, the Sb core level has one component and this is associated with the surface bonded Sb responsible for the reconstruction seen by LEED. With only one component fitted to the Sb spectrum we conclude that all Sb atoms have the same chemical environment. The parameters used in the fitting the core levels are listed in Table 5.1.

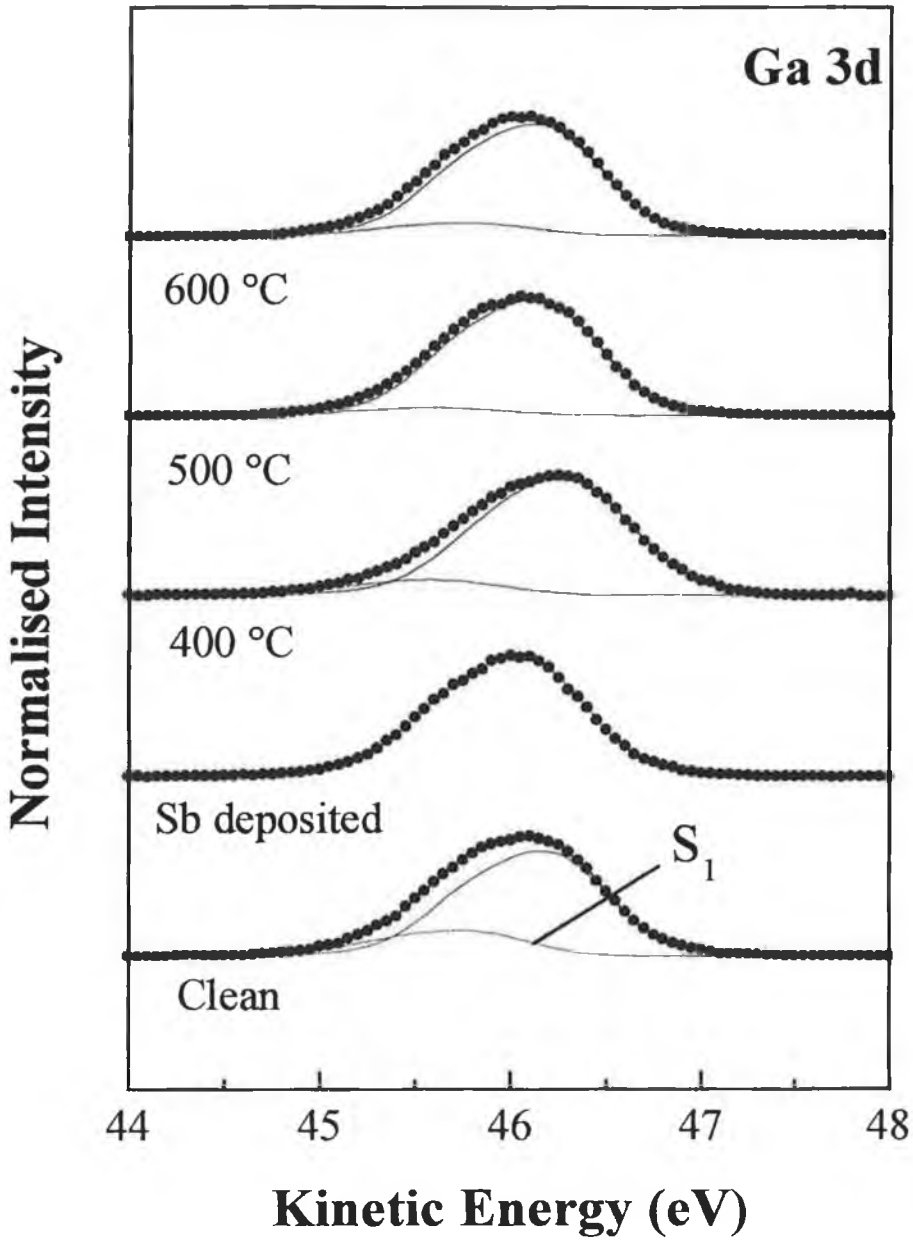

Figure 5.6 (a) Curve fitted photoemission spectra of the Ga 3d core levels from the Sb-GaAs(111)A surface as a function of annealing temperature. The photon energy was 70eV.

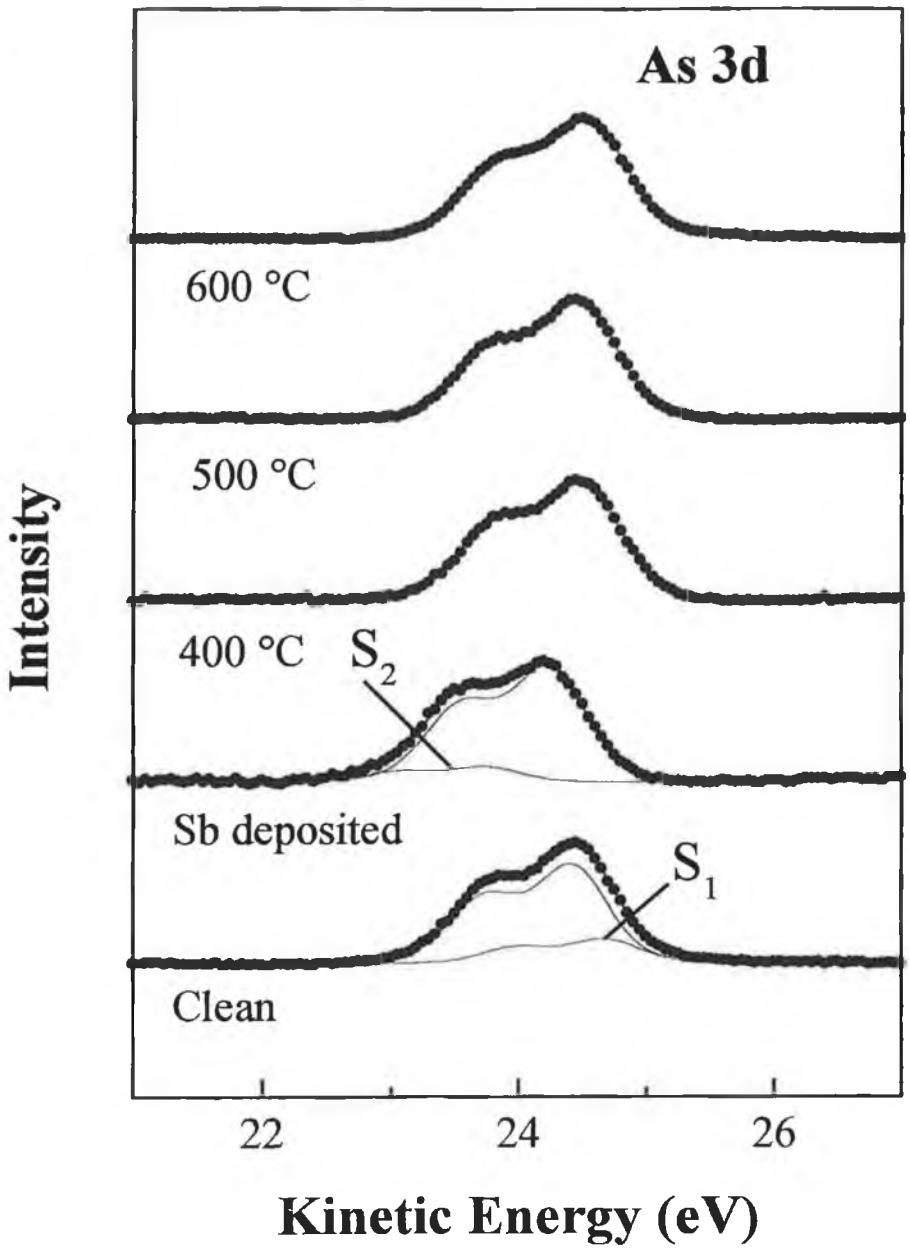

Figure 5.6 (b) Curve fitted photoemission spectra of the As 3d core levels from the Sb-GaAs(111)A surface as a function of annealing temperature. The photon energy was 70eV.

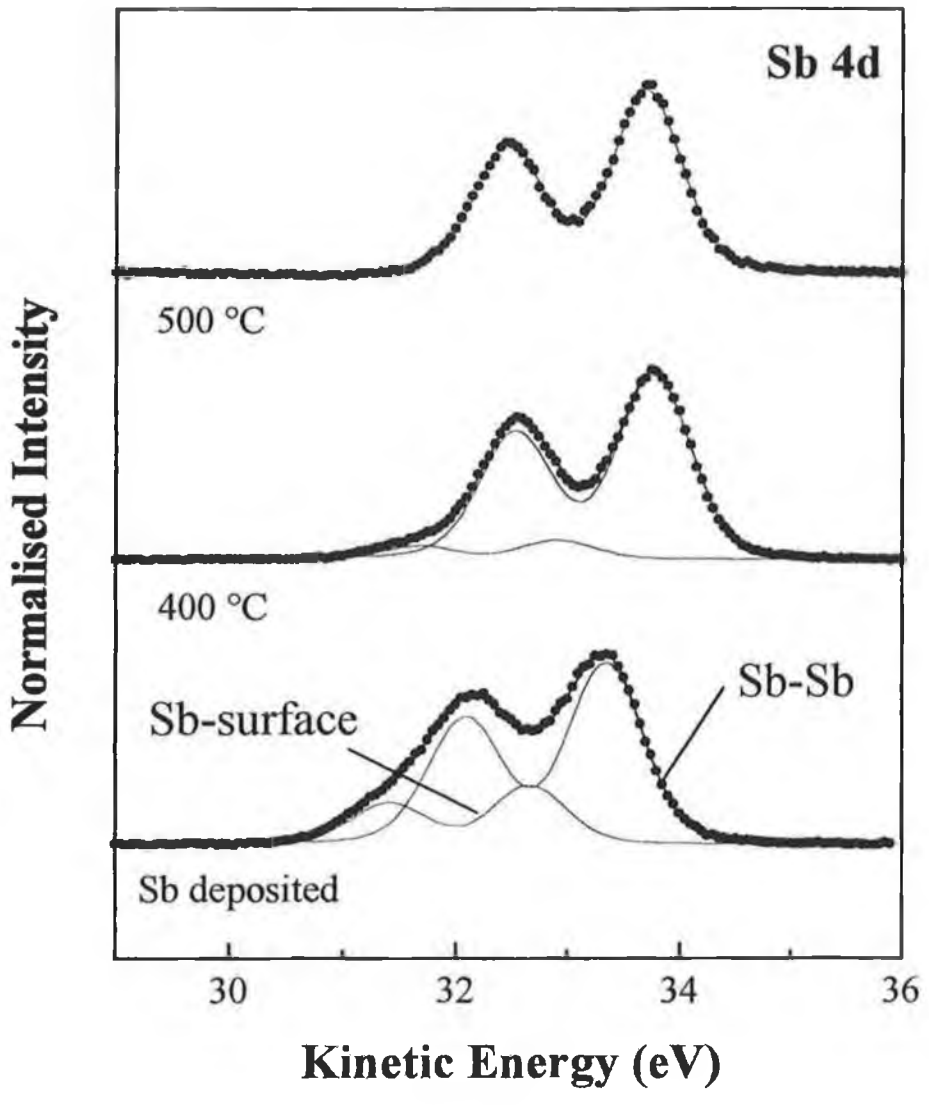

Figure 5.6 (c) Curve fitted photoemission spectra of the Sb 4d core levels from the Sb-GaAs(111)A surface as a function of annealing temperature. The photon energy was 70eV.

Table 5.1

	Ga 3d		As 3d		Sb 4d
	Clean	$2\sqrt{3}\times2\sqrt{3}$	Clean	$2\sqrt{3}\times2\sqrt{3}$	$2\sqrt{3}\times2\sqrt{3}$
Gaussian (eV)	0.47	0.57	0.50	0.58	0.62
Lorentzian (eV)	0.155	0.155	0.17	0.17	0.19
Spin-Orbit splitting (eV)	0.45	0.45	0.69	0.69	1.24
Branching Ratio	0.666	0.666	0.666	0.60	0.70
K.E. shift of S_1 (eV)	-0.40	-0.50	0.28		
Bulk K.E. position (eV)	46.18	46.22	24.39	24.48	33.70

5.4.2 Discussion on the parameters used in the fitting procedure

Listed in Table 5.1 are the parameters used to fit the photoemission core levels. Values for the Lorentzian and spin orbit splitting for all three core levels are consistent with other studies of GaAs surfaces [8,9,10]. Branching ratios were equal to the theoretical value of 2/3 except for two cases, the As 3d and Sb 4d levels when the reconstruction was formed. This is probably due to a diffraction effect where the intensity of one spin orbit component is reduced due to destructive interference of the emitted photoelectrons.

The Gaussian broadening for the As 3d and Ga 3d core levels of the clean surface differ by only 0.03 eV. For the $(2\sqrt{3}\times2\sqrt{3})$ reconstruction the Gaussian broadening is however significantly larger for both core levels. This increase in the Gaussian of 0.10 eV for As and 0.08 eV for Ga is quite large. The possibility of an extra core level component being needed to fit the spectra was discounted as an extra component in the fitting procedure reduced to zero intensity in both cases. The Sb 4d core level at 500°C was fitted with a Gaussian width of 0.62 eV. This broadening could be due to surface disorder, i.e. the surface at 500°C has more defects per unit area than the (2×2) clean surface and this broadens the photoemission features.

Another factor which was taken into account was the possibility of asymmetric Doniach-Sunjich (DS) broadening for the Sb 4d core levels. This effect is associated with core level photoemission spectra from metals [11] and has been observed for Sb overlayers of ~30 ML [12]. No DS broadening was needed to fit an Sb 4d doublet at any stage in the experiment - the relevant parameter was always zero when the DS line shape was included in the fitting.

5.5 The structure of Sb-GaAs(111)A ($2\sqrt{3}\times2\sqrt{3}$) R30°

A model for the Sb-GaAs(111)A ($2\sqrt{3}\times2\sqrt{3}$)R30° is proposed in the following way. An electron counting model [13] has been successful in describing III-V semiconductor surfaces. The model is based on the principle that no electron states above the valence band maximum (VBM) are allowed at the surface. For this condition to be fulfilled all Ga sp^3 dangling bonds must be empty at the surface whereas those of the As or Sb are full. There is, therefore, a charge redistribution at the surface which involves removing excess charge from the Ga atoms and placing it into the As or Sb dangling bonds. Ga is a Group III element so each of the four tetrahedral bonds contains 3/4 valence electrons. The Group V atoms contain 5/4 electrons per tetrahedral bond. In the case of bulk material each Ga-As bond therefore contains the requisite two electrons, but at the surface charge redistribution is necessary to ensure that the surface is semiconducting. As every unit cell of the surface reconstruction is identical we only need to consider the redistribution of charge within one unit cell to satisfy the electron counting model for the whole surface. Consider a Ga terminated surface with a ($2\sqrt{3}\times2\sqrt{3}$) unit cell : this has an area of 12 times the (1×1) unit cell of a bulk (111) plane. There are therefore 12 Ga atoms or $12 \times \frac{3}{4} = 9$ electrons per surface unit cell which cannot remain on the Ga atoms but are used in filling the partially full dangling bonds of the adsorbed Sb atoms. This redistribution empties the Ga dangling bonds and ensures that there are no filled states above the conduction band minimum.

The most likely bonding configuration for a sub monolayer coverage of Sb is the trimer, in keeping with the manner in which isoelectronic As bonds to both the (111)A and (111)B surfaces [7, 14]. Single Sb adatoms might also be possible as one adatom requires that exactly the same amount of surface charge be transferred from the Ga atoms as does one trimer to satisfy the electron counting rule and therefore stabilise the surface. On other

(111) surfaces like Si and Ge Group V atoms can form sub monolayer coverages with either a trimer or an adatom basis so the two situations are generally similar [15, 16].

An Sb trimer consists of 3 atoms each with the usual 4 tetrahedral sp^3 hybrid bonds. Each trimer bonded to the surface then has 9 bonds, i.e. three Sb-Sb bonds, three Sb-Ga bonds and three full dangling bonds protruding into the vacuum. We can see that these 9 bonds need to be filled with 18 electrons, 15 of which already exist on the 3 pentavalent Sb atoms and the remaining three electrons are provided from the surface Ga atoms as described above. The 9 electrons available from the surface Ga atoms will therefore provide the extra charge needed to stabilise 3 Sb trimers per $(2\sqrt{3}\times2\sqrt{3})$ surface unit cell. A model for this is shown in figure 5.7. The model depicts Sb trimers over the H_3 sites but could also exist over the T_4 sites, i.e. directly above the As atoms in the surface bilayer underneath.

The growth study described above in section 5.2 above gave an estimate of the coverage of Sb on the surface at this point as 0.9±0.1Å. Also derived was an estimate of the thickness of 1 ML of adsorbate at 2.0±0.1Å. This means that the final coverage of Sb is 0.5±0.1 ML, which is below the coverage of the model described in this section. As mentioned in the last paragraph, there are 9 Sb atoms in the $2\sqrt{3}$ unit cell which has an area of 12 bulk plane (1×1) unit cells. So the structural model given above predicts a coverage of 9/12 = 0.75 ML of Sb terminating the surface. It is difficult to reconcile this difference between the coverage estimated from the growth study and that of the structural model.

A major structural difference exists between the structure shown in figure 5.7 and the original clean surface. The difference is that the Ga vacancies of the (2×2) clean surface have been filled by Ga atoms. Justification for this is found by looking at the structural transition which happens on the clean GaAs(111)B surface at the same temperature at which the $(2\sqrt{3}\times2\sqrt{3})$ structure forms on this, the (111)A surface. GaAs(111)B shows a transition from a (2×2) surface terminated by 1.75 ML of As to a $(\sqrt{19}\times\sqrt{19})$ R23.4° where the surface motif is a ring of 12 Ga atoms and 6 As atoms This surface is considerably more Ga rich than at the lower temperature (2×2) situation [14]. It has been found, by Avery et. al. [17], that if this transition took place under a flux of As_4, Ga began to form the hexagonal rings on top of the original trimer terminated surface. These Ga atoms could have migrated across the surface as free adatoms but must have originated from the bulk material as there was no molecular flow of Ga to the surface nor Ga back-

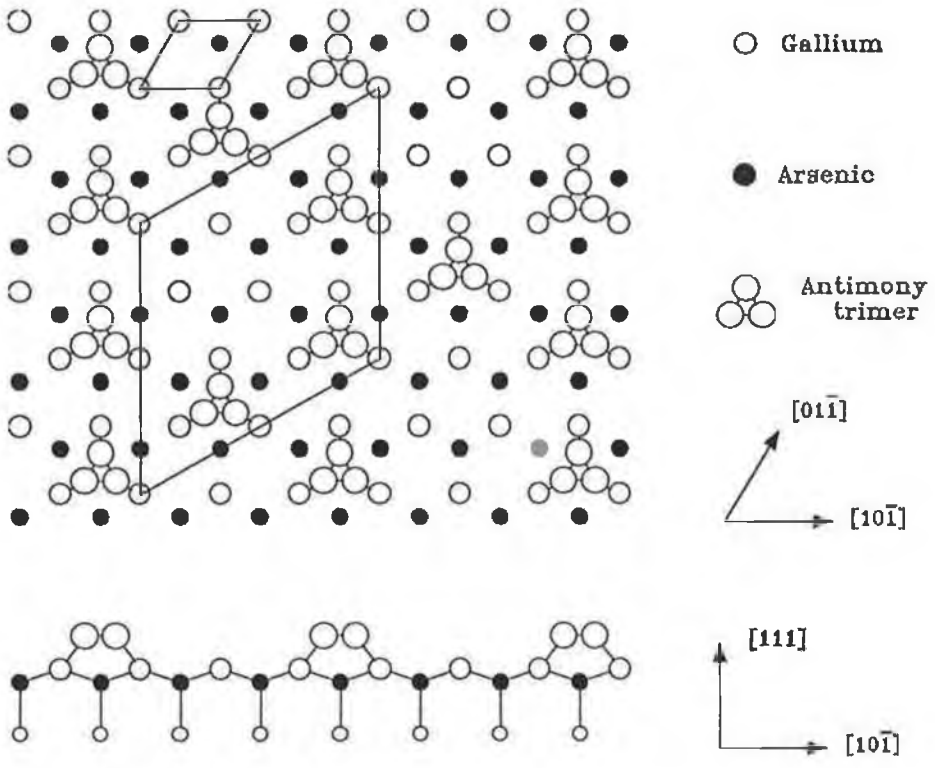

Figure 5.7 A model for the (2√3×2√3) reconstruction of the Sb-GaAs (111)A surface, based on photoemission and LEED evidence, in agreement with the electron counting model. The (2√3×2√3) unit cell and the bulk (1× 1) unit cell are shown for comparison.

pressure in the chamber. This diffusion of Ga to the surface was found to take place at 500-525°C and could be the early stages of Ga droplets forming at the surface which occurs at ~650°C. At this high temperature all GaAs surfaces contain metallic gallium but at the temperature range concerning the $(2\sqrt{3}\times2\sqrt{3})$ surface it is possible that Ga diffuses from the bulk and becomes involved in surface reconstruction.

Further annealing to 600°C causes the complete desorption of Sb and sharp (2×2) LEED pattern with a low background is recovered. It is likely that the surface is described at this stage by the (2×2) Ga vacancy model, the Ga 3d core level is consistent with this but there is no surface shifted component in the As 3d spectrum. A further photoemission study with higher experimental resolution could clarify the exact nature of the surface at this stage.

5.6 LEED Simulation of the structural model

Shown in Figure 5.8 is the result of the LEED simulation of the structural model described above. The form of the $(2\sqrt{3}\times2\sqrt{3})R30°$ pattern is reproduced well but the spots have an unusual shape. The profile of the spots have the shape of the unit cell in reciprocal space. This is an artefact of the simulation program.

5.7 Electronic properties

The Fermi level (E_f) of the GaAs(111)A clean surface is pinned midgap due to inhomogeneous surface band bending. This is caused by defects in the surface crystal structure. It is useful to know whether an adsorbed species passivates the surface, i.e. reduces the band bending. Group IV elements such as S and Se, for instance, reduce band bending on GaAs(100) surfaces [18]. The clean surface position of E_f was found by comparing the energy of the valence band maximum with the Fermi level of the molybdenum holder on which the samples were mounted. An Ohmic contact between the spade and sample was assumed because of the high doping of the samples used and the Indium bonding used to mount the samples. The change in E_f was monitored by finding the binding energy of the bulk Ga component relative to that of the clean surface at each stage in the annealing process. Any shift in the binding energy of the Ga core level will be accompanied by an equal shift in the energy of the valence band maximum (VBM).

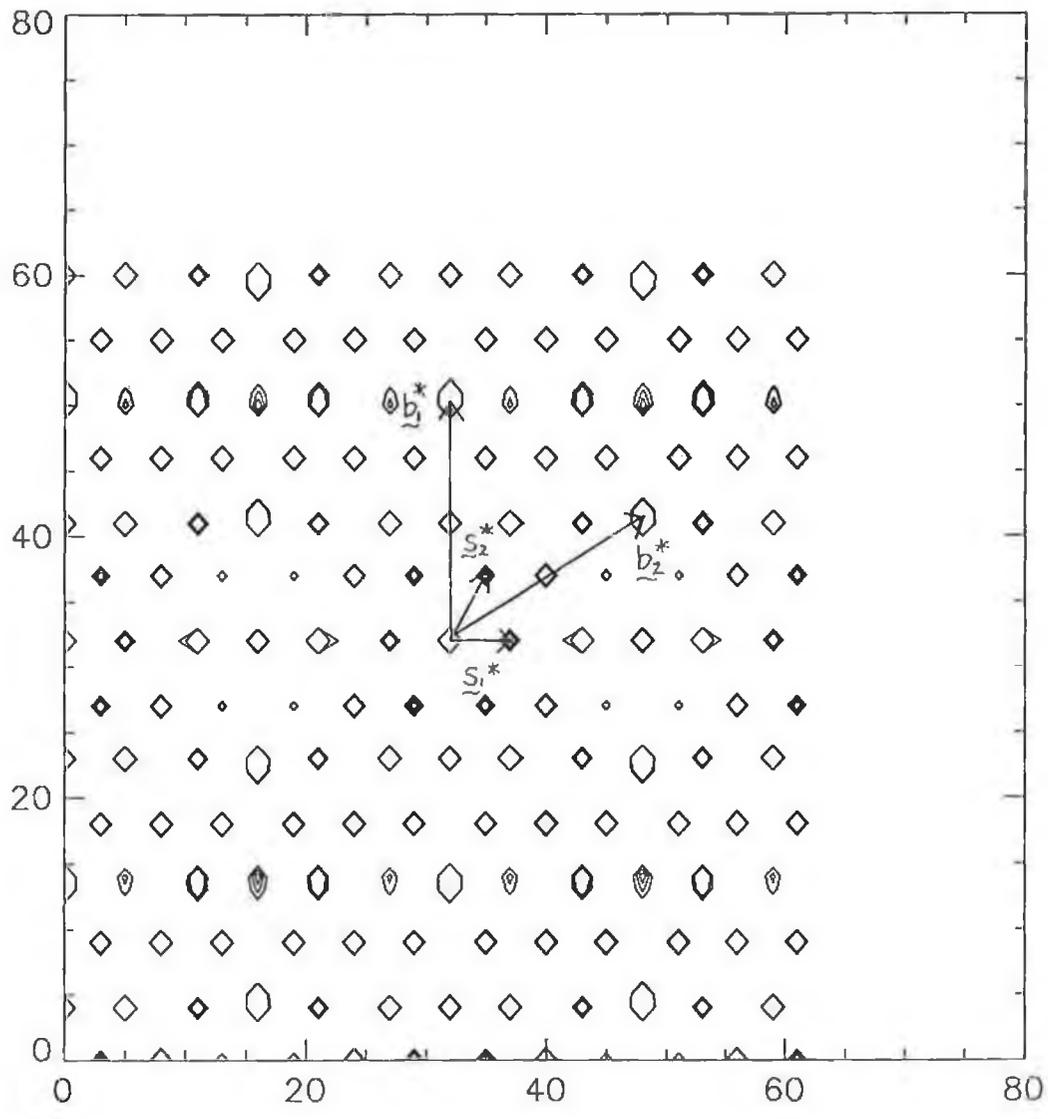

Figure 5.8 LEED simulation of the $(2\sqrt{3}\times2\sqrt{3})R30°$ pattern from the structural model described above. The axes are labelled in pixel numbers. Reciprocal lattice vectors are drawn to distinguish bulk and surface spots.

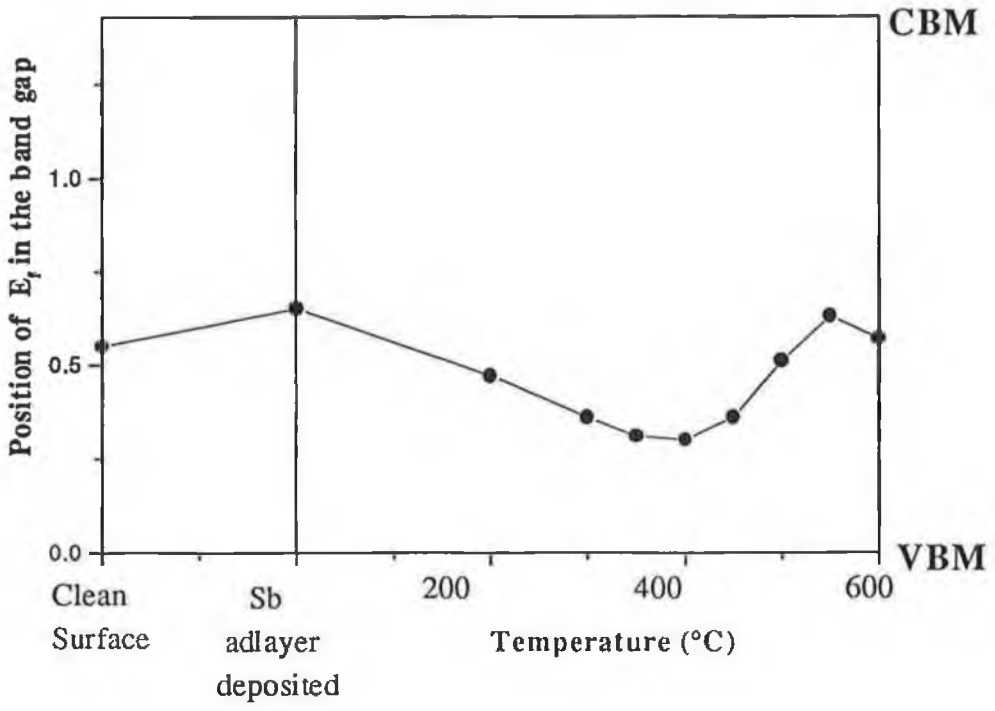

Figure 5.9 The position of E_f in the band gap as a function of temperature for Sb-GaAs(111)A. The samples were doped p-type so that in the bulk crystal E_f is just above the valence band maximum.

Variation in the binding energy of the VBM is conveniently expressed as the variation of the position of E_f in the band gap. Figure 5.9 shows the position of E_f through the experiment. Because the GaAs(111)A samples are doped p-type, E_f in the bulk is just above the valence band maximum.

The clean surface position of E_f was found to be 0.55 eV above the VBM. This is close to the middle of the band gap which is 1.46eV. The band bending reduced to 0.3 eV after annealing the sample at 400°C after which the band bending began to increase, reaching a maximum of 0.63 eV at 550°C. The clean surface restored after the desorption of Sb at 600°C had band bending of only 0.02 eV higher than the starting clean surface. These estimates of the changes in the band bending are relative to the starting clean surface and are accurate to 0.01 eV. Knowledge of the absolute value of the band bending at any stage is limited by the error in the estimate of the band bending of the clean surface which is ~0.05eV.

5.8 Summary

The initial growth of Sb on the GaAs(111)A surface is consistent with the Stranski-Krastanov mode. Annealing to a temperature of 500°C produced a $(2\sqrt{3}\times2\sqrt{3})R30°$ surface reconstruction. A possible model for this Sb termination of the surface contains 3 Sb trimers and 3 Ga rest atoms per surface unit cell. This structural model relies on a process where Ga diffuses from the bulk and fills the Ga vacancies of the clean surface. The deposition of Sb increased the clean surface band bending by 0.15eV. Annealing caused the surface band bending to increase to 0.08 eV above the clean surface value at the point where the reconstruction was formed. When the Sb desorbed at 600°C, the (2× 2) symmetry of the clean surface was restored as was the size of the clean surface band bending.

References for Chapter V

1. L.C. Feldman, J.W. Mayer, *Fundamentals of Surface and Thin Film analysis*, North Holland (1986)

2. R.M. Feenstra and P. Martensson, Phys. Rev. Lett. 61 447 (1988)

3. T.D. Golding, J. A. Dura, W.C. Wang, A. Vigliante, S.C. Moss, H.C. Chen and J.H. Miller, Appl. Phys. Lett. **63** (8) 1098 (1993)

4. D.G. Castner and G.J. Somorjai, Chemical Reviews, **79** (3) 233 (1979). This reference contains a tabulation of data reported by LEED studies on a wide variety of surfaces.

5. M.A. Van Hove, W.H.Weinberg and C.M. Chan, *Low Energy Electron Diffraction*, (Springer-Verlag, Berlin, 1983)

6. S.Y. Tong, G. Xu and W. N. Mei, Phys. Rev. Lett. **52**, 1693 (1984)

7. J.M.C. Thornton, P.Weightman, DA. Woolf and C. J. Dunscombe, Phys. Rev. B **51** 14459 (1995)

8. J. M. C. Thornton, P. Weightman, D. A. Woolf, and C. J. Dunscombe, Phys. Rev. B **51**, 14459 (1995).

9. G. LeLay, A. Kahn, D. Mao, Y. Hwu and G. Magaritondo, Phys. Rev. B **43** 14301 (1991)

10. T. Miller and T._C. Chiang, Phys. Rev. B **29** 7034 (1984)

11. L.Ley and M. Cardona, *Photoemisssion in Solids Vol. I*, Cap. 5 (Springer-Verlag, 1979)

12. Colm Stephens, PhD thesis, University of Dublin, 1993

13. M.C. Pashley, Phys. Rev B **40**, 10481 (1989)

14. D.K. Biegelsen, R.D. Bringans, J.E. Northrup and L.E. Swartz, Phys. Rev. Lett. **65**, 452 (1990)

15. K.J. Wan, T. Guo, W.K. Ford and J.C. Hermanson, Surf. Sci. **261** 69 (1992)

16. K.J. Wan, W.K. Ford, G.J. Lapeyre and J.C. Hermanson, Phys. Rev. B **44** 6500 (1991)

17. A.R. Avery, E.S. Tok and T.S. Jones, Surf. Sci. Lett. **376** L397 (1997)

18. T. Scimeca, Y. Watanabe, R. Berrigan and M. Oshima, phys. Rev. B **46** 10210 (1992)

Chapter VI

Bismuth on GaAs(111)A

6.1 Introduction

In this chapter, the growth of Bi on the GaAs(111)A-(2×2) surface is discussed. No change in the clean surface symmetry is induced by the Bi deposition or by the annealing process. Two chemical environments for the Bi overlayer are observed. One is associated with a Bi-Ga chemical bond at the surface and the other with bulk-like Bi. Above this Bi interfacial layer, further growth was in a layer plus island mode. The interfacial Bi remained on the surface up to 350°C. The remaining Bi had fully desorbed at 425°C. A structural model with (2×2) symmetry is suggested to explain the Bi-Ga bonding in the R.T. to 350°C temperature range. The effect of the Bi overlayer on the surface band bending is also discussed.

Core level photoemission spectroscopy is used to find the growth mode of Bi and to investigate the chemical bonding at the surface. A photoemission spectrum of the relevant core levels is shown in figure 6.1.

6.2 The growth of Bismuth on GaAs(111)A

For the series of Bi depositions on the GaAs(111)A surface, the Bi 5d core levels are fitted with two components. Figure 6.2 shows fitted Bi 5d core levels for three depths of Bi on the substrate. This was also found for the Sb-GaAs(111)A system described in chapter V and in a similar manner, one core level component is associated with Bi lying directly on the surface and the other is associated with Bi on top of this interfacial layer. The two components are labelled 'Bi_S' and 'Bi_B' respectively, the Bi_B component having the lower binding energy (higher kinetic energy).

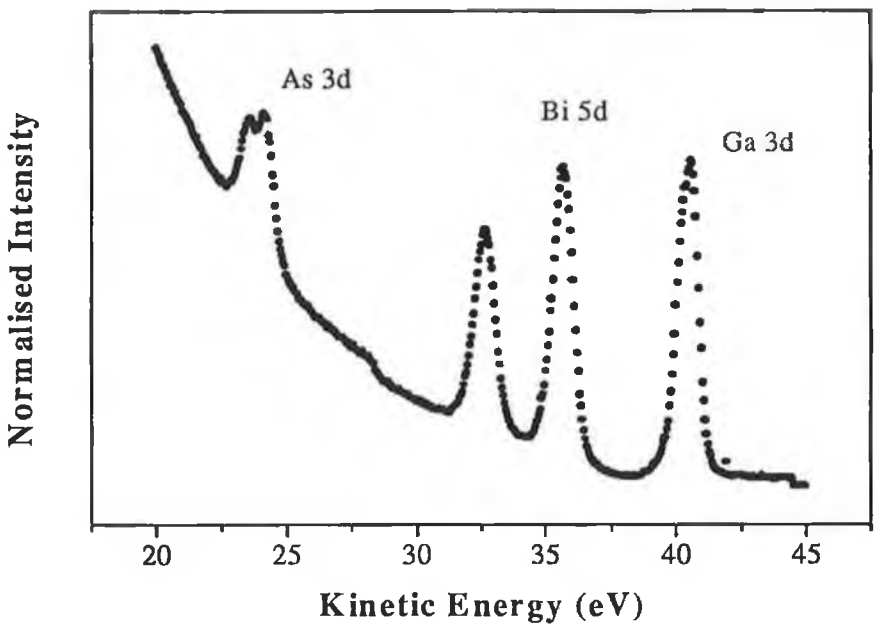

Figure 6.1 A wide scan spectra of the As 3d, Ga 3d and Bi 5d core levels recorded at a photon energy of 70eV.

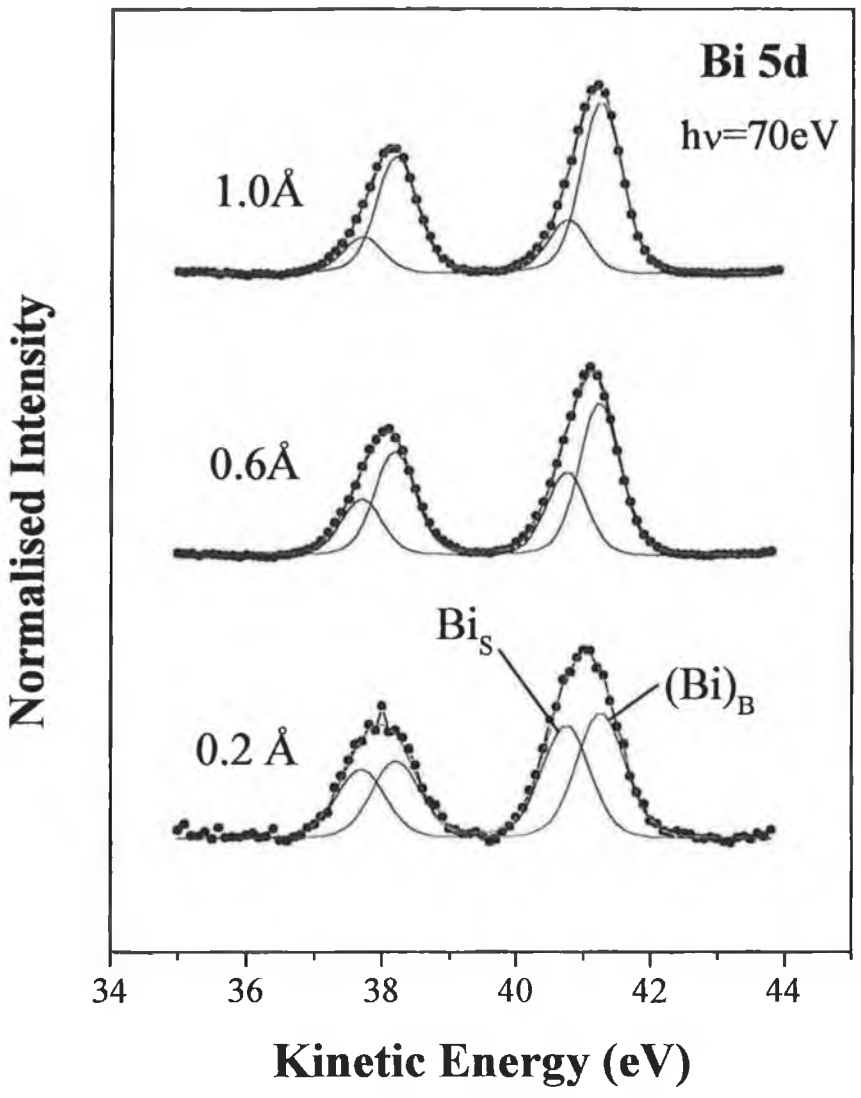

Figure 6.2 Fitted Bi core levels at successive coverages during the Bi growth study.

The intensities of the two Bi core level components are plotted as a function of the depth of Bi on the surface in figure 6.3. Also shown is the effect of annealing on these photoemission intensities. This graph is qualitatively similar to that for Sb growth in the preceding chapter. The Bi_B component increases linearly and than the slope of the curve changes at 1.4±0.1 Å. This change in slope of this component's intensity is indicative of the completion of one layer of Bi. As the change in slope occurs at 1.4±0.1 Å it is unlikely

that a full monolayer was deposited. It is proposed that this Bi layer is on top of an interfacial Bi layer which is identified with the Bi_S component. The growth curve shows that this photoemission feature saturates in intensity when the total Bi coverage is approximately 0.5Å.

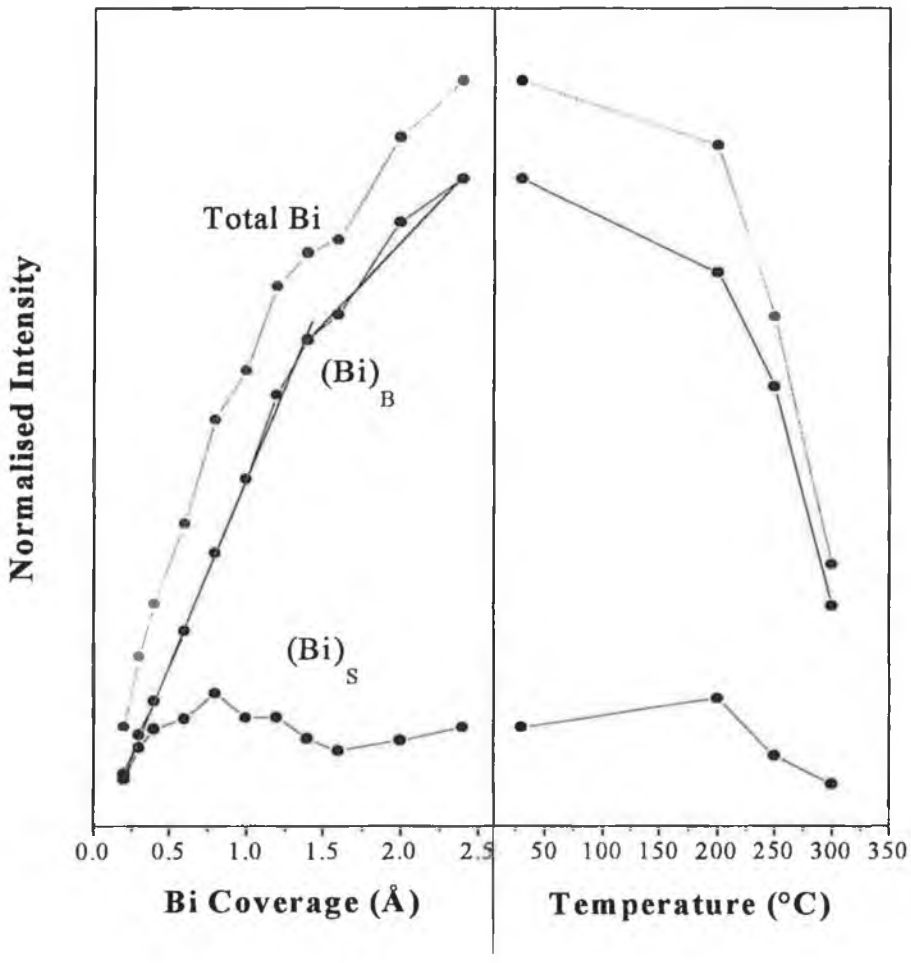

Figure 6.3 Normalised intensities of the $(Bi)_B$ and $(Bi)_S$ core level components. The lines are drawn to guide the eye.

At the start of the experiment, the decapped GaAs(111)A substrate gave a sharp (2×2) LEED pattern. The As 3d and Ga 3d core level photoemission spectra (figure 6.4 (a) and (b)) were, as in the case of the Sb-GaAs(111)A experiment, consistent with the Ga vacancy model (figure 4.1, section **4.2.1**). It is therefore assumed that this vacancy

structure describes the initial clean surface. There were two chemical environments for the deposited Bi after the initial deposit of 0.25Å. As the growth curve is consistent with the completion of a Bi layer on top of an interfacial layer, a suggestion as to how the interfacial Bi is bonded to the surface is now given. There are four possibilities:

(i) Interfacial Bi is bonded to the surface at crystal defects. There is no evidence for this. Even if the defect sites were most favourable for bonding, the surface would need to be at high temperature to allow diffusion of adatoms across the surface.

(ii) The Bi atoms of the interfacial layer rest in the Ga vacancies. If this is the case, the Bi could be bonded to the As atoms in the layer below the surface which are exposed due to the existence of the Ga vacancy. This situation violates the electron counting principle because there would be a shortfall of three electrons per (2×2) unit cell. It is therefore assumed unlikely.

(iii) Bismuth is bonded directly to the Ga atoms in the top layer of the substrate. This situation is difficult to justify as the clean surface photoemission data is consistent with the vacancy model structure. The formation of Bi-Ga bonds would violate electron counting for a (2×2) unit cell where there is a Ga vacancy. Electron counting violation is a possibility as in (ii) above but there is not enough evidence in this work to be sure that this is the case.

(iv) A variation on (iii) is that there are some regions of the starting surface which do not have the vacancy structure. If this is the case than the only other acceptable alternative is the As trimer termination. The As trimer termination was predicted by theoretical calculations [1] and later verified by STM [2]. The STM study also included photoemission results and the two surface structures show Ga 3d and As 3d core levels which are significantly different. The starting surface here has surface shifted core level components to low binding energy for Ga and to high binding energy for As (figure 6.4(a) ,(b)). In this trimer model, the surface core level components are on the opposite side of the bulk component for both As and Ga. Although the clean surface photoemission data here does not give evidence for the As trimer structure, if some small domains of the As trimer structure exist, than As trimers could be replaced with Bi trimers without violating the electron counting principle.

Of the four possibilities for the bonding of interfacial Bi given above, it is not possible to definitively choose the correct one with the growth study results. There is, however, more information with regard to the nature of Bi growth. The Ga 3d core level spectrum recorded when the Bi overlayer was deposited is shown in figure 6.4(a). A surface shifted core level component on the high kinetic energy side is needed to obtain a good curve fit. This is consistent with surface Ga atoms bonded to Bi trimers - the same type of core level shift was found for surface Ga bonded to As trimers in the work of Thornton et. al. (As and Bi are both Group V elements). It is most likely that the Bi bonded to Ga at the surface is the Bi associated with the low kinetic energy Bi 5d component, i.e. the 'interfacial' Bi. If this is correct, then possibility (iv) above is the most likely situation for the bonding of the interfacial Bi.

The main conclusion drawn from this study of Bi growth concerns the Bi 'on top' of the interfacial layer. This Bi, identified with the Bi_B core level component, grows initially in the form of a full layer over the interfacial Bi. The change in slope of the growth curve at 1.4±0.1 Å is consistent with the completion of a full layer. Upon completion of this layer, further growth could be in the form of islands, more layers or possibly statistical deposition [3]. In statistical deposition, the adatoms are randomly distributed on the surface and at higher coverages coalesce to form patches whose areas have a Poissonian distribution. For the case of continued layer by layer growth, the curve could not be successfully fitted to an exponentially increasing envelope function [4], so this growth mode is discounted. The possibility of continued growth by islanding (Stranski-Krastanov growth) is the most probable growth mode. As there is an interfacial Bi layer and a Bi layer on top of this, if further growth is by islanding then the growth mode is 'modified SK growth', i.e., two layers plus islanding. This was found for Bi growth on the GaAs(110) surface in a photoemission study by J.J. Joyce et. al. [5]. Ludeke et. al. [6] found that the growth mode for that system was orthodox SK growth - one layer plus islanding but this conclusion was based on a plot of the *total* Bi core level intensity only.

The point at which the intensity of the Bi_S component changes in figure 6.3 is 1.4±0.1 Å. The covalent radius of Bi is 1.46 Å and for Bi-GaAs(110) surface the first Bi monolayer is a height of 2.38Å (ab initio) to 2.52Å (LEED) above the surface [7]. There is some discrepancy here which may be explained by the definition of one monolayer as one atom per surface unit mesh. In this study it seems that one Bi atom is not adsorbed on the surface for each unit mesh. If the Bi coverage is less than this, then the 1.4 Å 'break point'

above corresponds to the deposition of a Bi layer where there is less than one Bi atom per (1×1) unit mesh.

In figure 6.3, the effect of annealing on the intensity of the Bi 5d core level components is also shown. Both components simply reduce in intensity over the temperature range for which Bi remained on the surface. The slight increase in the intensity of the Bi_S component at 250°C is due to the fact that some of the Bi above the interfacial Bi layer had desorbed at this temperature. This means that the photoelectrons emitted from the interfacial Bi are less attenuated than was the case before the anneal process. In chapter V, this effect for Sb on the GaAs(111)A was shown to be more extreme. This was because there was relatively more Sb deposited on the surface in that growth study.

6.3 LEED Results

At the start of the experiment, the clean surface showed a clear (2×2) LEED pattern. During the growth study described in the preceding section, a poor quality (1×1) LEED pattern was observed when 0.8Å Bi was deposited on the surface. No LEED pattern was observed at the end of the series of depositions. The (1×1) pattern was seen again upon annealing the sample to 110°C. After annealing to 250°C a (2×2) LEED pattern was observed with intense (1×1) spots due to the bulk GaAs while the (2×2) spots were clear but of apparently lower intensity than was the case for the clean surface. When the Bi had desorbed from the surface at 425°C a clear (2×2) pattern was observed.

These LEED results are unusual, especially where no pattern was seen at the end of the deposition sequence - a (1×1) pattern due to the bulk GaAs should be seen with only 2.4Å of Bi on the surface. In this work an energy range of approximately 20-200eV was used for the low energy electrons. The electron mean free path in this energy range in (111) oriented GaAs is approximately 10-25Å [8]. This was calculated from an empirical expression which models the universal curve of electron mean free path as a function of electron energy above the Fermi level (section 2.3). In terms of the kinetic energy of the electron, Van Hove et. al. [9] quote the sampling depth of LEED as 10-20Å for 10-300eV electrons incident on metal surfaces. For this reason the LEED system should have imaged the (1×1) pattern when 2.4 Å of Bi was present on the surface. That no LEED pattern was observed at this stage is not understood.

A separate study of this system where a total of 1.6Å of Bi was deposited initially was also carried out. In this case a clear (2×2) LEED pattern was observed throughout the whole experiment, from the initial clean surface, through three Bi depositions and the anneal series and for the recovered clean surface after the Bi had desorbed. Photoemission core level spectra in both experiments were successfully fitted using the same number of core level components. The fitted core levels of figure 6.4 (a)-(c) were taken from this latter experiment.

The anneal to 110°C restored the (1×1) LEED pattern. At this stage there was no significant surface reconstruction. The recovery of the (2×2) pattern after some further Bi desorption at 250°C shows that a surface reconstruction was present. The possible surface structure of the system at this stage is discussed in relation to the core level photoemission results in section 6.5.

6.4 Photoemission Results

Core level photoemission spectra for the As 3d, Ga 3d and Bi 5d states are shown in figure 6.4. A (2×2) LEED pattern was observed at each stage in this experiment. Spectra are shown for all three core levels at temperatures where any one of them changed significantly. These spectra were difficult to fit and the usual criteria of ensuring consistent fitting parameters was impossible to strictly adhere to in respect of the Gaussian broadening. This value was increased from the clean surface value for the As and Ga levels to ensure good fits at the higher annealing temperatures. The same was found for the systems described in other chapters in this thesis and is assumed to be due to surface disorder.

Thornton et. al. [2] have published core level photoemission data for the GaAs(111)A surface. In their study the transition from the As trimer surface termination to the Ga vacancy termination in the 315°C to 400°C temperature range was studied in detail. The As 3d and Ga 3d core levels of the clean surface in figure 6.4 (a) and (b) are consistent with the Ga vacancy model ([2] & section 4.2.1). A comparison between their results for the Ga vacancy structure and those of figure 6.4 is now given. The clean surface core level shifts (SCLS's) are labelled S_1 for both core levels. Shown in Table 6.1 are the fitting parameters which differ between the two studies. Other parameters such as Lorentzian,

branching ratio and spin orbit splitting are the same in both studies. It is important to note that in the work of Thornton et. al. the intensity ratios were quoted for core levels recorded with 95 eV radiation, while this work was done with 70 eV radiation. The intensity ratios are therefore not comparable.

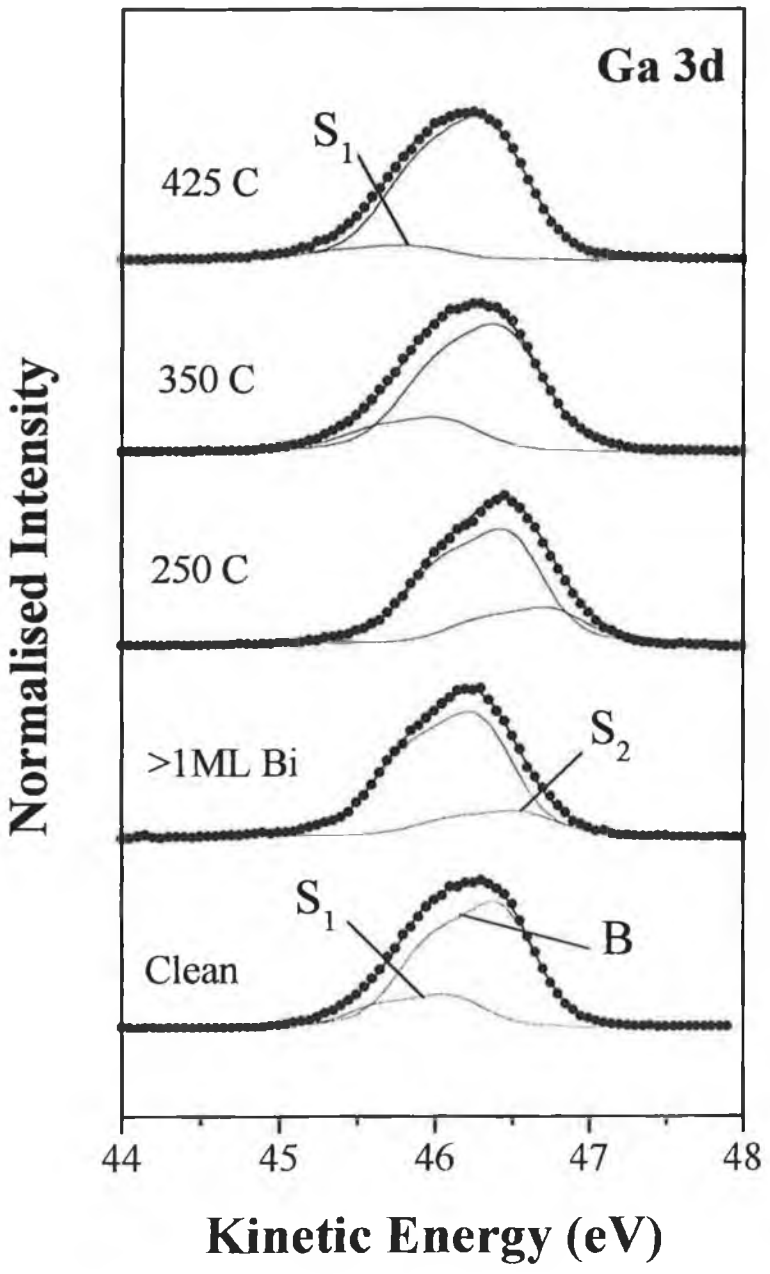

Figure 6.4(a) Fitted Ga core levels for Bi-GaAs(111)A recorded at a photon energy of 70 eV.

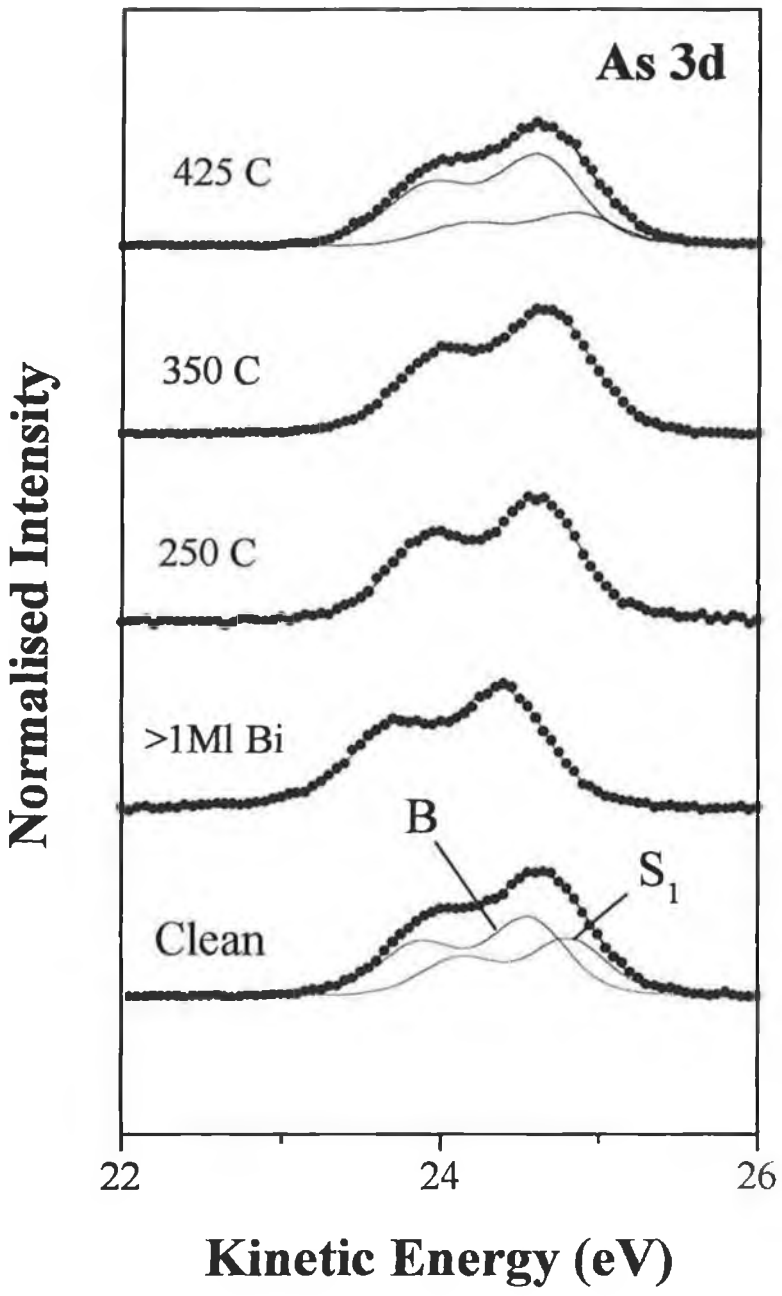

Figure 6.4(b) Fitted As core levels for Bi-GaAs(111)A recorded at a photon energy of 70 eV.

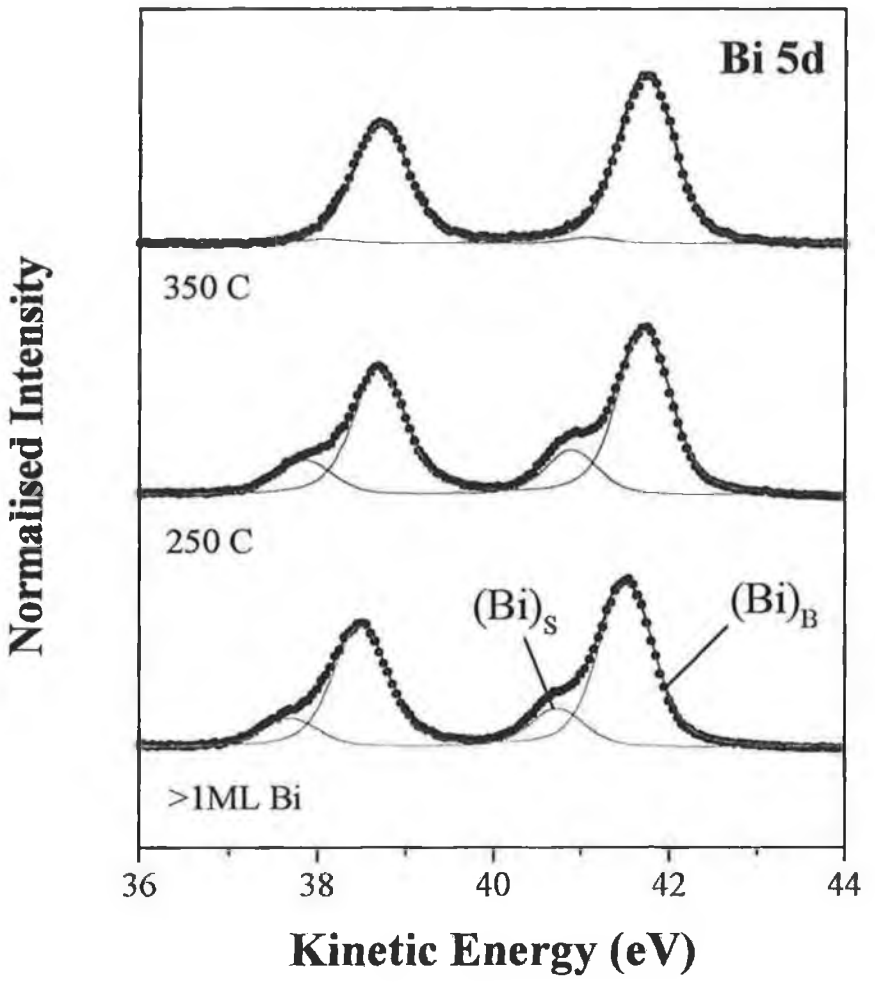

Figure 6.4(c) Fitted Bi core levels for Bi-GaAs(111)A recorded at a photon energy of 70 eV.

Table 6.1

	As 3d		Ga 3d	
	Figure 6.4(a)	Thornton et. al.[2]	Figure 6.4 (b)	Thornton et. al.
K.E. shift of S_1	0.26 (eV)	0.31	-0.32	- 0.31
Intensity Ratio S_1/Bulk	0.73 (hν = 70 eV)	0.62 (hν = 95 eV)	0.27 (hν = 70 eV)	0.39 (hν = 95 eV)
Gaussian	0.45 (eV)	0.40	0.48	0.43

The agreement is good for the SCLS's. The Gaussian width is higher in this work by 0.05 eV, so the experimental resolution here was lower. The S_1/Bulk intensity ratios are for different photon energies so a direct comparison cannot be made because Thornton et. al. give intensity ratio values for 95 eV radiation only. The binding energy difference between the As 3d and Ga 3d bulk components should be constant. The energy separation for the GaAs(111)A surface was quoted as 21.95 eV [2]. It is 21.85eV for the GaAs(001) surface [10]. In this work $\Delta E = 21.87 \pm 0.05$eV.

Core level spectra recorded when the Bi was deposited are now discussed. Significant changes in the chemical bonding of the surface took place (figure 6.4). Only one bulk component is needed to fit the As 3d core level after the deposition of Bi and this remains the case until the Bi had desorbed at 425°C. For the Ga 3d core level, one surface shifted component, labelled S_2, on the high kinetic energy side of the bulk peak is needed to fit the data. It is assumed that this Ga surface environment is due to the Ga bonding to some of the deposited Bi. This Bi is identified with the Bi_S component in the Bi 5d core level spectra as discussed in the section 6.3.

As the surface was annealed, the core levels were qualitatively unchanged until the 250°C anneal. A slight increase in the relative intensity of the Bi and Ga surface components was

recorded. By annealing to 350°C, the Bi_S component had reduced to almost zero intensity and the Ga 3d S_2 component was no longer needed to fit the data. This is further evidence that the surface atoms producing the Ga S_2 and Bi_S are bonded together.

After the desorption of Bi at 425°C the Ga 3d and As 3d core levels are consistent with the Ga vacancy structure. The S_1/Bulk intensity ratios at the stage are 0.10 and 0.37 for Ga and As respectively. These ratios are within 40-50% of the clean surface intensity ratios shown in Table 6.1. This result shows that the clean surface left after the desorption of Bi is most likely of poorer crystalline quality than the original starting surface.

Core level fitting parameters are shown in Table 6.2. For comparison the parameters for the clean surface and the Bi covered surface at 250°C are given. It is unusual that the Gaussian for the Ga core level is lower for the 250°C anneal then for the clean surface. Usually the surface is more disordered when an overlayer is deposited and the Gaussian increases.

Table 6.2

	As 3d		Ga 3d		Bi 5d
	Clean Surface	(2×2)-Bi 250°C	Clean Surface	(2×2) - Bi 250°C	(2×2) - Bi 250°C
Gaussian	0.45	0.55	0.48	0.46	0.54
Lorentzian	0.17	0.17	0.155	0.155	0.23
Spin -Orbit splitting	0.69	0.69	0.45	0.45	3.03
Branching Ratio	0.666	0.666	0.666	0.62	0.666
K.E. shift of S_1 (eV)	0.26		-0.32	0.28	-0.82
Bulk K.E. position (eV)	24.55	24.62	46.42	46.48	41.71

6.5 The Structure of Bi-GaAs(111)A

A structural model for this system is difficult to propose. In the growth study experiment, only by annealing to the 250 -350°C temperature range was a LEED pattern indicative of a surface reconstruction observed. When the experiment was repeated, a (2×2) pattern was seen throughout the annealing process. There are four factors to take into account:

(i) The LEED pattern seen after annealing to 250 -350°C is (2×2).

(ii) The Ga 3d S_2 core level component at this stage is consistent with surface Ga bonded to Bi.

(iii) There is still a bulk like Bi structure above the Bi bonded to surface Ga

(iv) There is no evidence for a surface environment for As at this stage. If there are surface As atoms with bonding different to that of the bulk, they are not distinguishable from bulk As by core level photoemission.

There is no exact structural model that can be proposed from this. There are possibly domains of (2×2) structure with one Bi trimer per surface unit cell (figure 6.5) and some bulk like Bi elsewhere on the surface. Thermally induced diffusion of Bi might help to form this situation. If the Bi trimer model is correct, then these regions have no Ga vacancies. It is unlikely that Ga could diffuse from elsewhere to fill the vacancies at these low temperatures so vacancy-free domains would have to have been present from the start. This is a possibility even though the clean surface core levels are not consistent with it as described above.

6.6 Electronic Properties

The position of the Fermi level in the bulk band gap is shown in figure 6.6. The change in position of the Fermi level could be monitored by the change in the binding energy of the bulk component of the As or Ga 3d core level. These binding energies should vary with annealing temperature by exactly the same amount. This condition should be met to ensure accuracy in the core level fitting procedure. For the E_f position there is not perfect agreement between the two methods. There are discrepancies of up to 0.05eV, the

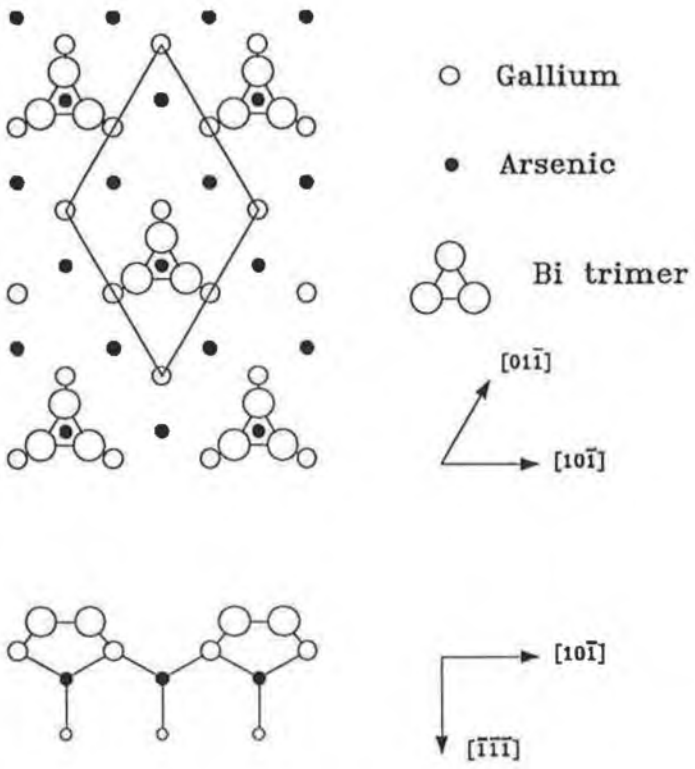

Figure 6.5 Structural model for a (2×2) Bi trimer termination of the GaAs(111)A surface.

separation of the data points in the core level spectra (figure 6.4(a)-(c)). This shows the difficulty of fitting this data. The disagreement is not large however.

Initially the band bending at the surface is increased, by approximately 0.15 eV, due to the deposition of Bi. On annealing, the band bending is reduced. After the desorption of Bi the total decrease in the band bending was 0.10-0.15 eV relative to the starting clean surface.

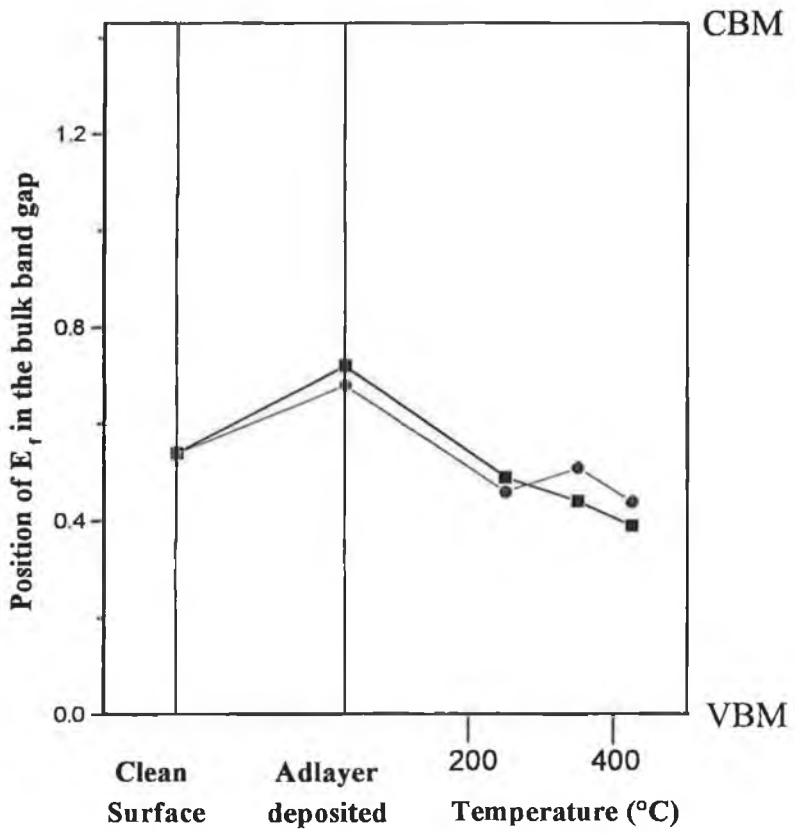

Figure 6.6 The position of the Fermi level in the bulk band gap throughout the experiment. Data shown are measured from the binding energy of the As core level bulk component (●) and the Ga core level component (■).

6.7 Summary

The initial growth of Bi on the GaAs(111)A surface is consistent with modified Stranski-Krastanov growth. No lowering of the clean surface (2×2) symmetry takes place due to the deposition of Bi. There was strong evidence for the formation of a Ga-Bi bond at the surface when the overlayer was deposited. During annealing, the (2×2) symmetry remained as did the Ga-Bi surface bond. The band bending at the surface was increased by 0.15eV by the deposition of Bi but began to increase as the sample was annealed. After the desorption of Bi, the band bending reduced by 0.10-0.15 eV relative to that of the clean surface.

References for Chapter VI

1 E. Kaxiras, et. al., Phys Rev. B **35** 9625 (1987)

2. J. M. C. Thornton, P. Weightman, D. A. Woolf and C. J. Dunscombe, Phys. Rev B **51** 14459 (1994)

3. Feldman, L.C. and Mayer, J. W., *Fundamentals of Surface and thin film analysis* (North-Holland 1986)

4. Luth, H, *Surfaces and Interfaces of Solids*, (Springer-Verlag 1993)

5. J.J. Joyce, J. Anderson, M.M. Nelson and G. J. Lapeyre, Phys. Rev. B, **40** 10412 (1989)

6. R. Ludeke, A. Taleb-Ibrahami, R.M. Feenstra and A. B. McLean, J. Vac. Sci. Technol. **B7**, 936 (1989)

7. These values are given in G.P. Srivistava, Rep. Prog. Phys. **60** 561 (1997) - ab initio calculation is from A. Umerski and G.P. Srivistava, Phys Rev. B **51** 2334, the LEED study is from W. K. Ford, T. Guo, D.L. Lessor and C.B. Duke, Phys. Rev. B **42** 8952.

8. Seah, M. P. and Dench, W. A., Surface and Interface Analysis, **1**, page 2 (1979)

9. Van Hove, M. A. et. al. *Low Energy Electron Diffraction*, (Springer-Verlag, 1979)

10. G. Le Lay, D. Mao, A. Kahn and G. Magaritondo, Phys. Rev. B **43** 14301 (1991)

Chapter VII

Antimony on GaAs(111)B

7.1 Introduction

A determination of the growth mode of Sb on GaAs(111)B was made from photoemission experiments. With a few monolayers of Sb deposited on the sample, a series of anneals was performed over the temperature range for which Sb remained on the surface. LEED and XPS data were taken at each stage in order to study the interaction of the overlayer with the substrate. The photoemission spectrum in figure 7.1 shows the three relevant core levels, Ga 3d As 3d and Sb 4d. Analysis of the core levels and changes in the LEED pattern are discussed and a model is described for a new reconstruction in the 500 to 550° C temperature range. During the annealing process the band bending at the surface was found to increase and the resulting Schottky barrier formation is also described.

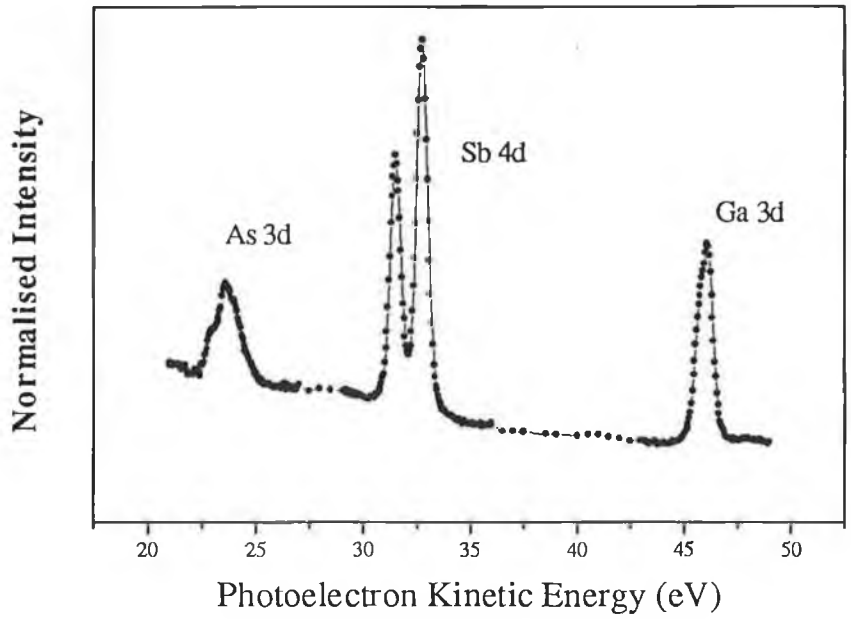

Figure 7.1 A wide scan photoemission spectra of the GaAs(111)B surface with ~8.0Å Sb deposited.

7.2 The growth of Antimony on GaAs (111)B

When the GaAs(111)B sample was decapped a clear (2×2) LEED pattern was observed. A gradual deterioration in quality of this pattern was noticed as Sb was deposited. A (2×2) pattern was still visible, though very diffuse, at the end of the deposition sequence. Approximately 11Å of Sb was on the surface at this stage. This diffuse patttern is indicative of domains of clean surface which are at least comparable in size with the coherence length of the LEED system (~100Å).

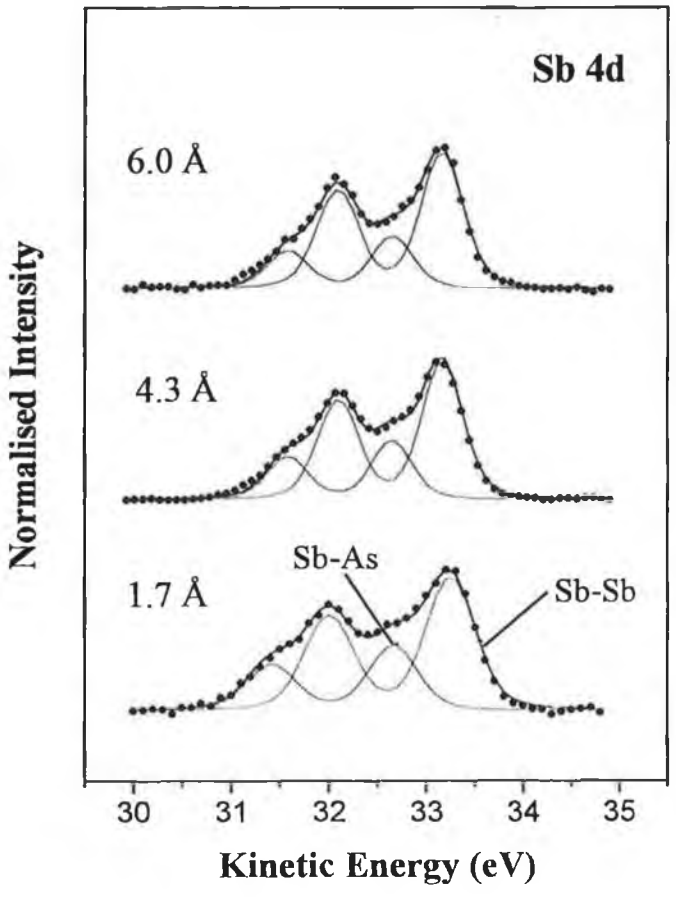

Figure 7.2 Fitted Sb core levels at various relative coverages during deposition. The photon energy used was 70eV.

Fitted Sb core levels from the initial stages of the deposition process are shown in figure 7.2. This core level has two components separated by 0.71eV, indicating two chemical environments for the deposited layer. One component is labelled Sb-Sb and the other Sb-As. As growth continues, the intensity of the Sb-Sb component increases linearly with the amount of Sb deposited while the Sb-As component almost saturates. This is illustrated in figure 7.3 where the total area under each of the two Sb components is plotted as a function of the depth of Sb on the surface. The linear increase of the Sb-Sb component is consistent with the growth of islands [1], i.e., the formation of three dimensional bulk-like structures containing Sb-Sb chemical bonds only (figure 7.4). Given that islanding accounts for the Sb growth, a justification is needed for labelling the Sb 4d core level component on the low kinetic energy side of the spectrum as 'Sb-As'. It could be proposed here that the Sb in the interfacial layer at the island/substrate interface is bonded to the As of the substrate. This Sb would have a different chemical environment than the bulk Sb and therefore give rise to a second component in the Sb 4d photoemission spectrum.

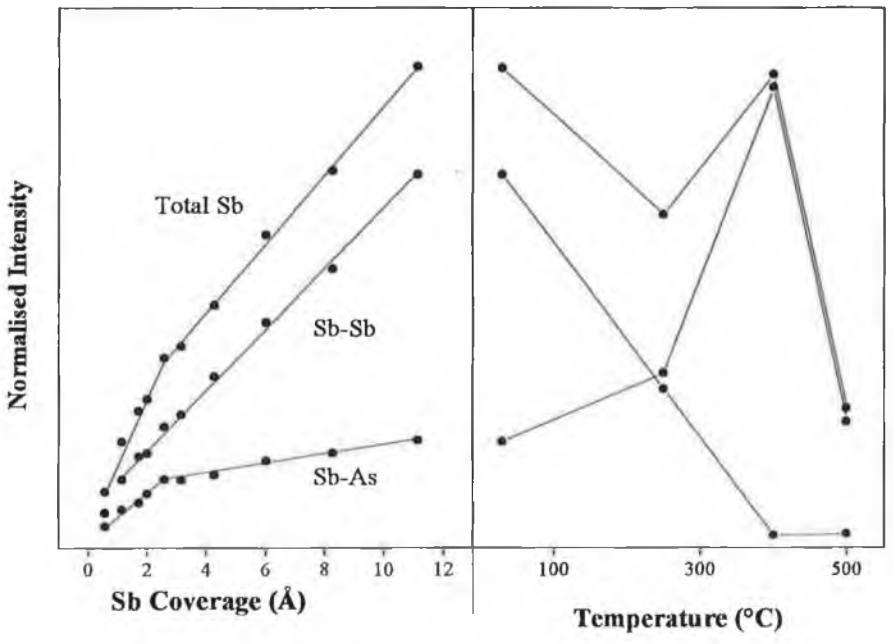

Figure 7.3 Normalised intensities of the bulk (Sb-Sb) and interfacial (Sb-As) components in the Sb 4d core level as a function of the amount deposited.

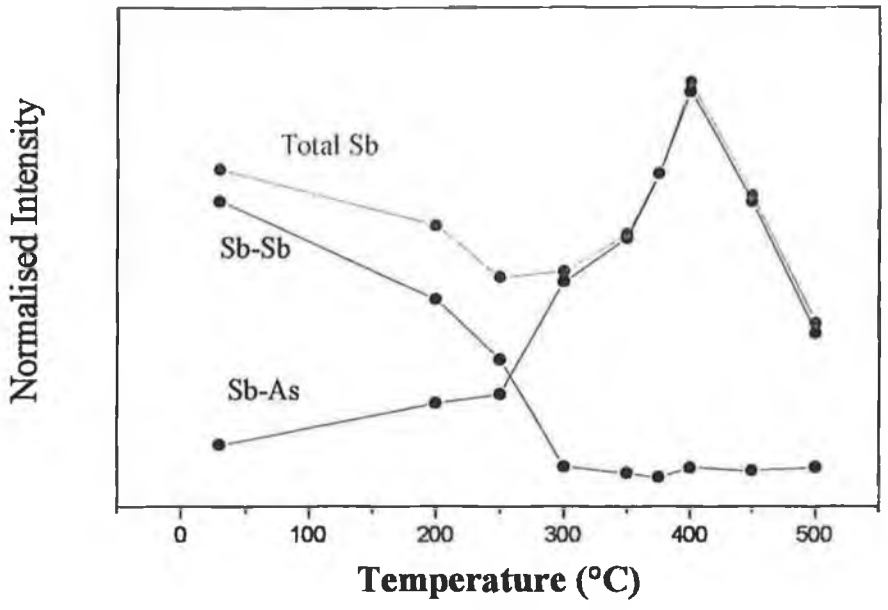

Figure 7.3 (b) A plot of the areas under the Sb 4d core level components during annealing. The data here is from a repeat of the above experiment.

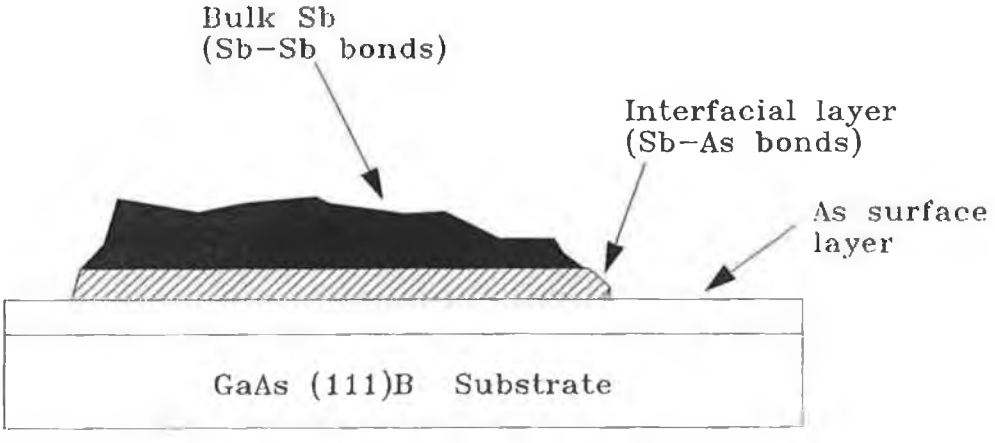

Figure 7.4 Schematic drawing of an island of Sb on a surface. The Sb of the interfacial layer is assumed to have different bonding than the Sb above it.

An STM study of this system by Moriarty et. al. [2] showed islanding in the early stages of growth which is consistent with the data presented here - bulk Sb grows on domains of an interfacial Sb layer. There was no evidence for any chemical substitution as the structure of the initial clean surface is, by photoemission evidence, unaltered. The intensity ratio of As trimer to As bulk components in the As 3d core level (figure 7.10(a)) is the same (0.62) for both the clean surface and after the deposition of 4 ML of Sb. The rest atom to bulk ratio is also unchanged at 0.19. No surface substitution has taken place and the interfacial Sb must be either bonded to As trimer atoms or else have fewer Sb-Sb bonds then the bulk Sb above them.

Even if the exact chemical nature of the interfacial layer is not known, the islanding model for the growth mode is appropriate. In the growth curve of figure 7.3, the total Sb core level intensity is plotted and this has a change in slope where 2.6Å of Sb was deposited. This depth of Sb is equivalent to aproximately 1 ML on the GaAs(110) surface where the average vertical height of Sb above the surface was found by LEED and ab initio calculation to be 2.35±0.05 Å [3, 4]. The point at which the curve changes slope is not however taken to be indicative 1ML point as it can be seen that there is a gradual increase in the intensity of the Sb-As component above 2.6Å indicating that a full monolayer has not been completed. The growth mode is therefore consistent with Volmer-Weber growth.

The effect of annealing on the intensities of the Sb 4d core level components is also shown in figure 7.3. As the annealing temperature increases there is an initial drop in the total Sb intensity. This might suggest that the Sb is simply desorbing but this is not the case as the total intensity then increases to a maximum at 400°C. An explanation for this is that initially some Sb desorbs from the tops of the islands and so the total Sb intensity decreases and this is followed by a thermally driven diffusion of the remaining Sb across the surface. If this is the case, the Sb should then form a layer on the surface which produces photoelectrons contributing to the Sb-As core level component. These photoelectrons are emitted straight into the vacuum without attenuation due to the bulk-like Sb islands on top as these islands no longer exist (the Sb-Sb component has almost reduced to zero at 400°C). It is only if the Sb spreads over the surface in this way that this decrease followed by an increase in the total intensity of the Sb core level can be explained. Figure 7.3 (b) shows a similar graph from a separate and more detailed study of the same system. The graphs agree qualitatively and the temperature where the intensity of the Sb-As component rises to maximum is the same for both. In the more detailed study it can be seen that at 400°C this Sb-As intensity is greater than the total Sb core level

intensity at room temperature. This further supports the explanation that the spreading out of the Sb enhances the signal precisely because there is no Sb 'on top' to attenuate these photoelectrons.

7.3.1 LEED Results

A diffuse (2×2) LEED pattern was observed after the deposition of ~4ML of Sb on the clean GaAs(111)B substrate. This pattern remained after annealing to 200°C and a series of temperature anneals were then performed with the annealing temperature increased in 50°C steps: increases of 25°C were used if the LEED pattern was seen to change radically. After annealing to 350°C the 'surface' or fractional order spots in the pattern began to form streaks which indicates that a new reconstruction was forming. At 375°C the pattern showed diffuse spots along the bulk reciprocal lattice vectors i.e., along the lines joining the bulk spots. These fractional order spots had 8× periodicity but were not indicative of an (8×8) reconstruction as there were no spots in the middle of the bulk reciprocal lattice unit cell (see figure 7.5). The pattern shown below is a triple domain (8× 1) pattern but this was not observed exactly as only some of the spots shown in the diagram were actually present.

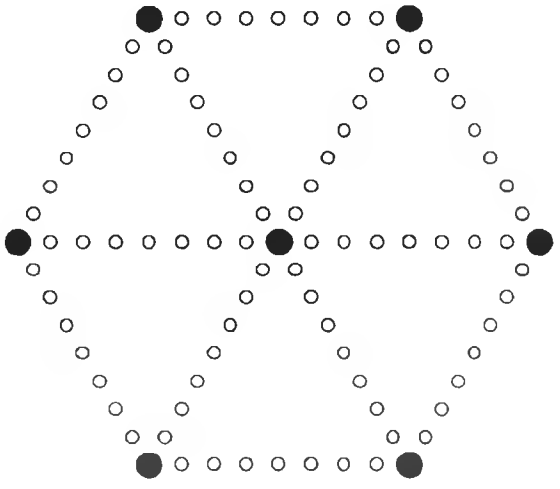

Figure 7.5 A schematic (8×1) LEED pattern produced by a triple domain surface.

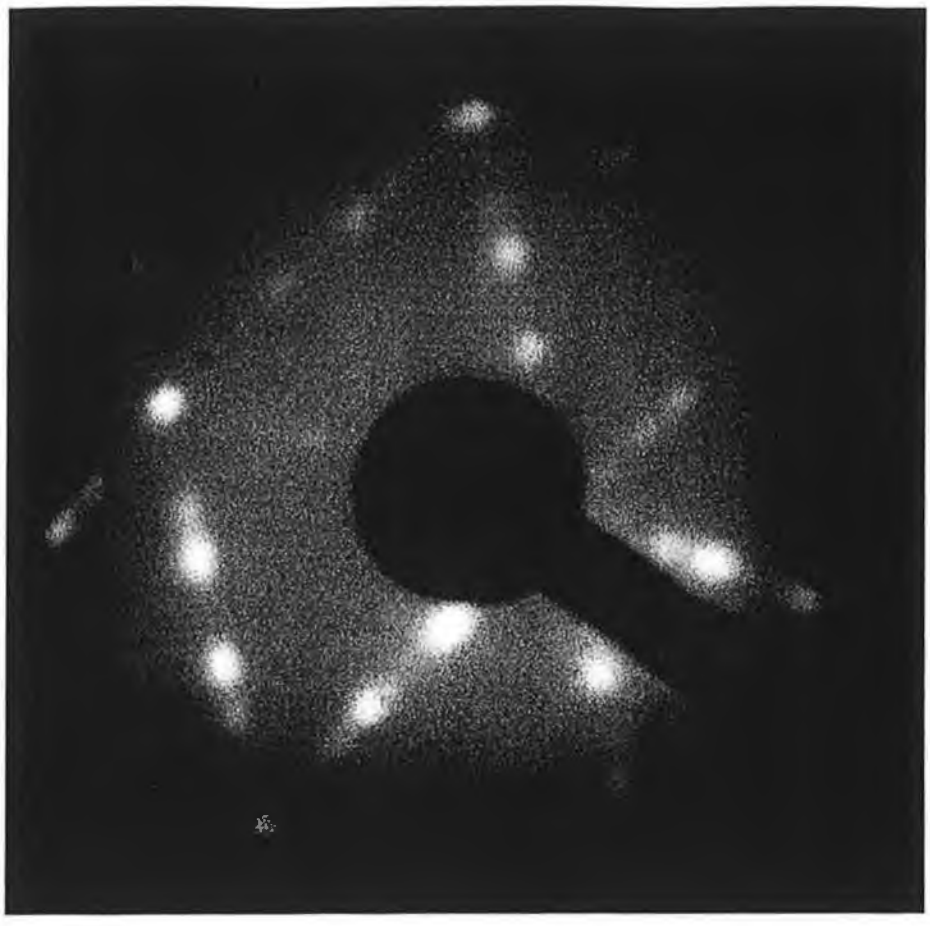

Figure 7.6 Photograph of the LEED pattern observed in the 400-450°C temperature range. The pattern shows evidence for (3×8) periodicity. As the lines of 3× and 8× spots overlap as the surface is triple domain.

In the temperature range 400°C to 450°C a more complicated LEED pattern was observed. At this stage the partial (8×1) pattern remained but additional spots in (3×1) positions were apparent as the photograph in figure 7.6 shows. This pattern is partial (3× 8) because there are no fractional order spots within the bulk reciprocal lattice unit cell. Also, the overlapping of the lines of 3× and 8× spots show the triple domain nature of the surface at this stage: if the surface was single domain these lines of spots would lie along inequivalent bulk reciprocal lattice directions (see figure 7.7). In an STM study of this system Moriarty et. al., [2] and Chapter IV, found that at this temperature the surface exhibited different domains of complex reconstructions. The most predominant of these reconstructions had (3×8) symmetry which is compatible with the LEED pattern observed here. It is plausible that if other reconstructions are also present they add background to the LEED pattern so that fractional order LEED spots cannot be seen inside the bulk unit cell of the pattern.

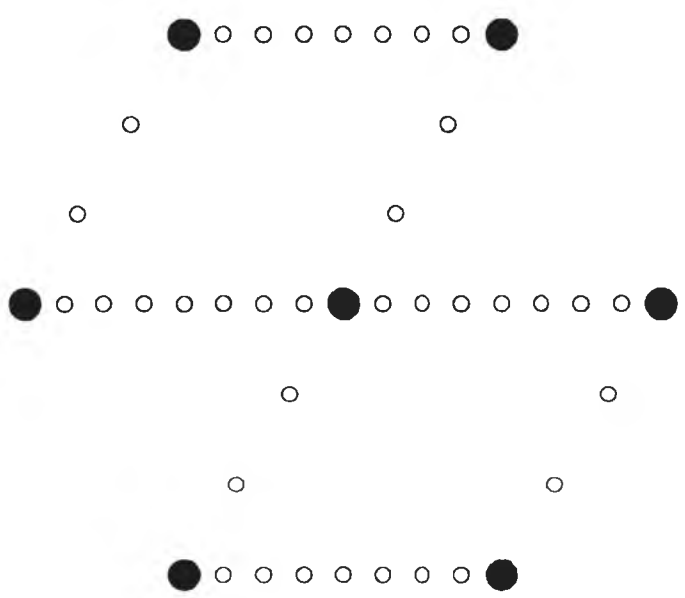

Figure 7.7 A partial LEED pattern for a single domain (3×8) surface. The fractional order spots are omitted from the centre of the bulk reciprocal unit cell.

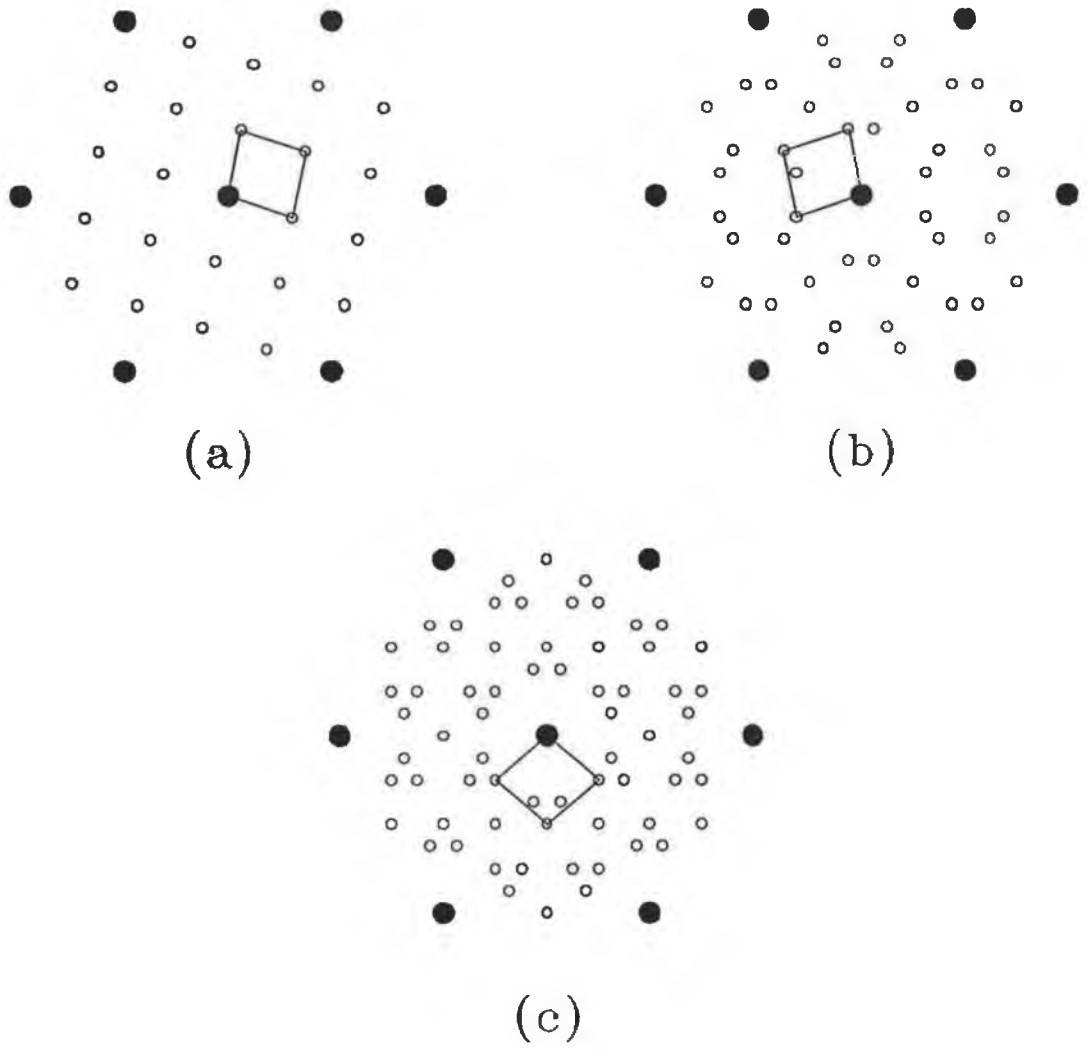

Figure 7.8 Schematic of the LEED pattern for the Sb-GaAs(111)B surface in the 500°C to 550°C temperature range. The actual pattern observed is (c). A photograph of this is shown on the following page. Three rotations of (a) produce the pattern as described in the text.

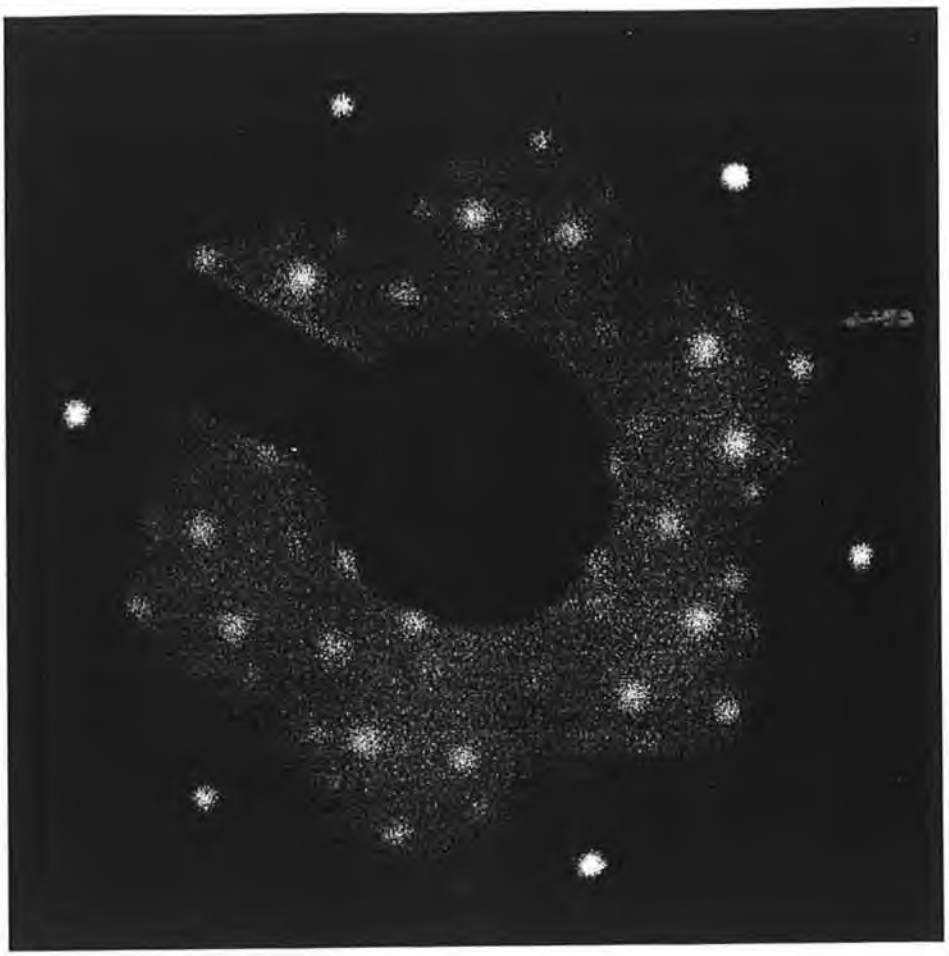

The $\begin{pmatrix} 3 & -1 \\ -1 & 3 \end{pmatrix}$ LEED pattern

A full (3×8) pattern was not observed at a higher temperature. By annealing the sample to 475°C the LEED pattern changed to (1×1). At this stage the adsorbate was either disordered or in the process of desorbing. A (1×1) Sb reconstruction is very unlikely as it would contradict the electron counting rule. This (1×1) pattern was due to the Sb being disordered and in the process of forming a new reconstruction.

At 500°C a very clear although complex pattern was recorded. Figure 7.8 shows this LEED pattern which is described in the matrix notation as $\begin{pmatrix} 3 & -1 \\ -1 & 3 \end{pmatrix}$. This matrix is described in the next section. The LEED has the characteristics expected a triple domain surface. The actual pattern is shown in figure 7.8(c) where bulk spots are in black and the empty circles represent the diffraction spots due to the surface reconstructed layer. The surface reciprocal lattice unit cell shown in (a) generates 1/3 of the spots in the pattern and the other spots are caused by diffraction from two other surface domains which have the same structure but are rotated by 120° with respect to each other. Diagram (b) shows the effect of rotating (a) by 120° and superimposing while a third rotation gives the full LEED pattern as in (c). This illustrates the 'triple domain' nature of the surface. A photograph of this LEED pattern is shown on the preceeding page.

Further annealing above 550°C led to the desorption of the Sb. At 600°C the Sb had desorbed completely leaving a faceted surface. This was clear from a LEED pattern showing the bulk spots of the $(\bar{1}\,\bar{1}\,\bar{1})$ plane with three patterns of rectangular spots rotated at 120° with respect to each other. These rectangular arrays were identified with the set of {110} planes which make tetrahedral facets on the $(\bar{1}\,\bar{1}\,\bar{1})$ surface.

7.3.2 Derivation of the Surface Unit Cell

A complex LEED pattern was recorded after the Sb-GaAs(111)B surface was annealed to between 500°C and 550°C. A derivation of the surface unit cell is presented here. Because the pattern is triple domain the problem is twofold. First a single domain LEED pattern has to be extracted (shown in figure 7.8(a)). Secondly, the surface real space lattice vectors have to be found. This is done by identifying the two inequivalent lines of fractional order spots which also contain bulk spots and using these as the directions of the

surface reciprocal lattice vectors ($\mathbf{s_1}^*$ and $\mathbf{s_2}^*$). This is described by Van Hove et. al. [5]. The length of $\mathbf{s_1}^*$ and $\mathbf{s_2}^*$ is equal to the separation of the spots. Bulk and surface reciprocal lattice vectors are shown in figure 7.9.

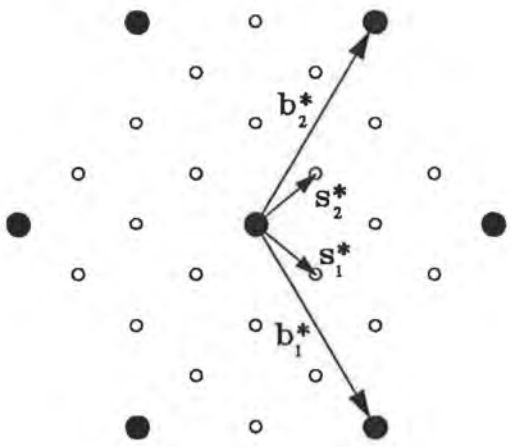

Figure 7.9 A 'reduced' LEED pattern for a single domain of the Sb-GaAs(111)B surface at 500 - 550°C.

In the diagram of the reduced LEED pattern (figure 7.9) the reciprocal lattice vectors for the substrate/bulk ($\mathbf{b_1}^*$,$\mathbf{b_2}^*$) and the overlayer/surface ($\mathbf{s_1}^*$,$\mathbf{s_2}^*$) are defined. These are related by

$$\mathbf{s}_1^* = \frac{3}{8}\mathbf{b}_1^* + \frac{1}{8}\mathbf{b}_2^*$$
$$\mathbf{s}_2^* = \frac{1}{8}\mathbf{b}_1^* + \frac{3}{8}\mathbf{b}_2^* \qquad (7.1)$$

or
$$\begin{pmatrix} \mathbf{s}_1^* \\ \mathbf{s}_2^* \end{pmatrix} = \frac{1}{8}\begin{pmatrix} 3 & 1 \\ 1 & 3 \end{pmatrix}\begin{pmatrix} \mathbf{b}_1^* \\ \mathbf{b}_2^* \end{pmatrix} = M^*\begin{pmatrix} \mathbf{b}_1^* \\ \mathbf{b}_2^* \end{pmatrix} = \begin{pmatrix} m_{11}^* & m_{12}^* \\ m_{21}^* & m_{22}^* \end{pmatrix}\begin{pmatrix} \mathbf{b}_1^* \\ \mathbf{b}_2^* \end{pmatrix}$$

From this we can write down the matrix M which relates the substrate/bulk ($\mathbf{b_1}$, $\mathbf{b_2}$) and overlayer/surface ($\mathbf{s_1}$, $\mathbf{s_2}$) lattice vectors in real space [5],

$$M = \frac{1}{\det M}\begin{pmatrix} m_{22}^* & -m_{21}^* \\ -m_{12}^* & m_{11}^* \end{pmatrix} = \begin{pmatrix} 3 & -1 \\ -1 & 3 \end{pmatrix}$$

$$\therefore \quad \begin{pmatrix} s_1 \\ s_2 \end{pmatrix} = \begin{pmatrix} 3 & -1 \\ -1 & 3 \end{pmatrix} \begin{pmatrix} b_1 \\ b_2 \end{pmatrix} \qquad (7.2)$$

With equation (7.2), the real space overlayer unit cell is known. With the aid of the photoemission results and the electron counting principle a structural model can be proposed. This is done in the following sections. There are alternative matrices M* which could be derived from the LEED pattern to give real space unit cells different from (7.2) but the overall symmetry of the resulting surface would be identical. The real space surface unit cell given by 7.2 is shown in the diagram of the structural model below (figure 7.11).

7.4 Photoemission Results

Photoemission results for the Sb/GaAs(111)B system are shown in figure 7.10(a)-(c) for the series of temperature anneals over the R.T. to 600 °C range. The parameters used in the fitting procedure are listed in Table 7.1 at the end of this section. There are two components in the 'as-deposited' Sb 4d core level as described above, the smaller of which (Sb-As) increases in intensity with anneal temperature and at 400°C dominates the spectrum. Only a small trace of the bulk like (Sb-Sb) component remains at 400°C. The increase in intensity of the higher binding energy component (Sb-As) is accompanied by a decrease in the intensity of the trimer component (S_1) of the As core level and with no change in the Ga spectra. This indicates a gradual replacement of the As trimers with an Sb structure. This substitution of As trimer atoms by Sb has been verified by STM studies [2,6] where it was found that at 370 °C the Sb forms trimers and a double chain structure with a predominantly (3×8) unit cell with some regions of (12×7) and (6×10). As described above, the LEED pattern of the surface in this work showed 8× and 3× periodicity in the 375 - 450 °C temperature range, a clear (3×8) pattern probably not being observed due to the coexisting domains of different periodicity. In the STM study of the Sb-GaAs(111)B surface the double chain-trimer structure was present at ~380 °C without any evidence for As trimers. In this study, As trimers are still present in the 375 - 400 °C

temperature range: in the As 3d core level spectra, the As trimer (S_1) component is still present at this stage with the LEED pattern showing 3× and 8× spots. This inconsistency is slight and might be due to differing conditions between this work and the STM study. It is possible that the method of annealing, for instance, could be different Also, the initial amount of Sb deposited was approximately 4.0ML in this study while Moriarty et al. initially deposited 3.0ML of Sb. Further differences between the two studies arise at the higher temperature range of 475°C to 550°C.

Signifigant changes in the core level spectra are seen after annealing to 500°C, the temperature where the $\begin{pmatrix} 3 & -1 \\ -1 & 3 \end{pmatrix}$ LEED pattern was observed. A shift of +0.40eV is apparent in the Sb 4d core level and new surface shifted component is observed in the Ga 3d core level. For Sb, this shift is quite large and indicates a new chemical environment entirely. In the earlier stages of the experiment the Sb-Sb and Sb-As components were separated by 0.71eV so the shift in position at this stage is signifigant. This shift of 0.40 eV in the Sb component is not due to band bending effects as the As and Ga 3d core levels shift by only 0.05 eV in the 400 - 500°C temperature interval. A possible explanation for the Sb 4d binding energy shift is that only at this stage is the Sb fully bonding to the As of the substrate. This would mean that the component labelled Sb-As in the spectra up to this point is due to Sb not fully bonded to the surface but simply 'resting on top'. This was also suggested from the growth study in section 7.2 and would explain the lack of a clear (3×8) pattern in the 375°C to 450°C range. It is likely that only after annealing to 500°C is the Sb fully bonded to the As of the substrate.

The change in the Ga 3d core level at 500°C is signifigant. An entirely new component can be seen in the spectrum, its binding energy is 0.29 eV higher than the bulk component. This indicates that a surface environment has been created for some of the Ga atoms. This surface core level shift is consistent with an empty dangling bond. These bonds are observed in the case of the GaAs(111)A clean surface and coincidentally have exactly the same binding energy shift of 0.29eV [7]. In the earlier work in this thesis however, this surface shift for the GaAs(111)A clean surface was found to be 0.40eV, but the principle of the empty Ga dangling bond is valid. An explanation for this new Ga surface component would necessitate the creation of an As vacancy in the top layer of the substrate. This vacancy, together with Sb trimers or adatoms give the basis for suggesting a structural model which is described below.

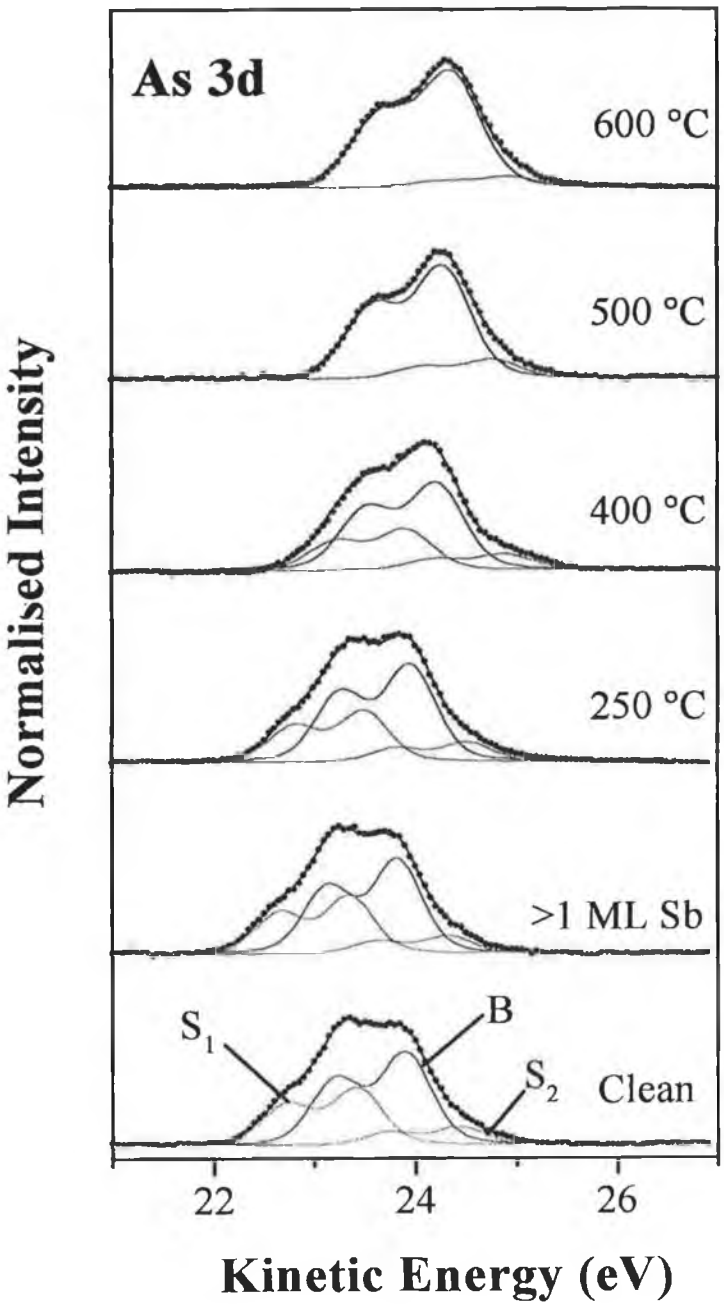

Figure 7.10 (a) Fitted As 3d core levels for the Sb-GaAs(111)B surface recorded at a photon energy of 70eV.

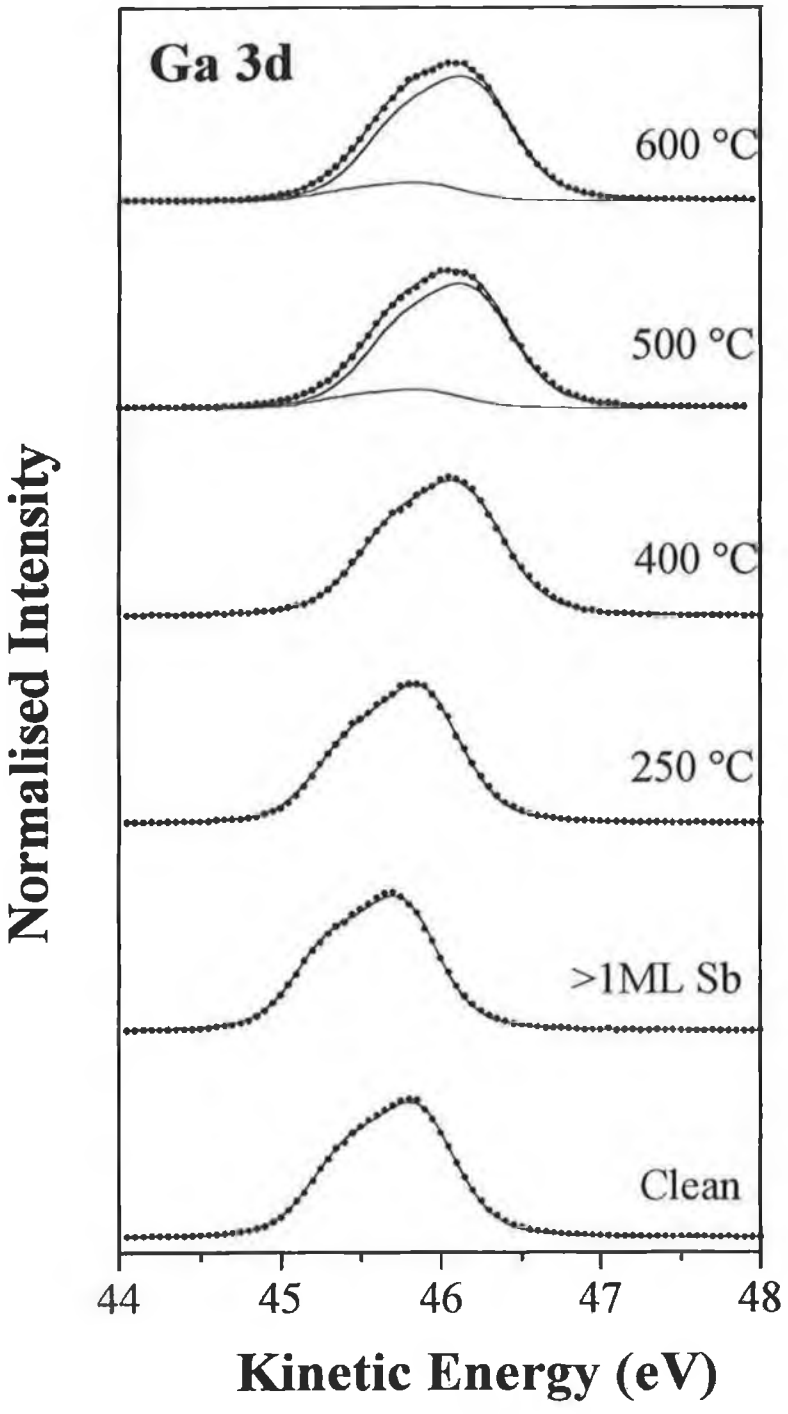

Figure 7.10 (b) Fitted Ga 3d core levels for the Sb-GaAs(111)B surface recorded at a photon energy of 70eV.

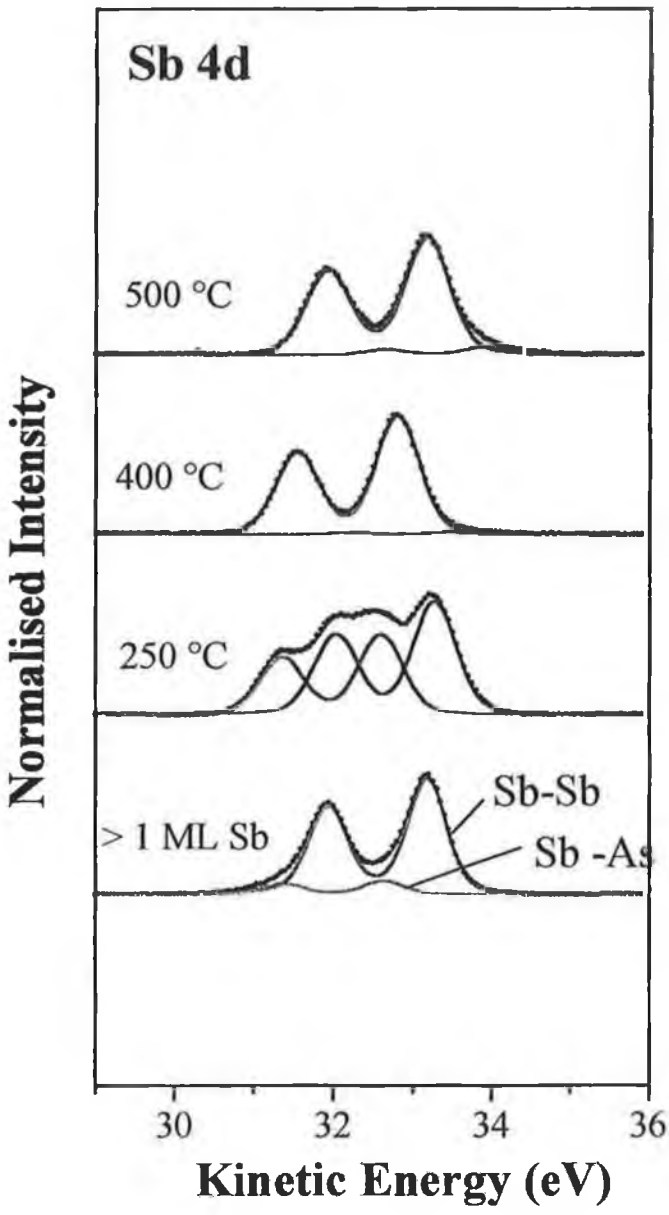

Figure 7.10 (c) Fitted Sb 4d core levels for Sb-GaAs(111)B recorded at a photon energy of 70eV.

To summarise the photoemission results for the system at 500°C, a chemical shift occurred in the Sb 4d spectrum which indicates a change in the chemical bonding of the Sb and there is evidence for a new surface environment for some of the Ga atoms in the sample.

A second STM study of the Sb-GaAs(111)B surface in the 475 - 525°C temperature range by Moriarty et. al. [6] gave results which are at variance with what is seen in this study. These authors found that in this temperature range a gradual transition to a (1×3) reconstruction took place. This reconstruction comprises Sb chains extending across the surface in <110> directions and separated by two (1×1) unit cells. Such a structure is not compatible with the LEED pattern observed here (figure 7.8). The $\begin{pmatrix} 3 & -1 \\ -1 & 3 \end{pmatrix}$ unit cell is not oriented in the <110> directions. This discrepancy between the two studies is not understood.

To complete this discussion of the photoemission results, the As and Ga 3d core levels are described for the anneal to 600°C. At this point all the Sb had desorbed from the surface and the substrate was clearly faceted. Both core levels have a surface shifted component as they had at 500°C, that of the As core level due to the As rest atoms which were present for the entire experiment and the Ga surface core level component compatible with an empty dangling bond. Each facet is composed of three planes of atoms with {110} orientations. The known core level shifted components for the (110) surface [8] are similar to those shown here and this explains why there are core level shifts on the recovered clean surface at 600°C which are not uniquely seen on the GaAs(111)B surface.

7.4.2 Discussion on the Parameters used in the fitting Procedure

Listed in Table 7.1 are the parameters used to fit the photoemission core levels. Values for the Lorentzian and spin orbit splitting for all three core levels are consistent with other studies of GaAs surfaces [7,9,10]. Branching ratios are equal to the theoretical value of 2/3 except for the case of As 3d when the final reconstruction was formed where there is a slight increase. This can be caused by diffraction effects as mentioned in chapter V. For the GaAs(100) (4×2)-c(2×8) surface the branching ratio was found to be 0.71 [9].

Table 7.1

	As 3d		Ga 3d		Sb 5d
	Clean Surface	$\begin{pmatrix} 3 & -1 \\ -1 & 3 \end{pmatrix}$-Sb	Clean Surface	$\begin{pmatrix} 3 & -1 \\ -1 & 3 \end{pmatrix}$-Sb	$\begin{pmatrix} 3 & -1 \\ -1 & 3 \end{pmatrix}$ -Sb
Gaussian (eV)	0.46	0.53	0.42	0.52	0.60
Lorentzian(eV)	0.17	0.17	0.155	0.155	0.17
Spin -Orbit splitting (eV)	0.69	0.69	0.45	0.45	1.243
Branching Ratio	0.666	0.68	0.666	0.666	0.666
K.E. shift of S_1(eV)	0.57	0.54		-0.29	0.71
K.E. shift of S_2 (eV)	-0.49				
Bulk K.E. position (eV)	24.20	24.31	46.13	46.21	33.22

The Gaussian broadening for the As 3d and Ga 3d core levels of the clean surface, 0.46 eV and 0.42 eV respectively, agree within an acceptable error for the experiment - the data points in the spectra are 0.05 eV apart. A slight increase in the Gaussian width is needed to fit the spectra when the final reconstruction is formed. This can be due to surface disorder, i.e. the surface at 500°C has more defects per unit area than the (2×2) clean surface and this broadens the photoemission features. By the same reasoning, the Gaussian for the Sb 4d core level is quite high at 0.60eV. The broadening effect of roughening is more extreme for Sb than Ga or As as it has a completely surface environment.

The values for the surface core level shifted components of As 3d core level also agree with another study of the GaAs(111)B clean surface [7] to within 0.04eV.

As mentioned in chapter V for the Sb-GaAs(111)A surface, the possibility of asymmetric Doniach-Sunjich (DS) broadening [11] for the Sb 4d core levels was considered. No DS broadening was needed to fit an Sb 4d doublet at any stage in the experiment. The relevant parameter was always zero when the DS lineshape was included in the fitting.

7.5.1 The structure of Sb-GaAs(111)B -$\begin{pmatrix} 3 & -1 \\ -1 & 3 \end{pmatrix}$

A possible structure for this system at 500°C is given in figure 7.11. This structure is suggested by the electron counting model [13], with the assumption that each unit cell contains at least one As vacancy and at least one Sb trimer. Evidence for the As vacancy comes from photoemission and the Sb trimer is assumed to be the simplest way in which Sb may bond to the surface. Alternatives, such as Sb single adatoms, chains or other structures are assumed less likely. As adatoms have been found to be energetically unfavourable compared to As trimers on this substrate [14]. An Sb chain structure is not compatible with the LEED pattern because Sb chains are oriented in the <110> directions and the surface unit cell is not (see figure 7.11).

The unreconstructed surface unit cell contains 8 surface As atoms. This is because the unit cell has an area equal to 8 (1×1) cells on the unreconstructed (111) surface, i.e., $\det\begin{pmatrix} 3 & -1 \\ -1 & 3 \end{pmatrix}$ =8. The creation of x As vacancies leaves (8-x) As atoms and 3x Ga dangling bonds in the unit cell. The Ga dangling bonds are in the layer immediately below the surface. They are created by the breaking of the Ga-As bond when the As vacancy is created. Ga and As sp^3 orbitals contain 3/4 and 5/4 electrons respectively, i.e., the number of valence electrons distributed among the four tetrahedral bonds. Therefore the total number of surface electrons involved in bonding is

$$(8-x)\frac{5}{4}+(3x)\frac{3}{4} \qquad (7.3)$$

This number of electrons must be involved in filling As surface dangling bonds, using 2 electrons or else used in the bonding of an Sb adstructure to the surface which requires 3 electrons for an Sb trimer as described before in relation to the GaAs(111)A surface. A Ga dangling bond is empty. If y is the number of trimers there are 8-x-3y As dangling bonds

and 3y As atoms bonded to Sb, so the total number of electrons needed to fill the relevant bonds is

$$2(8-3x-y)+3y \tag{7.4}$$

Setting (7.3) = (7.4) gives x+y=2 meaning that 1 As vacancy and 1 Sb trimer per unit cell is the only possible structure allowed by the electron counting model with the assumptions made. This is the structure as shown in figure 7.11 where there are four As rest atoms per unit cell. Structures involving chain pairs of Sb atoms parallel to the <110> directions, as seen at lower temperatures by STM [2], were not considered as the LEED pattern shows that the unit cell of the surface is not oriented in the <110> directions.

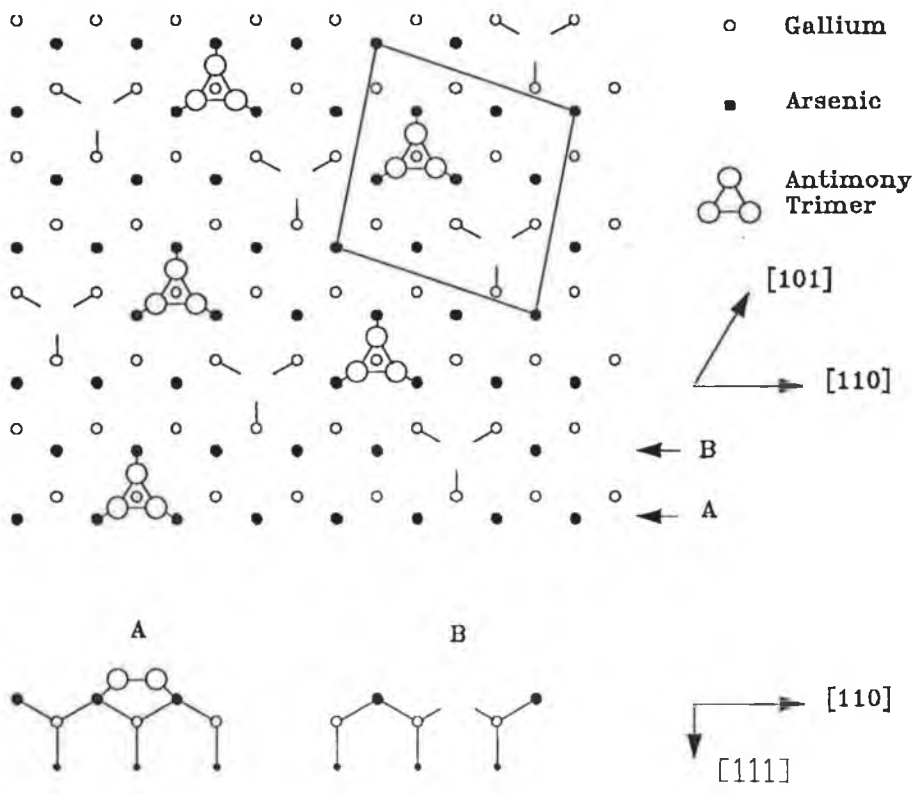

Figure 7.11 The structural model proposed for Sb-GaAs(111)B at 500 - 550°C. The viewpoints for the side views A and B are indicated by arrows.

Some justification is now given for the creation of the As vacancy as it seems unusual in regard to other studies of the GaAs(111)B surface. A (2×2) array of As vacancies was found to be energetically less favourable than a (2×2) trimer structure on the GaAs(111)B clean surface [15]. This was found by total energy calculations which simulate the growth conditions of the MBE process. This result was confined to a surface with (2×2) symmetry. It is well known that at 500°C the (111)B clean surface lowers its symmetry to ($\sqrt{19}\times\sqrt{19}$) [15,16,17,18]. The transition involves the desorption of As and the formation of empty Ga dangling bonds which is what was suggested for the model in figure 7.11. Although the ($\sqrt{19}\times\sqrt{19}$) surface does not contain As vacancies similar to those described here, the As desorption at 500°C is well documented and this is used as additional support for the vacancies suggested in this work.

7.5.2 The Antimony Coverage of the Surface

The Sb coverage of the structural model presented above is 3/8 ML, i.e. 3 Sb atoms per surface unit cell. It is useful to estimate the Sb coverage of the surface at this stage to see if it is in agreement with the model. This estimate is made from the plot of the Sb core level intensities during the growth and annealing processes (figure 7.3). By comparing the Sb core level intensity at 500°C with an equal intensity in the Sb growth curve, the coverage might be determined. A dotted line is drawn in figure 7.3 to illustrate this. The Sb coverage was found to be 1.7±0.2 Å. If the Sb-As bond length is equal to that found for the Sb-GaAs(110) surface (2.35±0.05Å) [3,4] then the final Sb coverage is actually 0.7±0.1 ML. This value is larger than the 3/8 of the model by a factor of 2. Either the model is incorrect or else the Sb-As bond length in this study is signifigantly different than 2.35Å. Also, the estimate of the coverage could be flawed. At the point where 1.7Å of Sb had been deposited there were two components in the Sb core level spectrum. Photoelectrons from the interfacial Sb could be attenuated by the Sb above and so absolute certainty about coverages from this type of photoemission evidence may be inconclusive for this surface. In other chapters of this thesis, coverage estimates were made in the manner described here. There is no evidence that the Sb-GaAs(111)B system is so different that the coverage for a specific reconstruction cannot be found in this way. Also, Sb does not replace As on deposition, so the possibility of this effect compromising the coverage determination is discounted.

Given that the estimate of the Sb coverage at 500°C is approximately twice that of the structural model and to propose more one more Sb trimer per $\begin{pmatrix} 3 & -1 \\ -1 & 3 \end{pmatrix}$ unit cell would violate electron counting, it is concluded that more work is necessary to fully understand this reconstruction. An STM study where the LEED pattern observed here is also observed might resolve the problem.

7.6 Electronic Properties

As the GaAs(111)B samples used in this work are doped n-type, the Fermi level (E_f) is just below the conduction band minimum (CBM) in the bulk of the crystal. At the surface, the band bending is quite large and the Fermi level is pinned midgap. For the clean surface, the valence band maximum (VBM) was found to be 0.80eV below E_f. This means that due to the raised potential of the surface, the valence band maximum is shifted upwards in energy towards the Fermi level by an amount equal to E_{gap}-0.80eV = 0.66 eV. Figure 7.12, shows how the position of E_f in the bulk band gap varied as Sb was deposited and the sample subsequently annealed.

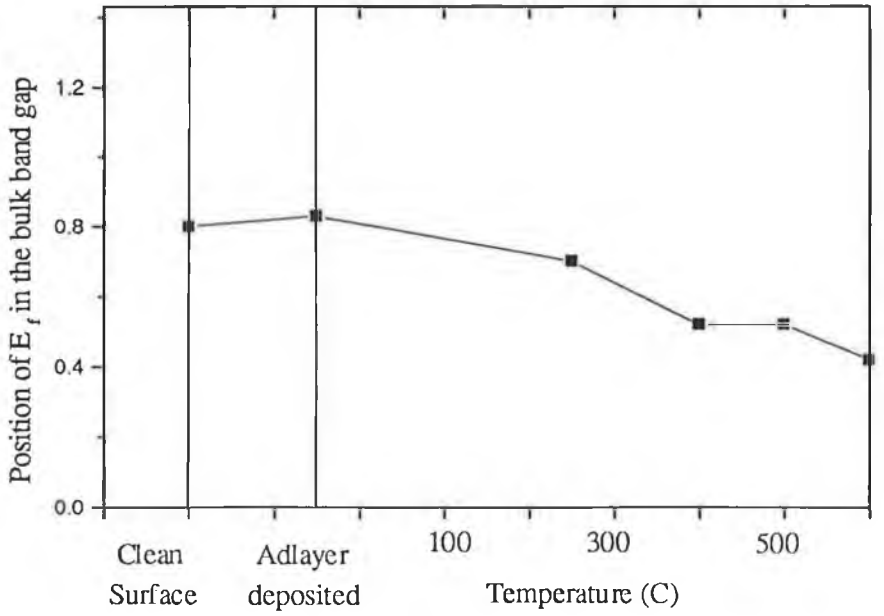

Figure 7.12 The position E_f in the bulk band gap as a function of temperature for Sb-GaAs(111)B. The GaAs(111)B samples were doped n-type so that in the bulk, E_f is just below the conduction band minimum.

When the Sb was deposited the band bending was practically unchanged but with annealing, the position of E_f in the band gap moved towards the VBM. This means that the band bending increases with annealing temperature. For the final reconstruction observed at 500°C, the band bending is ~0.28 eV higher than for the clean surface. The Schottky barrier is therefore ~1.08eV.

7.7 Summary

The growth of Sb on the GaAs(111)B surface was found to be consistent with Volmer-Weber growth. When the system was annealed, Sb spread over the surface and excess Sb desorbed. From room temperature to 475°C, the LEED pattern gradually changed to a partial (3×8) pattern. A $\begin{pmatrix} 3 & -1 \\ -1 & 3 \end{pmatrix}$ reconstruction was stable in the 500 to 550°C temperature range. The structural model suggested for the surface at this stage contains Sb trimers bonded to the surface and As vacancies. Annealing the system caused the surface band bending to gradually increase to a value of 0.28 eV above that of the clean surface.

References for Chapter VII

1. *Fundamentals of Surface and thin film analysis,* by L.C. Feldman and J.W. Mayer, (North-Holland, 1986)

2. P. Moriarty, P.H. Beton, D. A. Woolf, Phys. Rev. B **51**, 7950 (1995).

3. W. K. Ford, T. Guo, D. L. Lessor and C. B. Duke, Phys. Rev. B **42** 8952 (1990).

4. W. G. Schmidt and G.P. Srivistava, Surf.Sci. **331-333**, 540 (1995).

5. M. A. van Hove, W.H. Weinberg and C.-M. Chan, *Low Energy Electron Diffraction*, (Springer-Verlag, 1979)

6. P. Moriarty, P.H. Beton, M. Henini and D. A. Woolf, Surf. Sci. Lett., **365** L663 (1996)

7. J. M. C. Thornton, P. Weightman, D. A. Woolf, and C. J. Dunscombe, Phys. Rev. B **51,** 14459 (1995).

8. F.Schaffler, R. Ludeke, A. Taleb-Ibrahimi, G. Hughes and D. Rieger, J. Vac. Sci. Technol. B5 (4) 1048 (1987)

9. G. LeLay, A. Kahn, D. Mao, Y. Hwu and G. Magaritondo, Phys. Rev. B **43** 14301 (1991)

10. T. Miller and T._C. Chiang, Phys. Rev. B **29** 7034 (1984)

11. L.Ley and M. Cardona, *Photoemisssion in Solids Vol. I*, Cap. 5 (Springer-Verlag, 1979)

12. Colm Stephens, PhD thesis, University of Dublin, 1993

13. M. D. Pashley, Phys. Rev. B **40**, 10481 (1989).

14. D. K. Biegelsen, R. D. Bringans, J. E. Northrup, and L.-E. Swartz, Phys. Rev. Lett. **65**, 452 (1990).

15. E. Kaxiras, Y.Bar-Yam, J. D. Joannopoulus, and K. C. Pandey, Phys. Rev. B **35**, 9636 (1987).

16. A. R. Avery, E.S. Tok and T.S. Jones, Surf. Sci. Lett. **376** L397 (1997)

17. A. Y. Cho, J. Appl. Phys., **41** 2780 (1970)

18. J. R. Arthur, Surf. Sci. **43** 449 (1974)

Chapter VIII

Bismuth on GaAs(111)B

8.1 Introduction

The growth of Bi on the GaAs(111)B surface is described first. Following the establishment of the growth mode, a temperature induced reconstruction is described and a structural model proposed. These separate studies of Bi growth and of the reconstruction formed are linked by an estimate of the final Bi coverage of the surface. This estimate of the coverage justifies the structural model proposed. The surface band bending is also measured.

8.2 The growth of Bismuth on GaAs(111)B

Throughout the Bi deposition there are two components in the Bi photoemission spectrum (figure 8.1). The lower binding energy component is assigned to bulk Bi bonds (Bi-Bi) and the higher binding energy component is identified with a Bi-As bond. The reason for this is seen by noting the change in relative normalised intensities of the two components as a function of coverage. As the coverage increases, the core level component with higher kinetic energy increases in intensity while intensity of the lower kinetic energy component saturates after an initial increase. The intensity versus coverage for the two components are plotted in figure 8.2. It is the area under the Voigt lineshape of the relevant components as shown in figure 8.1 which are plotted here. The black lines are drawn to guide the eye. The red line is drawn to relate the intensity of the Bi-As component to an equivalent surface coverage from the initial growth study. This coverage was evaluated at the temperature where the intensity of the Bi-Bi component had fallen to zero, i.e. at the temperature where the Bi on the surface in bulk form had entirely converted to surface bonded Bi. The final coverage is discussed in section 8.5.1 below.

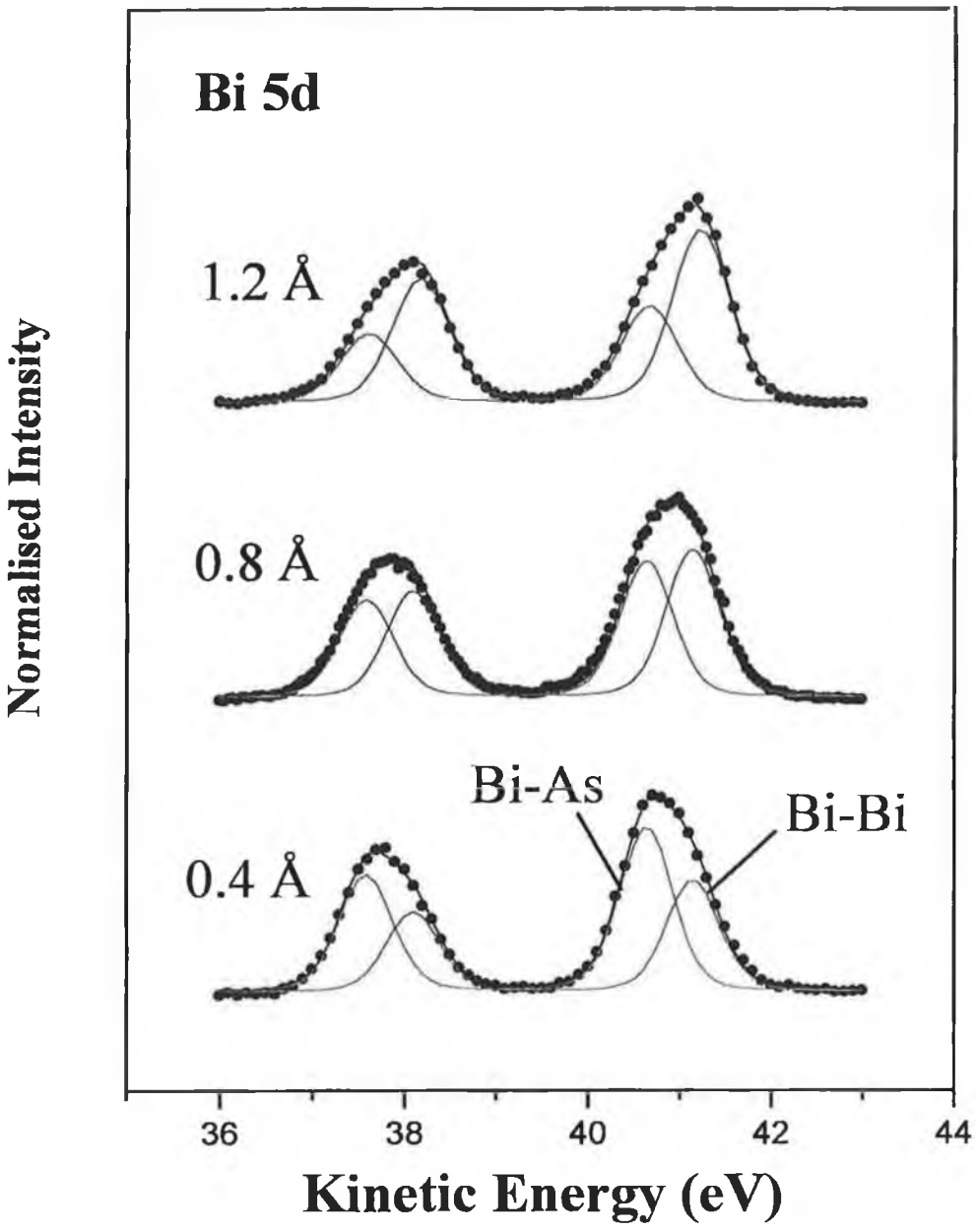

Figure 8.1 Fitted Bi core levels at successive coverages before temperature annealing. Spectra were recorded at a photon energy of 70eV

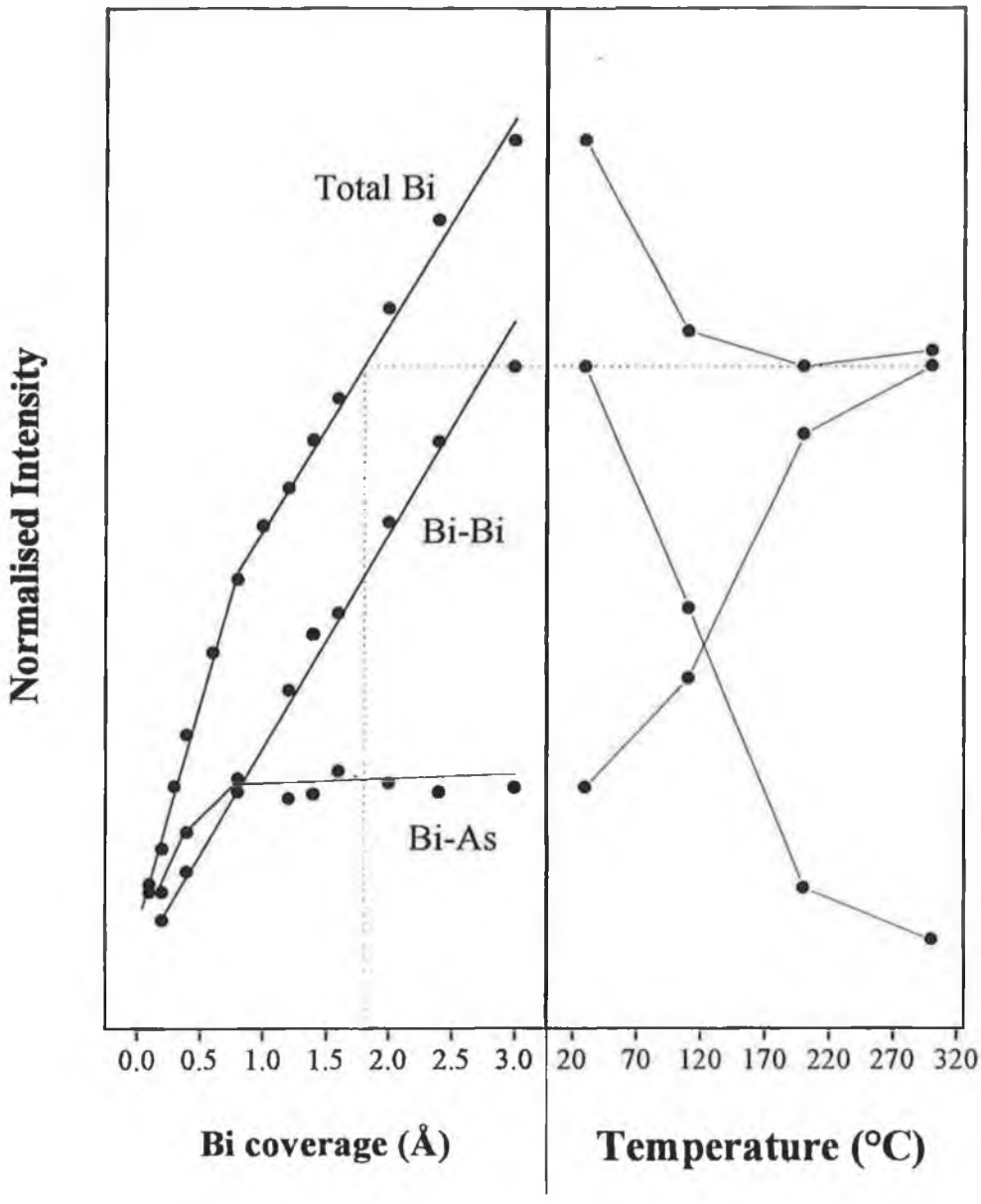

Figure 8.2 The normalised intensities of the bulk (Bi-Bi) and interfacial (Bi-As) components as a function of Bi coverage and annealing temperature.

The Bi-Bi component in figure 8.2 increases linearly with the amount of Bi deposited - this is typical of islanding [1] and is therefore taken to be the Bi-Bi component, while the

intensity of the second component rises to a maximum and then saturates. This component is identified with Bi bonded directly to the surface, i.e. Bi-As bonds. The Bi-As bonding is justified on comparing the As 3d core level of the clean surface with the same core level after the deposition of Bi (figure 8.5(a)). The As trimer component (S_1) is immediately reduced (by ~30 % relative to the bulk As component) after the deposition, so Bi has replaced a proportion of the As trimer atoms before annealing takes place. It is this Bi which is associated with the Bi-As component in figures 8.1 and 8.2. The surface As atoms to which the As trimers are bonded are not distinguishable from the bulk As atoms in photoemission.

Growth of Bi on this surface therefore involves partial substitution of the As trimers with Bi atoms which saturates after a certain coverage and bulk like growth of Bi accounts for further growth. This is consistent with islanding (Volmer-Weber growth) as the presence of an As trimer component in figure 8.5 (a) after the Bi deposition indicates areas of clean surface coexisting with Bi islands. For the growth of the other group V metal Sb on this surface, islanding was also observed [2].

Although the mode of Bi growth has been labelled as Volmer-Weber (VW) growth, there is a slight difference between the growth curve shown here and what is normally seen (description given in chapter II, section 2.4). The graph of the *total* Bi core level intensity versus coverage shows a change in slope at a coverage of 0.75 Å when usually, in perfect VW growth this line should have constant slope. A change in slope is indicative of layer-plus-island or Stranski-Krastanov (SK) growth, but this only refers to growth where the first layer covers the entire surface. In this study it is deduced that this initial layer of Bi covers only patches or domains of the surface and as stated above substitutes for the original As trimers. Aspects of this growth of Bi is actually similar to both SK and VW growth but labelling the process with the latter name is more appropriate as no complete layer is initially formed. A coverage of 0.75 Å is consistent with a coverage of 0.3 monolayers which is equivalent to saying that the Bi islands cover approximately 1/3 of the surface with the As trimer terminated (2×2) clean surface remaining everywhere else.

An observation from the annealing process is that the total intensity of the Bi core level decreased with increasing temperature but remained approximately constant after about 110°C. At this temperature the LEED pattern changed to c(4×2) as described below, so that although some of the Bi on the surface is unstable against desorption initially, the formation of a new reconstruction stabilises the surface and therefore lowers the total surface energy. Above 110°C, Bi diffuses along the surface and the formation of a new reconstruction as opposed to simple desorption is preferred.

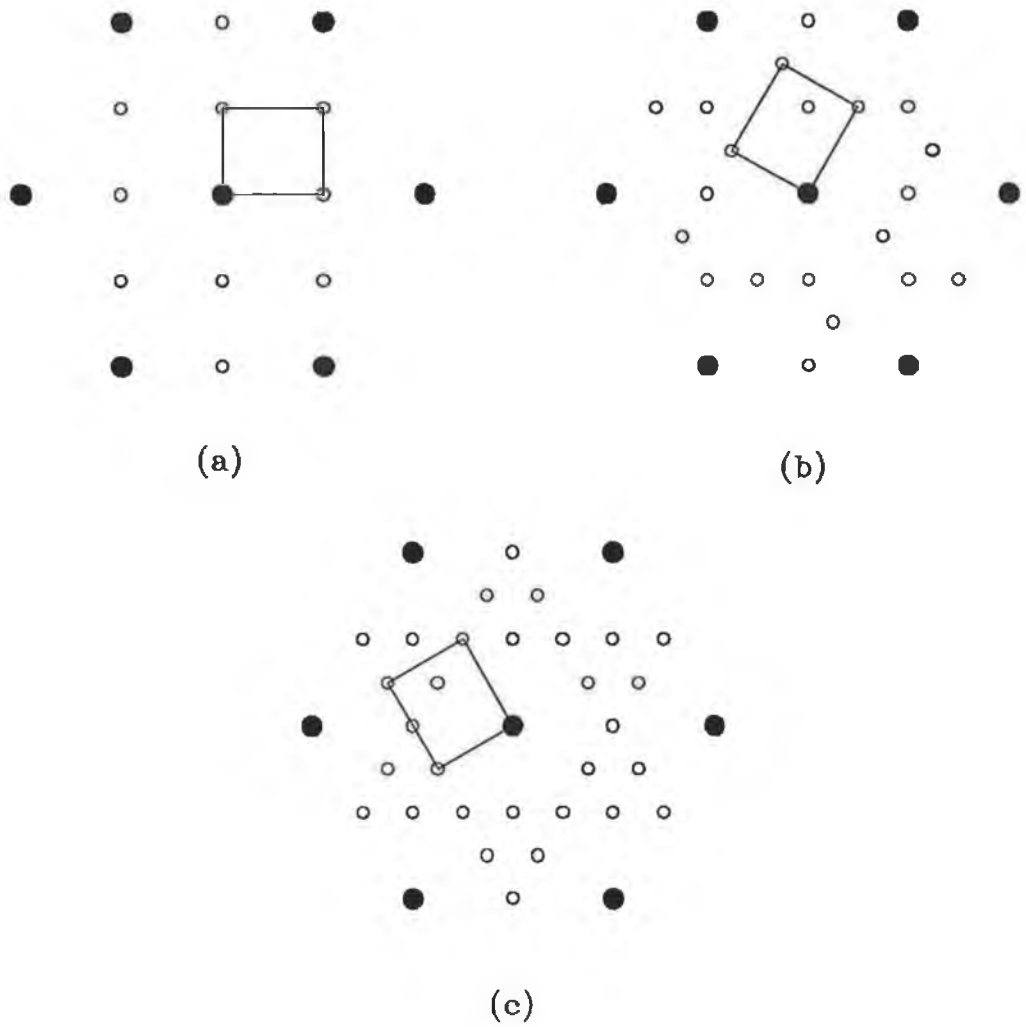

Figure 8.3 Schematic of the LEED pattern for the Bi-GaAs(111)B system in the 110 - 375°C temperature range. A photograph of this pattern is shown on the following page.

The c(4×2) LEED pattern

8.3.1 LEED Results

Following the deposition of Bi on the GaAs(111)B surface a series of temperature anneals were carried out over the temperature range for which Bi remained on the surface (R.T. to 450°C). After the deposition of 1-2 ML of Bi a (2×2) LEED pattern was still visible but with a more diffuse background and lower intensity in the bulk and surface diffraction spots. This (2×2) pattern is due to the portion of the surface still exhibiting the clean surface reonstruction as discused above. Upon annealing to >110°C the LEED image changed to a c(4×2) triple domain pattern (figure 8.3(c)), the image becoming sharper with increasing temperature. The pattern remained up to 375 °C. Above 375 °C, the Bi began to desorb, as judged from the photoemission data, and the LEED pattern changed to (1×1) with the Bi desorption complete at 475 °C.

In figure 8.3 the actual pattern is shown on the bottom (c) where bulk spots are in black and the empty circles represent the diffraction spots due to the surface reconstructed layer. The surface reciprocal lattice unit cell shown in (a) generates 1/3 of the spots in the pattern and the other spots are caused by diffraction from two other surface domains which have the same structure but are rotated by 120° with respect to each other. Diagram (b) shows the effect of rotating (a) by 120° and superimposing while a third rotation gives the full LEED pattern as in (c). This illustrates the 'triple domain' nature of the surface. A photograph of this LEED pattern is shown on the following page.

8.3.2 Derivation of the surface unit cell

In the preceding section the LEED pattern was labelled c(4×2). This is not immediately obvious from the pattern and centred nets in hexagonal LEED patterns are hard to recognise. A rigorous interpretation of the pattern is given in this section. Although the c(4×2) label has been used for the pattern, a rectangular mesh is more convenient to use in order to demonstrate that the LEED pattern has been interpreted correctly. A section of the LEED pattern is shown in figure 8.4 with the bulk and surface reciprocal lattice vectors labelled.

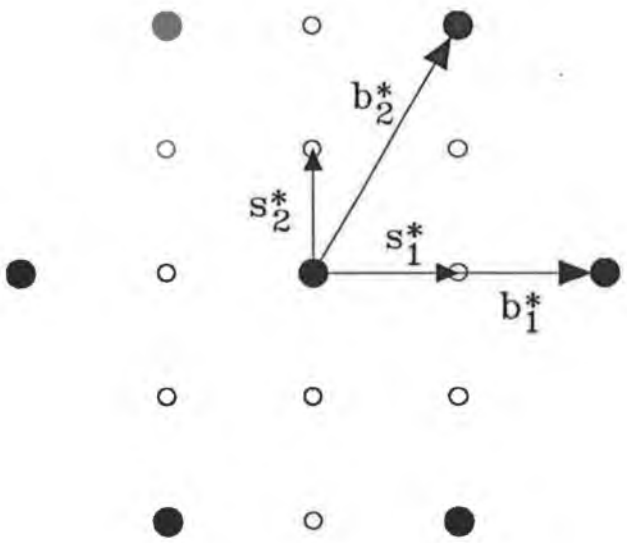

Figure 8.4 A single domain of the c(4×2) LEED pattern showing the substrate and overlayer reciprocal lattice vectors

The schematic LEED pattern shows the reciprocal lattice vectors for the substrate ($\mathbf{b}_1^*$,$\mathbf{b}_2^*$) and the surface ($\mathbf{s}_1^*$,$\mathbf{s}_2^*$) which are related by

$$\mathbf{s}_1^* = \mathbf{b}_1^*/2$$

$$\mathbf{s}_2^* = -\mathbf{b}_1^*/4 + \mathbf{b}_2^*/2$$

or

$$\begin{pmatrix} \mathbf{s}_1^* \\ \mathbf{s}_2^* \end{pmatrix} = \frac{1}{4}\begin{pmatrix} 2 & 0 \\ -1 & 2 \end{pmatrix}\begin{pmatrix} \mathbf{b}_1^* \\ \mathbf{b}_2^* \end{pmatrix} = \mathrm{M}^*\begin{pmatrix} \mathbf{b}_1^* \\ \mathbf{b}_2^* \end{pmatrix} = \begin{pmatrix} m_{11}^* & m_{12}^* \\ m_{21}^* & m_{22}^* \end{pmatrix}\begin{pmatrix} \mathbf{b}_1^* \\ \mathbf{b}_2^* \end{pmatrix} \quad (8.1)$$

From this we can write down the matrix M which relates the substrate and overlayer lattice vectors in real space (cf. Chapter II),

$$\mathrm{M} = \frac{1}{\det \mathrm{M}}\begin{pmatrix} m_{22}^* & -m_{21}^* \\ -m_{12}^* & m_{11}^* \end{pmatrix} = \begin{pmatrix} 2 & 1 \\ 0 & 2 \end{pmatrix}$$

$$\therefore \quad \begin{pmatrix} s_1 \\ s_2 \end{pmatrix} = \begin{pmatrix} 2 & 1 \\ 0 & 2 \end{pmatrix} \begin{pmatrix} b_1 \\ b_2 \end{pmatrix} \tag{8.2}$$

With equation (8.2), the real space overlayer unit cell can be drawn and a structural model proposed. Because the substrate lattice vectors form an hexagonal net and the overlayer net is rectangular, the matrix notation is needed instead of the Woods notation. The real space rectangular unit cell is shown in figure 8.6 with a structural model based on the photoemission results.

8.4.1 Photoemission Results

With the crystallographic information obtained from the LEED study, suggestions can be made as to the crystal structure of the surface. As with the other surfaces studied in this work, core level photoemission spectroscopy was used to obtain evidence for the changes in chemical bonding occurring during and after the formation of the reconstructed surface. Figures 8.5 (a) - (c) shows the changes in the relevant core levels up to 475°C. The Ga 3d core level remains unchanged indicating that no reaction takes place between the deposited Bi and Ga in the layers below the surface. The As 3d spectra reveal a gradual loss of the trimer component (S_1) up to 300 °C which is accompanied by a change in the Bi core level from predominantly Bi-Bi (S_1) to Bi-As (S_2). These changes are consistent with the As trimers being replaced by a Bi ad structure associated with (S_2) and a model for the resulting c(4×2) structure can be suggested by information about the chemical bonding from these photoemission results and with electron counting reasoning [4]. This structural model is discussed below.

At 375°C the LEED pattern changed to (1×1) with some Bi still present on the surface without any evidence from photoemission for a change in the bonding of the Bi. This remained the case until the Bi had fully desorbed at 475°C. With regard to the Ga 3d and As 3d core levels at this point it is seen that they are qualitatively unchanged with respect to the case of the Bi c(4×2) reconstruction - the As still has a bulk and surface rest atom component and the Ga is entirely bulk like. After the Bi desorbs the surface is therefore disordered with some full dangling bonds on the surface As atoms. Table 8.1 below lists the parameters used in the core level fitting procedure.

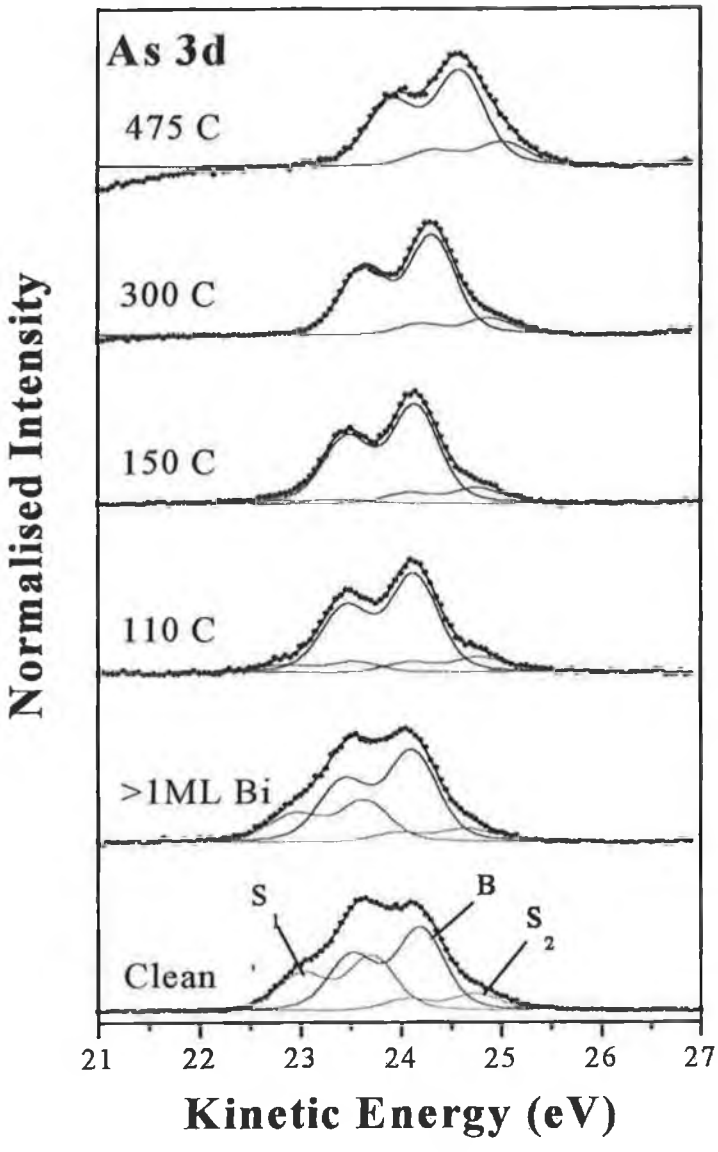

Figure 8.5 (a) Fitted As core levels for Bi-GaAs(111)B recorded at a photon energy of 70eV.

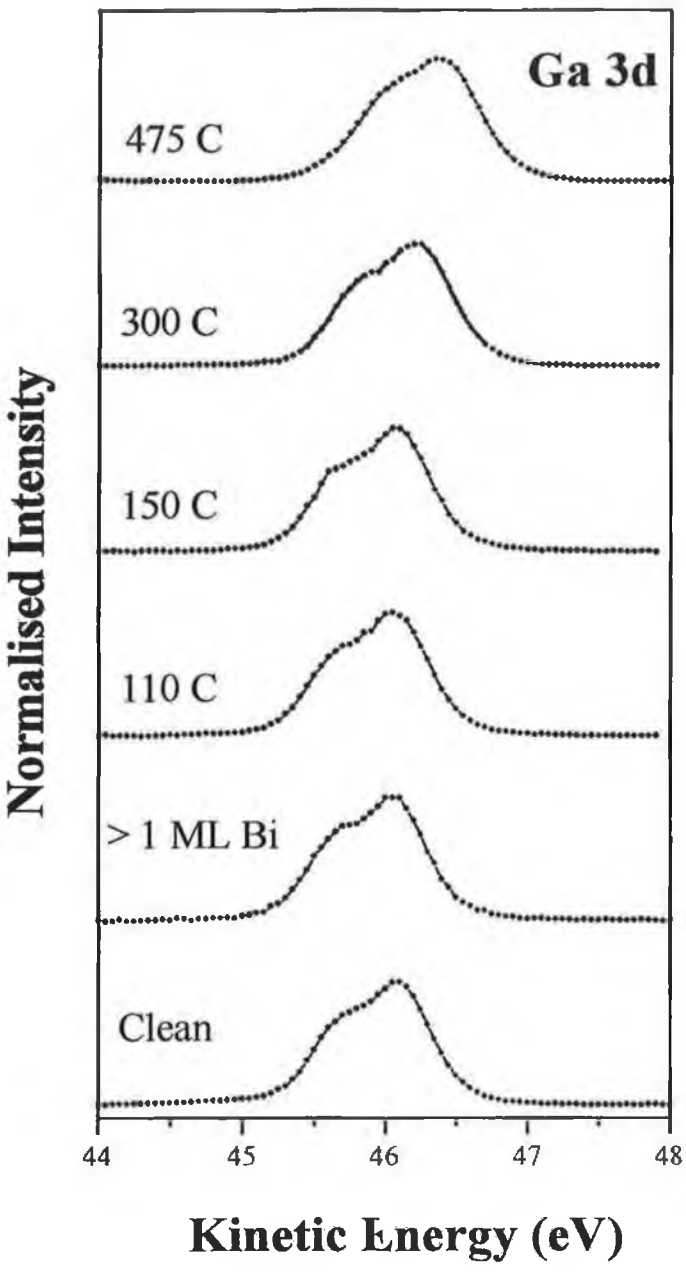

Figure 8.5 (b) Fitted Ga core levels for Bi-GaAs(111)B recorded at a photon energy of 70eV.

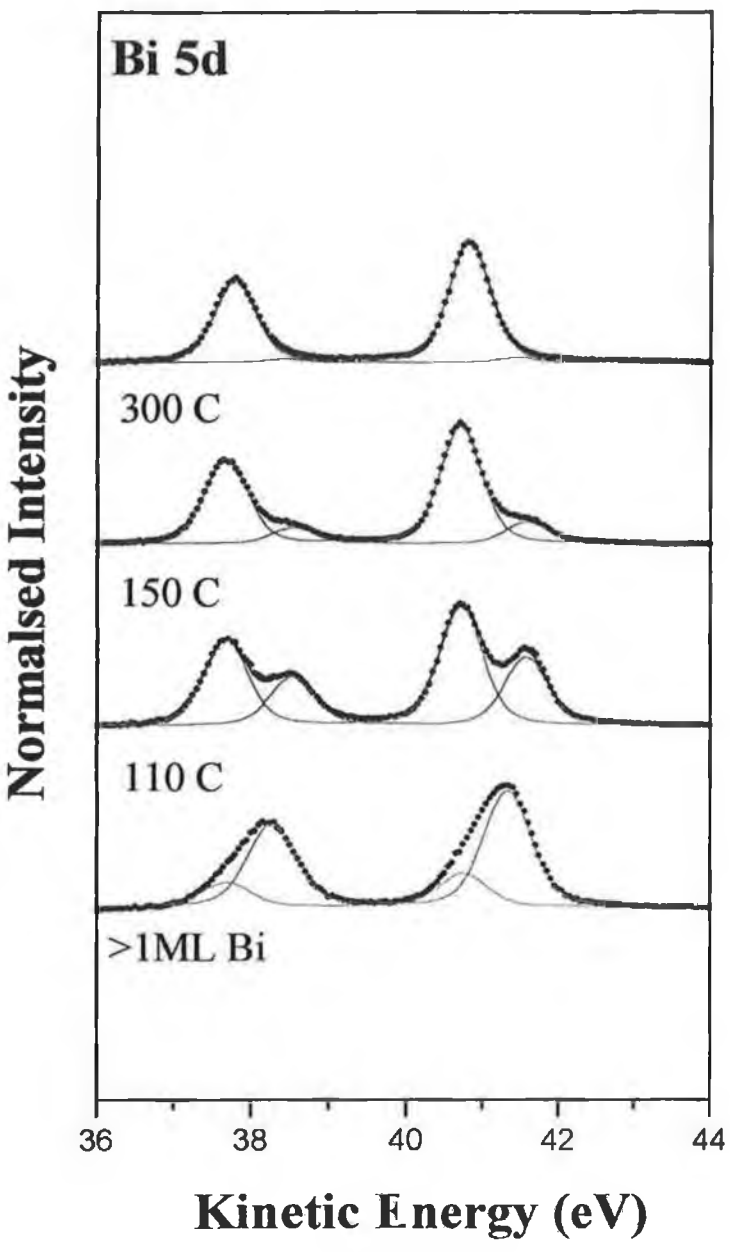

Figure 8.5 (c) Fitted Bi core levels for Bi-GaAs(111)B recorded at a photon energy of 70eV.

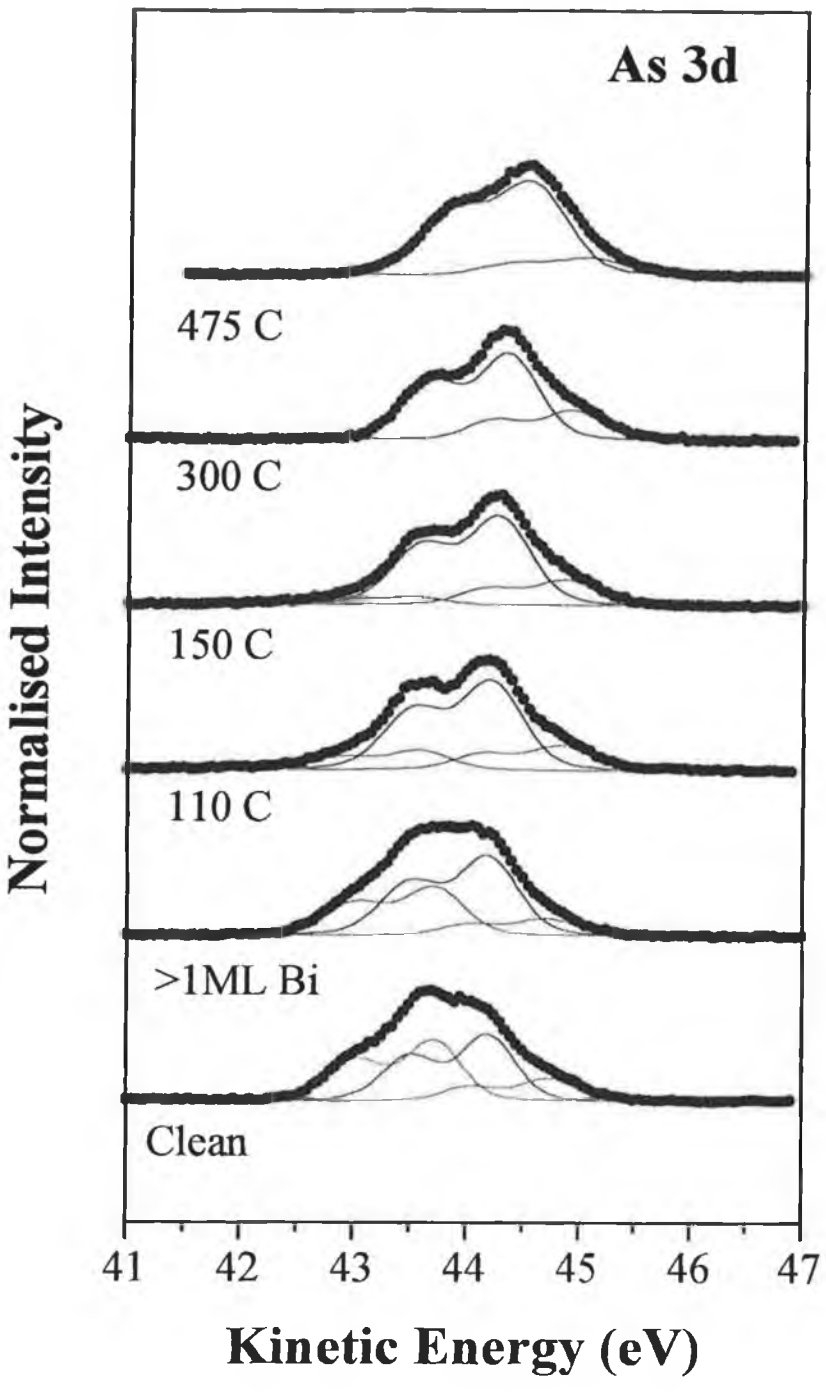

Figure 8.6 (a) Fitted As 3d core levels for Bi-GaAs(111)B recorded at a photon energy of 90eV.

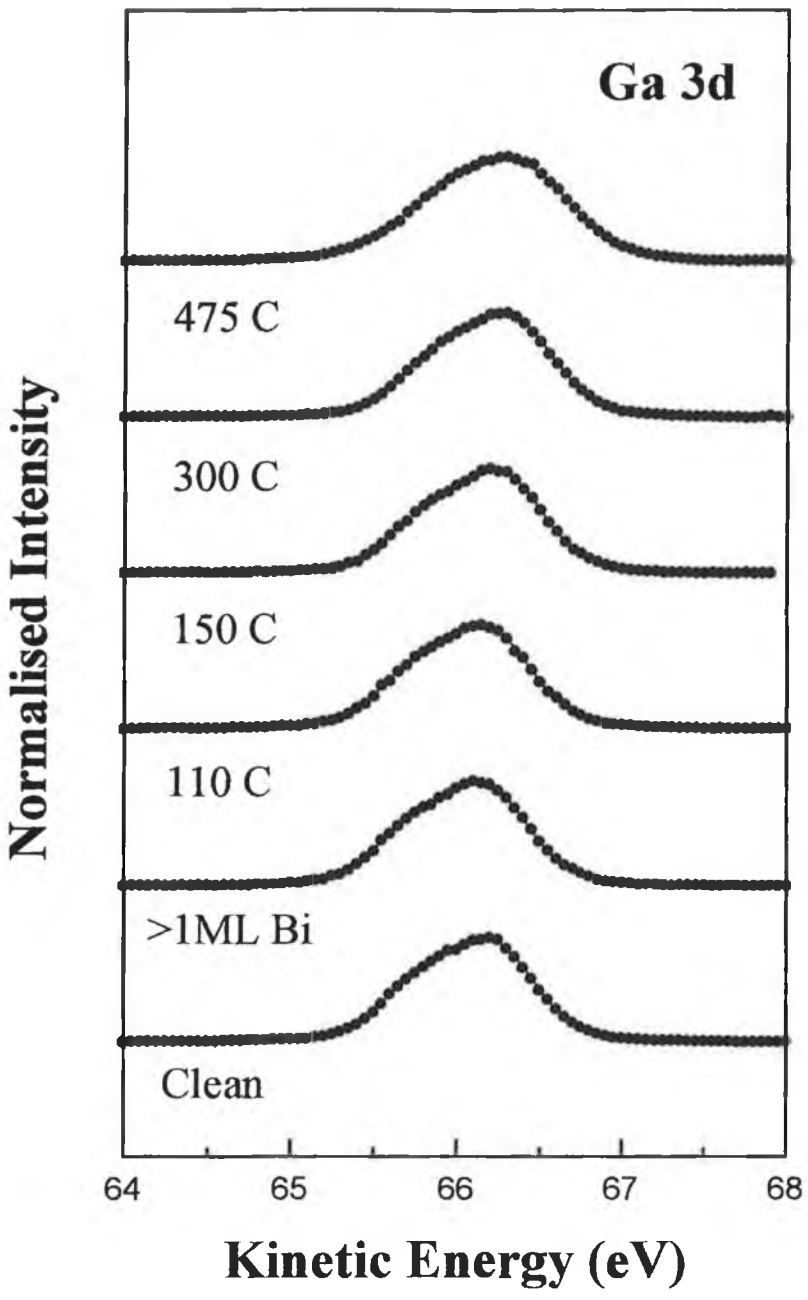

Figure 8.6 (b) Fitted Ga 3d core levels for Bi-GaAs(111)B recorded at a photon energy of 90eV.

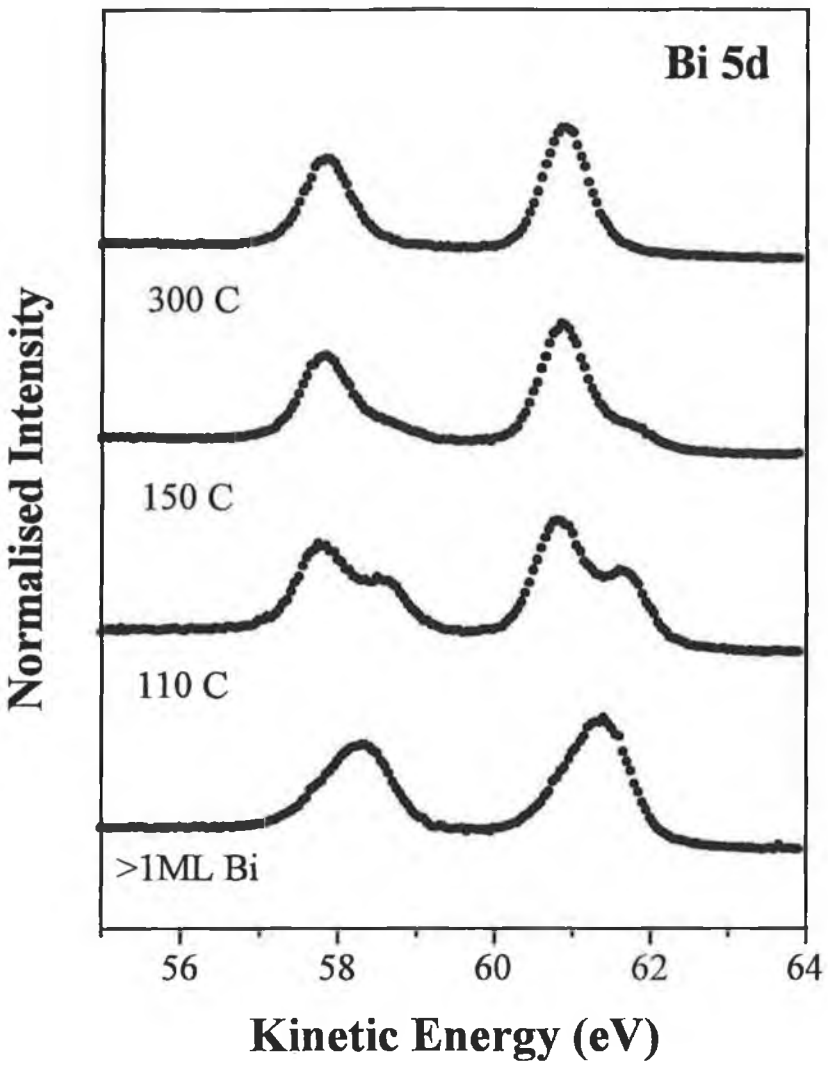

Figure 8.6 (c) Bi 5d core levels for Bi-GaAs(111)B recorded at a photon energy of 90eV.

Table 8.1

	As 3d		Ga 3d		Bi 5d
	Clean Surface	c(4×2) - Bi	Clean Surface	c(4×2) - Bi	c(4×2) - Bi
Gaussian (eV)	0.46	0.45	0.42	0.44	0.50
Lorentzian (eV)	0.17	0.17	0.155	0.155	0.23
Spin -Orbit splitting (eV)	0.69	0.69	0.45	0.45	3.03
Branching Ratio	0.666	0.666	0.666	0.62	0.666
K.E. shift of S_1 (eV)	0.57	0.57			0.66
K.E. shift of S_2 (eV)	-0.49				
Bulk K.E. position (eV)	24.20	24.32	46.13	46.26	40.82

Shown in Figures 8.6 (a)-(c) are core level photoemission data recorded at a photon energy of 90eV. It can be seen qualitatively that the SCLS's of the As 3d core level have higher intensity relative to the bulk peak than those recorded at 70eV. This illustrates how the surface sensitivity of the photoemission technique is increased by recording spectra where the photoelectrons have a kinetic energy such that their mean free path in the material is a minimum (section 2.3, figure 2.5).

8.4.2 Discussion on the parameters used in the fitting procedure

Consistent results for the parameters used in the core level fitting procedure is essential if the photoemission study is to be used to deduce the changes in chemical bonding at the surface. In Table 8.1 above the Gaussian broadening for the As and Ga core levels is consistent to within a small error of 0.04 eV. The Gaussian width represents the resolution of the light source and the electron spectrometer so this value should vary very little throughout the experiment and should be the same for all elements. Surface roughening can also be responsible for broadening the spectra : this justifies the slightly high Gaussian value of 0.50 for the Bi core levels. This surface effect is due to a higher proportion of the Bi atoms being involved in surface defects then would be the case for As and Ga.

Values for the spin orbit splitting are in exact agreement with other studies [5-9]. The Ga core level is fitted with a branching ratio of 0.62 at the stage when the c(4×2) reconstruction is present and is the only deviation for any core level from the ideal value of 2/3. This has been seen in other work [6] and is attributed to diffraction effects where the intensity of one line in the doublet is reduced relative to the other because of destructive interference caused by the layers of atoms above (As and Bi) the layers of Ga contributing to the phototemission spectrum.

8.5.1 The Structure of the Bi-GaAs(111)B - c(4x2) Surface

The structural model for the c(4×2) overlayer structure is suggested by the electron counting model [4] as follows. A c(4×2) mesh on an unreconstructed As terminated (111) surface contains 8 surface As atoms. Each As atom has a dangling bond containing 5/4 electrons due to the five valence electrons distributed among four tetrahedral bonds. Thus

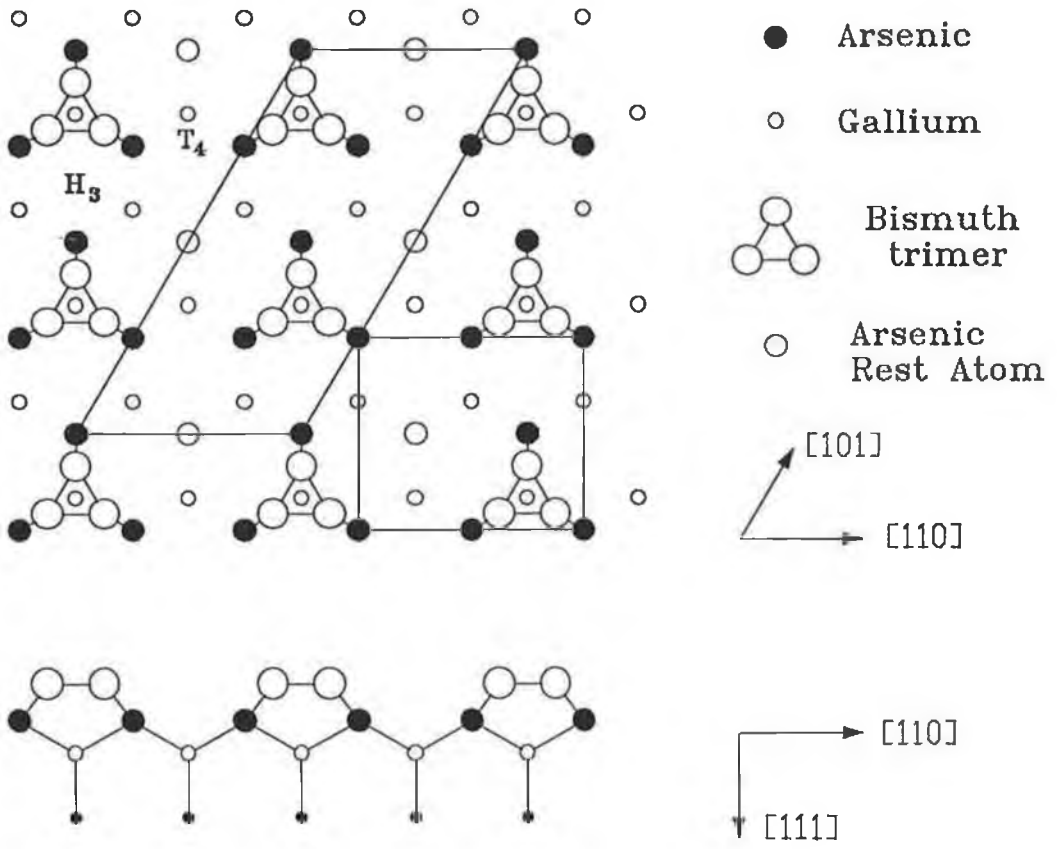

Figure 8.7 A structural model for Bi-GaAs(111)B. Two surface unit cells are shown which reproduce the symmetry of the surface but the surface is best described by the larger c(4×2) cell. The trimers are positioned in the T_4 sites which are above Ga atoms in the third layer.

the c(4×2) unit cell has 8×5/4=10 electrons available for bonding with the Bi overlayer. Bi trimers require three electrons to form bonds with the surface in exactly the same way as Sb required three electrons to bond to the GaAs(111)A surface (chapter VI, section 6.4). The possibility for single Bi adatoms is neglected as Group V adatoms are generally not found to be stable on GaAs (111) surfaces. [2, 10, 11]

Any surface As atom not involved in bonding to Bi - a rest atom - must have a full dangling bond containing two electrons. Therefore, the proposed structure, consistent with the electron counting model, consists of two Bi trimers and two As rest atoms, using 6 and 4 of the 10 available electrons respectively. A model for such a trimer structure is shown in figure 8.7, where trimers are shown in the T_4 sites (over a Ga atom in the sub-surface layer). In terms of the electron counting model, Bi trimers in the H_3 sites (adjacent to T_4 sites) would also be acceptable but we show trimers in the T_4 sites. Calculations have shown that As trimers rather than adatoms have a greater stabilising effect on the GaAs(111)B surface [11] and the T_4 site has the lowest energy [10]. It is suggested here that the same is true for Bi because As and Bi are both Group V elements. The Bi coverage of this model is 0.75ML. The c(4×2) structure bears a close relationship to the (2×2) trimer structure. If every second row of trimers oriented in the [110] direction are moved by one substrate lattice vector in the the [110] direction, then the reconstruction would be (2×2).

Although the Woods notation, c(4×2), is most convenient for labelling, it was shown above that the LEED pattern represents this structure by the matrix calculation using *rectangular* real and reciprocal lattice unit cells. This is because it is simply easier to see that the rectangular cell generates the LEED pattern as there is a fractional order spot at each corner of the cell. For a centred unit cell the equivalent reciprocal lattice unit cell does not have spots at all corners and is therefore more difficult to visualise.

8.5.2 The Bismuth Coverage of the Surface

When a structural model has been suggested it is necessary to compare its coverage with what was actually found on the surface. An estimate of the actual coverage is usually found from the plot of the Bi core level intensities during the growth and annealing processes (figure 8.2). Unfortunately this is difficult to do as the c(4×2) LEED pattern was present over the large temperature range 110°C to 375°C over which the Bi-As

component in the Bi spectrum is steadily increasing. This shows that the formation of the reconstruction is gradual in that the Bi islands gradually spread out on the surface. The c(4 ×2) structure is formed in domains which gradually increase in size as the Bi diffuses from the islands to replace the original clean surface (2×2) reconstruction. Because the spots of the (2×2) pattern overlap with c(4×2) spots the exact point at which the original clean surface structure was completely removed cannot be found from LEED. An alternative way to find the temperature and Bi coverage at which the domains of original clean surface had been replaced is to look at the As core levels (figure 8.5 (b)), to find the temperature at which the component associated with the As trimers (synonymous with the clean surface) disappears. This temperature is 175±25 °C, and the surface coverage of Bi bonded to As in the substrate at this point can be read from the growth study graph by comparing equal intensities during the deposition and annealing processes. The problem with this approach is that it is too indirect, the point where the (2×2) surface has been completely removed is not necessarily the same as that point where the Bi has successfully rebonded to the surface in the c(4×2) form. So the experimental determination of the final coverage is here taken at the point at which the Bi-Bi core level component has reduced to zero, 300±25°C. At this point, a maximum coverage of the surface with the c(4×2) structure is assumed. From the growth study, by comparing the Bi-As core level intensity at 300±25°C with the same intensity for the total Bi core level during growth, a final Bi coverage is found. The result is 0.75±0.06 ML. The Bi coverage in the suggested model shown below is exactly 0.75 ML, i.e. each (2×4) cell has an area of eight substrate (1×1) unit cells and contains six Bi atoms, so the Bi coverage is 6/8 or 0.75ML.

8.5.3 LEED Simulation of the structural Model

The structural model as described above was used to generate a LEED pattern using the double scattering simulation program [12] described in chapter III. Input to the program was the structural model shown in figure 8.7. The simulation was repeated twice with the surface model rotated by 120° and 240° and the three resulting patterns were superimposed. This simulates the effect of the triple domain nature of the surface. The c(4×2) triple domain LEED pattern produced by this method is shown in figure 8.8. It can be seen that both the spots due to the surface reconstruction and the bulk derived spots are not circular in cross section. These spots have a shape similar to that of the rectangular surface unit cell which was also the case for the simulation of the ($2\sqrt{3}\times2\sqrt{3}$) LEED pattern in chapter V. Some of the surface induced diffraction spots have very low intensity

and are not seen in this contour plot but any spot missing in figure 8.8 is accounted for by another which is equivalent by symmetry.

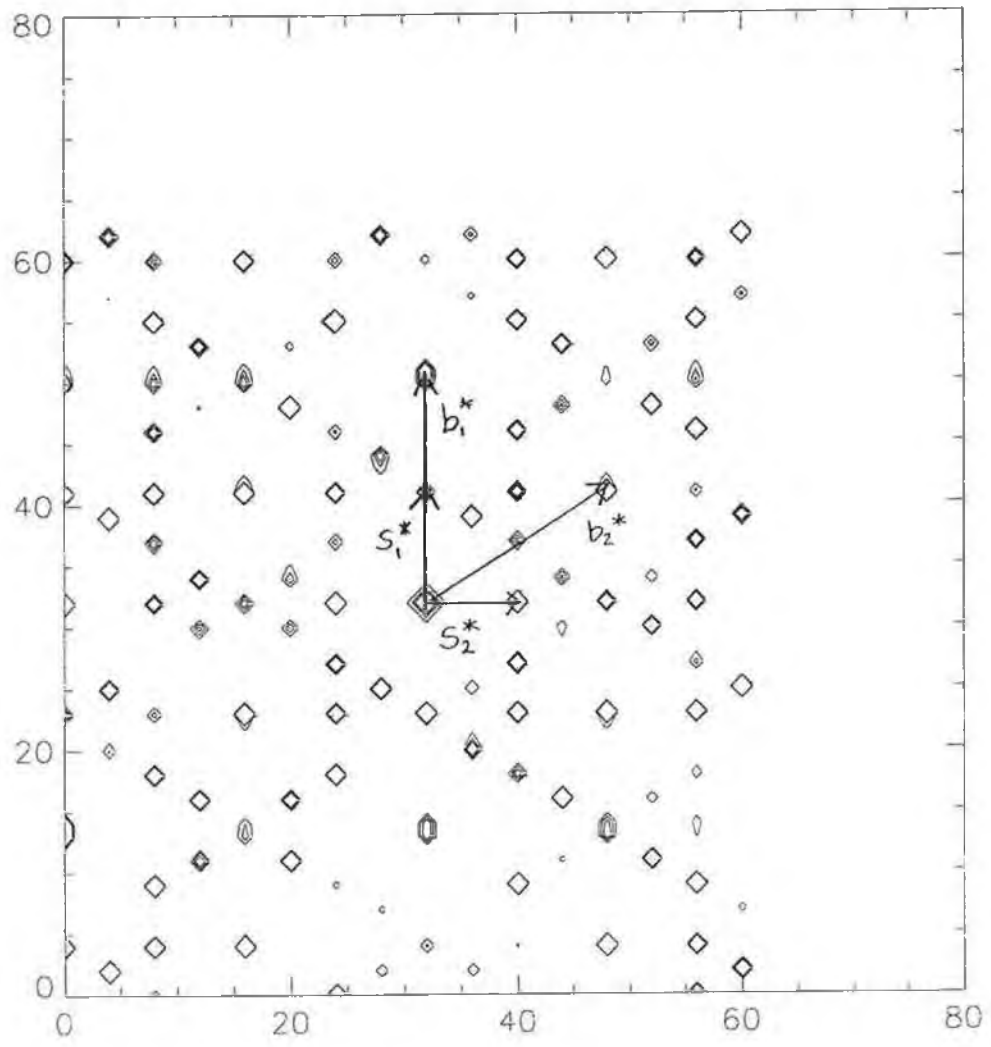

Figure 8.8 A computer generated LEED pattern resulting from the triple domain equivalent of the surface structure shown in figure 8.7.

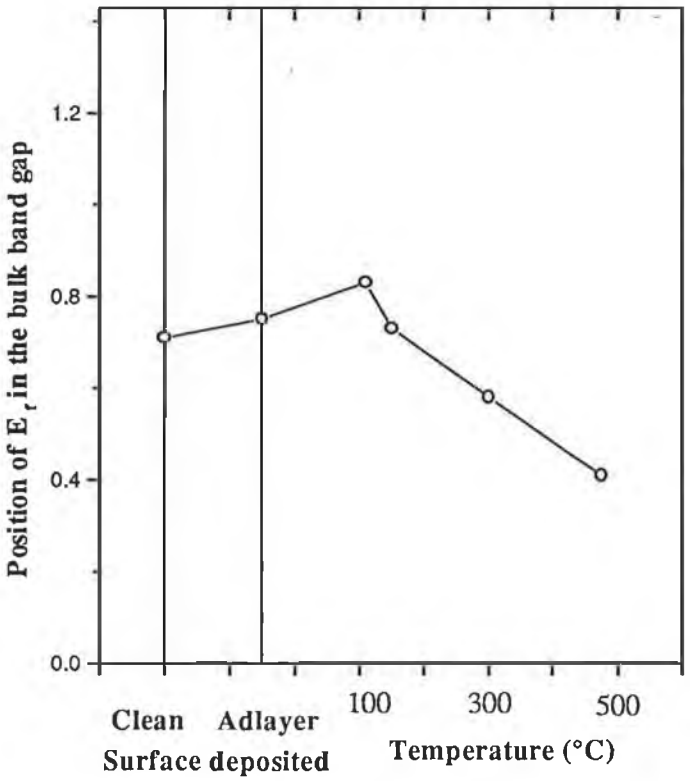

Figure 8.9 The position of the Fermi level in the bulk band gap throughout the experiment.

8.6 Electronic Properties

Figure 8.9 shows the position of E_f through the experiment. Because the GaAs(111)B samples are doped n-type, E_f in the bulk is just below the conduction band minimum (CBM). The clean surface position of E_f was found to be 0.76 eV above the VBM. This is close to the middle of the band gap which is 1.46eV. When the initial deposit of Bi was complete, the band bending was only slightly affected but as the reconstruction involving the Bi adlayer was formed at 110°C a slight flattening of the bands is noticable (the position of E_f moves back towards the conduction band minimum). This reduction of the band bending is by 0.08eV which is not signifigant enough to state that the Bi overlayer reduces surface defects. As the surface was annealed to higher temperatures the band bending increased and after the desorbtion of the Bi, the Fermi level had fallen below the original clean surface value by ~0.25eV.

8.7 Summary

As an experiment in the determination of the growth mode of Bi on GaAs(111)B - (2×2) and as a study of the reconstruction formed by annealing, this system has produced quite clear results. The change in chemical form of the deposited Bi is very clear from the core level studies as is the gradual elimination of the As trimers of the original clean surface. The c(4×2) reconstruction is stable over a reasonably large temperature range of approximately 270°C, a far larger range than the Sb reconstructions on the GaAs{111} surfaces described in chapters V and VII.

References for Chapter VIII

1. Fundamentals of Surface and thin film analysis, L.C. Feldman and J.W. Mayer, (North-Holland, 1986)
2. P. Moriarty, P.H. Beton and D.A. Woolf, Phys. Rev. B **51**, 7950 (1995)
3. D. G. Castner and G. A. Somorjai, Chemical Reviews, 79 **3** 233 (1979).
4. M.D. Pashley, Phys. Rev B **40**, 10481 (1989)
5. J.M.C. Thornton, P. Weightman, D. A. Woolf and C. Dunscombe, Phys. Rev. B **51** 14459 (1995)
6. G. Le Lay, A. Kahn, D. Mao, Y. Hwu and G. Magaritondo, Phys. Rev B **43** 14301(1991)
7. P. Moriarty, B. Murphy, L. Roberts, A.A. Cafolla, G. Hughes, L. Koenders and P. Bailey, Phys. Rev. B **50** 14237 (1994)
8. D. E. Eastman, T. C. Chiang, P. Heimann and F. J. Himpsel, Phys. Rev. Lett. **45** 656 (1980)
9. T. Miller and T. C. Chiang , Phys Rev B **29** 7034 (1984)
10. D. K. Biegelsen, R.D. Bringans, J.E. Northrup and L.E. Swartz, Phys. Rev. Lett. **65**, 452 (1990)
11. E. Kaxiras, Y. Bar-Yam, J.D. Joannopoulus and K.C. Pandey, Phys. Rev. B **35**, 9636 (1987)
12. N. Panagiotides, D. Batchelor and D. A. King, Chem. Phys. Lett **177** 419 (1991)

Chapter IX

Comparisons, Conclusions and Further Work

9.1 Growth

With regard to the growth of these overlayers on GaAs{111} substrates, the results are clear. Sb and Bi exhibit the Stranski-Krastanov growth mode on the (111)A surface and Volmer-Weber growth on the (111)B surface. The corrugation for the (111)A Ga vacancy terminated surface and the (111)B As trimer terminated surfaces have been measured by STM as approximately 1Å and 2Å respectively [1,2]. This simple difference in the size of the corrugation between the two surfaces can explain the difference in the growth modes - the growth of a complete layer is not favoured on the more corrugated surface. Another factor is the chemical reactivity of the surfaces. Because the (111)A surface is Ga terminated, the formation of a chemical bond with a group V element is more likely than for the As terminated (111)B surface.

9.2 Reconstruction

The reconstructions which were observed for Sb and Bi on the GaAs(111)B surface have not been found in the literature for metal overlayers on any semiconductor surface. A c(4×2) reconstruction has been observed for CO and/or NO overlayers on the (111) faces of Ni, Pd, Pt and Rh [3]. Because these transition metals have an fcc crystal structure, the (111) face has threefold symmetry as does the (111) face of a zincblende structure. The molecules C_2H_2 and C_2H_4 also form a c(4×2) overlayer on Rh(111) [4]. The only system found in the literature with $\begin{pmatrix} 3 & -1 \\ 1 & 3 \end{pmatrix}$ symmetry is Rh(111)-(C_6H_6 + CO) [5]. There is no significant similarity between the two classes of systems - organic molecules on Rh(111) and Group V on GaAs(111)B - to be able to make any deductions about the latter system. The coincidence is simply due to relative lattice sizes and two dimensional packing fractions.

The $(2\sqrt{3}\times2\sqrt{3})R30°$ reconstruction on the Sb-GaAs (111)A surface does not involve the removal of substrate atoms as in the case of the As trimers on the (111)B surface, but the proposed mechanism of Ga atoms originating in the bulk and becoming involved in the surface reconstruction highlights the complexity of the system. Further work as suggested below would be needed to verify the structural model.

An interesting comparison is the temperature range over which the observed reconstructions are stable. The c(4×2) LEED pattern for Bi-GaAs(111)B was clear at 110°C and remained up to 375°C. This stability is in contrast to both reconstructions found for Sb on the (111)A and (111)B surfaces where the reconstructions were observed for an interval of 50°C before the Sb desorbed. For this reason it is concluded that the Bi-GaAs(111)B system is the most 'ideal' system for further study of the interaction of a semimetal with a GaAs(111) surface.

There is a clear contrast between the state of the (111)A and (111)B surfaces after the desorption of the overlayers. A (2×2) LEED pattern was recovered for the (111)A surface after Sb or Bi desorption. For the (111)B surface, desorption of Bi gave a (1×1) LEED pattern and Sb desorption resulted in a faceted surface. The non-recovery of the (2×2) symmetry on the (111)B surface is of course to be expected since the cause of this symmetry, the As trimers, were removed by the Group V adatoms under the effect of annealing.

9.3 Band bending

The effect of the group V overlayers on the magnitude of the surface band bending is different for both surfaces. For the (111)A surface, the deposition of Sb and Bi increases the band bending by 0.15eV. Annealing had the effect of reducing the band bending with respect to the clean surface by 0.15eV and 0.25eV for Bi and Sb respectively. When the Bi had fully desorbed from this surface, the band bending remained at this value. As the (111)A samples were doped p-type, the effect of the Bi overlayer was to reduce the number of acceptor states at the surface. This seems unusual, that the deposition and subsequent desorption of Bi (at 425°C) should reduce the surface band bending. It is possible that the high temperature anneal simply removed some excess As from the surface and this reduced the number of electronic states at surface defects.

In the case of Sb\GaAs(111)A, the band bending began to increase above 400°C and was 0.08eV higher then that of the clean surface when the ($2\sqrt{3}\times2\sqrt{3}$) reconstruction was formed. After Sb desorption, the size of the surface band bending returned to the clean surface value. It is assumed that the reduction in band bending before the formation of the reconstruction is due to the filling of acceptor states at surface defects. The high temperature at which the surface reconstruction is formed may have the effect of creating more surface states hence the increase in the surface band bending.

Changes in surface band bending for Sb and Bi on the (111)B surface are qualitatively similar. The combined effect of deposition and annealing increases the band bending relative to the initial clean surface for both systems. After the desorption of the overlayer, the band bending had increased by 0.28eV and 0.15eV for the case of Sb and Bi respectively. In the case of Bi, however, there is a slight passivation or reduction of the surface band bending by 0.08eV when the c(4×2) reconstruction is formed. That the clean surface position of the Fermi level is not restored after the desorption of each overlayer is not surprising as the recovered surfaces have lost the As trimers. An increase in the number of surface states associated with defects after the overlayer desorption is inferred from this increase in the band bending.

9.4 Future Work

As the main conclusions of this work relate to the structure of Sb and Bi terminated GaAs{111} surfaces, further work should include an STM study of the four systems. The STM technique would easily verify if the structural models are indeed correct so that the exact determination of the surface structures could proceed by other methods. This work would need verification of the LEED patterns observed here, to ensure that the same situations as described in this work are repeated. A temperature versus coverage phase diagram study for each surface would be invaluable in this regard. Absolute determination of these surface structures could be found by I-V LEED. The difficulty of this technique is compounded by the complexity of these systems and the problem of preparing well ordered surfaces.

The theoretical calculations for the {111} surfaces have been highly successful in the prediction and verification of the (2×2) reconstructions. Total energy calculations have

been extended to include Group V adatoms on the (100) surface so a logical progression would be the study of these adlayers on the {111} surfaces.

Another proposal concerns measuring electronic band structure. This would not be possible, by the standard technique of angle resolved photoemission, for the reconstructed (111)B surfaces as the triple domain nature of the surfaces prevents this. The $(2\sqrt{3}\times2\sqrt{3})$ symmetry of the Sb-GaAs(111)A surface does not present this problem so the surface band structure could be mapped. Quality surface preparation would be essential for this type of work and the success of structural studies as mentioned above would help to solve this problem.

References for Chapter IX

1. K. W. Haberen and M. D. Pashley, Phys. Rev. B **41** 3226 (1990).
2. J. M. C. Thornton, P. Weightman, D. A. Woolf and C. J. Dunscombe, Phys. Rev. B **51** (14459).
3. D. G. Castner and G. A. Somorjai, Chemical Reviews, **79** 233 (1979).
4. D. G. Castner, B. A. Sexton and G. A. Somorjai, Surf. Sci. **71** 519 (1978).
5. M. A. Van Hove, R. F. Lin and G. A. Somorjai, J. Am. Chem. Soc. **108** 2532 (1986).